DISSERTATION

UNSATURATED FLUID FLOW AND VOLUME CHANGE BEHAVIOR OF FILTERED TAILINGS

Submitted by

Neelufar Aghazamani

Department of Civil & Environmental Engineering

In partial fulfilment of the requirements

For the Degree of Doctor of Philosophy

Colorado State University

Fort Collins, Colorado

Spring 2022

Doctoral Committee:

Advisor: Joseph Scalia IV

Christopher A. Bareither
Charles D. Shackelford
Jay M. Ham

ABSTRACT

UNSATURATED FLUID FLOW AND VOLUME CHANGE BEHAVIOR OF FILTERED TAILINGS

As the global demand for minerals continues to increase so does the generation of mine waste. Tremendous volumes of mine waste, viz. tailings and waste rock, are generated and placed in impoundments and piles. Improved methodologies are needed to enhance the sustainability of mine waste management. Tailings are typically discharged as a slurry of finely ground rock within water to a settling facility contained by an embankment. These facilities often necessitate long-term management of inherently weak materials. Tailings dewatered via filtration yields enhanced water stewardship and greater geotechnical stability; filtered tailings are readily amenable to progressive closure and environmental restoration. But, the high cost of tailings filtration, and the potential for acid rock drainage (ARD) due to oxygen ingress and internal unsaturated flow of water have limited the adoption of filtered tailings by the mining industry. The goal of this study is to advance the state of knowledge of filtered tailings. To this end, this dissertation consists of three components; (1) assessing the influence of filtered tailings placement conditions on filtered tailings unsaturated characteristics, (2) assessing excess pore pressure generation during compression of unsaturated filtered tailings, and (3) exploring hydrologic paths to minimize ARD and improve geochemical stability of filtered tailings stacks. Pressure plate, chilled mirror, and shrinkage curve tests were performed to produce soil water characteristic curves (SWCCs) for two precious metal mine tailings with varying initial water contents and dry densities. The resultant SWCCs illustrate that the placement water content and dry density have a significant influence on the unsaturated characteristics of the filtered tailings. Generation of excess pore water pressure

was assessed via undrained compression tests. Unsaturated filtered tailings started generating appreciable excess porewater pressure (> 10% of the incrementally applied total vertical stress) when the saturation of the tailings was at the range of 80 to 90%; this appreciable excess pore pressure did not fully dissipate after 24 h. Filtered tailings in this study followed a stress path with void ratios below the critical state line (i.e., dilative during undrained shear) unless placed initially loose and wet. The SWCCs produced were used to model the hydrology of filtered tailings and comingled filtered tailings columns via HYDRUS-2D in example wet, hemiboreal, and dry climates. Results of this study illustrate that for the filtered tailings evaluated in this study, ARD is anticipated to be minimized via varying climate-dependent mechanisms. In the arid climate, filtered tailings functioned as a water balance layer, storing, and releasing precipitation as evaporation not percolation. In the wet climate, filtered tailings became rapidly saturated and maintained a saturated surficial layer preventing inward movement of oxygen and potentially minimizing generation of ARD. In the hemiboreal and wet climates percolation was minimal due to the low hydraulic conductivity of the filtered tailings, and inclusion of a commingled capillary barrier layer further reduced percolation (further reducing the potential flux of ARD). Results from this study illustrate the potential efficacy of filtered tailings to maintain both geotechnical stability and limit ARD.

ACKNOWLEDGEMENTS

Getting my PhD from a world class university was my childhood dream. Even though I have worked hard to accomplish this goal, I would have never been at this position had I not have the supportive people around me throughout my life.

I feel very privileged and honored to have Dr. Joe Scalia as my supervisor and mentor. I sincerely appreciate for accepting me into your research group, Dr. Scalia, for giving me a chance, training me, and giving me courage and enthusiasm to work harder and harder every day. I am also thankful to Dr. Bareither and Dr. Shackelford for their guidance during my education, and to Dr. Ham for serving as my committee member.

I would like to express my utmost gratitude and love to my family in Iran, Canada, and the US, for their trust, sacrifice, and emotional support all these years. I am also very grateful to have made wonderful friends in our Geo-group and CSU, MohammadReza, Raquel, Anna, Rehman, Sajjad, Ragan, and Fatemeh, for creating some of my best memories in Colorado.

Finally, I thank god for blessing me and granting this opportunity to me.

TABLE OF CONTENTS

LIST OF TABLES

LIST OF FIGURES

LIST OF SYMBOLS

e	Void ratio
G_s	Specific gravity of solids
γ_d	Dry unit weight
$\gamma_{d,\,max}$	Maximum dry unit weight
K	Hydraulic conductivity
K_r	Relative hydraulic conductivity
LL	Liquid limit
PI	Plasticity index
φ_m	Matric potential
ψ	Matric suction
ρ_d	Dry density
$\rho_{d,\,max}$	Maximum dry density
SC	Solid content
S	Degree of saturation
S_e	Effective saturation
S_m	Maximum field saturation
S_r	Residual saturation
σ_v	Vertical total stress
σ	Total stress
σ'	Effective stress
σ^s	Suction stress
$\sigma^s{}_{ads}$	Adsorptive component of σ^s
$\sigma^s{}_{cap}$	Capillary component of σ^s
$\sigma^s{}_{dry}$	σ^s at the oven-dry state
u_e	Excess pore pressure
u_a	Gauge air pressure
w	Gravimetric water content
w_r	Residual gravimetric water content
w_s	Saturated gravimetric water content
w_{opt}	Optimum gravimetric water content
w_{tran}^{SS}	Transitional water content

LIST OF ACRONYMS

AEV	Acid Entry Value
ARD	Acid Rock Drainage
HAE	High Air Entry
MSE	Mean Squared Error
PAG	Potentially Acid Generating
PSD	Particle Size Distribution
SSCC	Suction Stress Characteristic Curve
SWCC	Soil Water Characteristic Curve

Executive Summary

INTRODUCTION

Mine waste in the form of tailings and waste rock is an unavoidable consequence of civilization. Tailings are fine residuum of milling and other mineral processing generated during the extraction of valuable metals. Conventional tailings facilities manage slurry deposited tailings behind containment embankments resulting in a loose fabric after placement and low strength that has resulted in recent flow-type failures (Mt. Polley mine in 2014, Samarco Mariana mine in 2015, and Córrego do Feijão mine in 2019; Morgenstern et al. 2015, Petticrew et al. 2015, Morgenstern et al. 2016; Fonseca do Carmo et al. 2017, Robertson et al. 2019). Slurry deposition of tailings also creates long times for consolidation necessitating long-term management of inherently weak materials. Finally, slurry deposition can hinder progressive reclamation during the life of a mine.

To achieve stability from the time of placement, tailings must be sufficiently dewatered prior to placement such that the resultant tailings can be compacted to create a sufficiently dense structure that is dilative during undrained shear, preventing the generation of positive excess pore water pressures and thus mitigating the potential for liquefaction and flow. As a result, filtration has become a widely practiced method of separating tailings mineral solids from water to enhance densification (Wang et al. 2014). The resulting filtered tailings are unsaturated material that can be placed in a denser condition than slurry tailings (Lupo and Hall 2010). Filtered tailings are deposited to form a tailings stack, often placed near or wet of standard optimum water content (ASTM D698; ASTM 2014) and compacted to 95% of standard Proctor energy maximum dry density.

Tailings filtration at a large scale has typically not been cost-competitive relative to conventional slurry tailings management. To minimize costs and maximize throughput, a maximally viable filtered tailings pile will be placed as wet as possible to minimize dewatering. However, the generation of positive excess pore water pressure in unsaturated filtered tailings can potentially prevent sufficiently dense placement and the achievement of geotechnical performance targets. Thus, relevant, and interrelated operational questions include, *how high a lift of filtered tailings can be built until a significant amount of excess pore water pressure is generated? At what gravimetric water content should a lift of filtered tailings be constructed*, or posed a different way, *how wet can filtered tailings be practically placed? Is compaction required while stacking filtered tailings? What is a significant amount of excess pore water pressure for a filtered tailings stack?* Further investigations are required to enable the optimized and purposeful construction of filtered tailings stacks. This investigation is one objective of this study.

Finally, although filtered tailings stacks have enhanced geotechnical stability, by virtue of being unsaturated, these stacks have an increased possibility for acid rock drainage (ARD) if the mineralogy includes sufficient sulfide minerals, insufficient buffering capacity, and the tailings are exposed to both oxygen and water. Acid rock drainage, when present, often requires leachate treatment in perpetuity (Wickland and Wilson 2005). If a filtered tailings stack is to be constructed out of potentially acid generating (PAG) material, keeping the structure near saturation will minimize ARD by preventing oxygen ingress. Alternatively, preventing percolation of atmospheric precipitation via a water balance achieved with dense filtered tailings may prevent ARD flux. Filtered tailings can also be co-disposed or comingled with layers or zones of waste rock or any available coarse-grained material to enhance the hydrologic, geotechnical, and geochemical behavior of the stack (Brawner 1978, Brussière 2007). Thus, a second objective of

this study is to evaluate how filtered tailings or commingled filtered tailings will maintain high saturation or low fluxes in different climatic conditions.

METHODS AND MATERIALS

Soil water characteristic curves (SWCCs) are required to assess the influence of filtered tailings placement conditions (density, water content, stack height) on the unsaturated behavior of filtered tailings. Pressure plate, chilled mirror hygrometer, and shrinkage curve tests were conducted to produce SWCCs for a variety of filtered tailings samples with different initial water contents and dry densities. The SWCCs were generated using well-recognized models in the literature (van Genuchten 1980 and Fredlund and Xing 1994). Initial conditions included standard Proctor optimum water content and 5% wet of optimum water content, with initial compaction to 80, 90, and 95% of the maximum dry unit weight of the tailings.

Tailings from two confidential precious metal mines were tested in this study. These tailings are the same used in Gorakhki et al. (2020). The tailings were filtered in the field and had particle size distributions of average silty and clayey tailings.

To further understand how density, water content, and stack height influence generation of excess porewater pressure in an unsaturated state, undrained compression tests were also performed on the same materials as SWCCs targeting the same initial conditions. Drying and wetting SWCCs were used to estimate suction stress of filtered tailings using methods by Lu et al. (2010) and Zhang and Lu (2020). Suction stress data were combined with results from compression tests to estimate effective stress using models developed by Zhang and Lu (2020). The effective stress and compression data could then be integrated with a critical state line to evaluate if the

stress paths of filtered tailings stayed below the critical state line (i.e., maintained conditions that would be dilative, not contractive, during undrained shear).

Finally, the combined results from shrinkage and SWCC tests were used to assess the maintenance of saturation and the impact on drawdown and percolation (downward flux) on filtered tailings stacks. The efficacy of internal capillary layers in maintaining a near saturation condition and thus minimizing the risk of ARD was also investigated. Parameters from drying SWCC were used to numerically model columns of filtered tailings via HYDRUS-2D. Tailings columns were also simulated above layers of coarse-grained materials as capillary barriers to test the concept of integrated capillary barriers. Simulations within HYDRUS-2D were conducted considering three different climate types: wet (Juneau-AK), hemiboreal (Bozeman-MT), arid (Tucson-AZ). Models were also run considering no atmospheric interaction as a baseline condition.

MAJOR FINDINGS

This study shows a combination of tailings SWCCs, and compression results from undrained compression tests, tailings-specific critical state line, and local climate data, can be used to identify required levels of dewatering and compacting to attain geotechnically and geochemically stable stacks. Each chapter has been prepared as a stand-alone document.

In Chapter 1, unsaturated tailings characteristics are identified and evaluated for two mine tailings with various initial gravimetric water contents and degrees of compaction. Generated SWCCs for filtered tailings are shown to vary with initial placement conditions. The placement condition of filtered tailings, however, only affects matric suction data (below 1000 kPa). In

general, highly compacted (≥ 90% compaction) filtered tailings maintain more moisture and higher degrees of saturation under suctions ranging from 15 to 600 kPa, when compared to loosely placed (80% compaction) filtered tailings. Similarly, filtered tailings compacted wet of optimum keep more water under suctions ranging from 15 to 600 kPa compared with filtered tailings compacted at standard Proctor optimum water content. A distinct desaturation of both tailings tested in this study started at the plastic limit of each tailings, viz., the plastic limits of these tailings were representatives of the suctions equal to the air entry values of the tailings for each test.

In Chapter 2, the generation of excess pore water pressure under varying as placed conditions of filtered tailings are assessed and quantified. Generation of positive excess pore water pressure in unsaturated filtered tailings is related to degree of saturation and compressibility of the as placed tailings. Drier tailings are less compressible for a given applied stress and have a lower degree of saturation. Wetter tailings are more compressible for a given applied stress and have a higher degree of saturation. Based on the results from undrained compression tests, appreciable positive excess porewater pressure was measured at 80% to 90% saturation for specimens with more than +3% optimum water content. In this research, appreciable excess pore pressure refers to when the ratio of generated excess pore pressure over the applied vertical stress is equal to or greater than 0.1, and the generated excess pore pressure is not fully dissipated after 24 h. The magnitude of generated positive excess porewater pressure increased under subsequent loadings because generated excess porewater pressure was not dissipated before next load was applied. In tests where no appreciable positive excess porewater pressure was observed, the specimens had not reached 78% saturation by the end of the test. These tests illustrate that filtered tailings should be kept at saturations less than 80% to avoid generation of excess pore water pressure. However, this saturation criterion is the inverse of what is needed to prevent oxygen ingress. Thus, the

magnitude of dewatering of a filtered tailings stack must balance the creation of a sufficiently density deposit while considering long-term geotechnical implications of the dryness necessary to achieve these conditions.

In Chapter 3, the impact of using water balance in minimizing ARD of comingled filtered tailings and sand in different climatic type settings (arid, hemiboreal, and wet) is assessed. The necessity of compaction of tailings to create a near saturation condition and limit oxygen ingress is shown to be climate dependent. Filtered tailings with relatively higher clay-size content ($\geq$ 23%) and lower unsaturated hydraulic conductivity successfully maintained the initial degree of saturation for 10 years, when no atmospheric impacts were considered (e.g., precipitation, evaporation). On the other hand, internal capillary barriers were found to be efficient in more silty tailings, when no atmospheric changes were considered, to maintenance of the as-placed saturation condition (drawdown resulted in saturation without such internal barriers).

In the arid climate, the surficial degree of saturation (up to 250 cm depth) decreased independent of capillary layer installation. Moreover, the seepage rates from simulated filtered tailings in an arid climate were minimal or zero. In the hemiboreal climate, significant fluctuations in the degree of saturation of tailings (up to 62% difference between the initial and final degrees of saturation) especially at the depths closer to the ground surface ($\leq$ 20 cm) were observed. However, saturations were maintained at depth due to the tight pores of the filtered tailings. In the wet climate, rapid surficial saturation was observed, with further percolation limited by the hydraulic conductivity of the filtered tailings. Thus, oxygen ingress and resultant ARD would be of greatest concern in the hemiboreal climate, but the magnitude of ARD flux was still substantially limited (e.g., the maximum flux from the bottom of the siltier tailings lift was 7.2% of the

percolated water at the end of the 2nd year of modeling) by the low hydraulic conductivity of the filtered tailings.

In both hemiboreal and wet climates internal capillary barriers further reduced the seepage rate from filtered tailings but did not affect the degree of saturation. For example, the cumulative flux at the end of the 2nd year of modeling was reduced up to 100% (depending on the initial placement of filtered tailings) in the hemiboreal and wet climates with the presence of internal capillary barriers.

Chapter 1. Effect of placement water content and dry density on moisture retention behavior of filtered tailings

1.1. INTRODUCTION

Filtered tailings are considered a best available technology for the management of tailings (Morgenstern et al. 2015). However, there is uncertainty as to how placement conditions (viz., gravimetric water content and dry density) impact geotechnical and geochemical behavior of the resultant filtered tailings stack. Compacting filtered tailings after placement is a common practice for filtered tailings stacks, but this added step makes filtered tailings a more costly tailings management strategy. To build geotechnically and geochemically stable filtered tailings stacks, we need to account for the unsaturated behavior of the placed materials that is derived from the placement condition. However, there is not adequate guidance on how the placement condition of filtered tailings influences unsaturated characteristics.

Soil water characteristic curves (SWCCs) are used to quantify water distribution and movement in unsaturated soils by providing a linkage between the mass and volume of water in a soil and the energy state of the water phase (Barbour 1998, Fredlund et al. 2012, Lu 2016). Soil water characteristic curves defining the relationship between soil suction (ψ) vs volumetric water content (θ) are used as inputs to model moisture movement in unsaturated soils (and tailings). Typically, data for matric suction and total suction (= matric suction + osmotic suction) are combined to define the SWCC (Fredlund et al. 2012). Although derived from soil science, many studies have used the SWCC to quantify unsaturated behavior of tailings (Bussière 2007, Qiu and Sego 2001).

Cyclic wetting and drying of filtered tailings stack is inevitable due to transient climatic conditions, and thus, the investigation of both wetting (absorption) and drying (desorption) SWCCs is paramount (Fredlund et al. 2012). Hysteretic behavior has been attributed to several mechanisms, including non-homogenous pore-size distribution (ink-bottle effect), entrapped air in dead-end pores, shrinkage, and contact angle (Childs 1969, Lu and Likos 2004). Limited data are available that evaluate the hysteretic behavior of filtered tailings.

The objective of this chapter is to evaluate the influence of filtered tailings placement conditions on unsaturated characteristics. Findings from this study also can be used to understand the evolution of SWCCs as a filtered tailings stack is built and guide the degree to which tailings are dewatered and potentially compacted after placement. The unsaturated characteristics of the filtered tailings were evaluated using both drying and wetting pressure plate, chilled mirror hygrometer, and shrinkage curve tests on two different precious metal mine tailings. Initial conditions were varied over gravimetric water contents ranging from 0 to 5% wet of standard Proctor optimum and dry densities 80, 90, and 95% of the standard Proctor maximum dry density (ASTM D698; ASTM 2014). Resultant data are analyzed using the van Genuchten (1980) and Fredlund and Xing (1994) models to fit SWCCs. The influence of initial conditions on SWCCs and SWCC parameters is demonstrated.

1.2. MATERIALS

Filtered tailings from two confidential precious metal mines (mine M and mine P) were used in this study. Geotechnical characterization of mine M and mine P filtered tailings (referred to as M tailings and P tailings henceforth) are described in Gorakhki et al. (2019) and are summarized in Table 1.1. Filtered tailings were dewatered at the mines during pilot-scale tests, prior to shipment to Colorado State University and testing. Characteristics of the tailings include

mechanical sieve and hydrometer (ASTM D422; ASTM 2007), Atterberg limits (ASTM D4318; ASTM 2014), specific gravity (ASTM D854; ASTM 2014), and standard effort compaction (ASTM D698; ASTM 2014).

Table 1.1 - Summary of physical characteristics and classification of mine M and P tailings (from Gorakhki et al. 2019).

Property/Characteristic	Standard	Tailings	
		M	P
Atterberg limits:	ASTM D4318		
Liquid limit, LL (%)		30.1	20.9
Plastic index, PI (%)		9.2	1.3
Classification (USCS)	ASTM D2487	CL	ML
Particle sizes (%):	ASTM D422		
Gravel (4.75 mm – 76.2 mm)		0	0
Sand (0.075 mm – 4.75 mm)		14.3	35.8
Fines (< 0.075 mm)		85.7	64.2
Clay (< 2 μm)		23.6	17.4
Specific gravity of solids, G_s	ASTM D854	2.715	2.62
Compaction:	ASTM D698		
Optimum water content, w_{opt} (%)		15.8	14.2
Maximum dry density, ρ_d (Mg/m^3)		1.69	1.82

The particle-size distributions (PSDs) for M tailings and P tailings are shown in Figure 1.1, along with an average, upper-bound, and lower-bound PSD based on a compilation from literature for other mine tailings (Gorakhki et al. 2019). Based on Table 1.1 and Figure 1.1, tailings from

both mines are comparable to average tailings properties. The fines content and clay-size content (particle size < 0.002 mm) of M tailings are higher than P tailings and are closer to the upper bound for tailings from the literature; the greater clay-size content is consistent with the higher plasticity (LL and PI) of M tailings and illustrate that M tailings are more clayey than the average tailings.

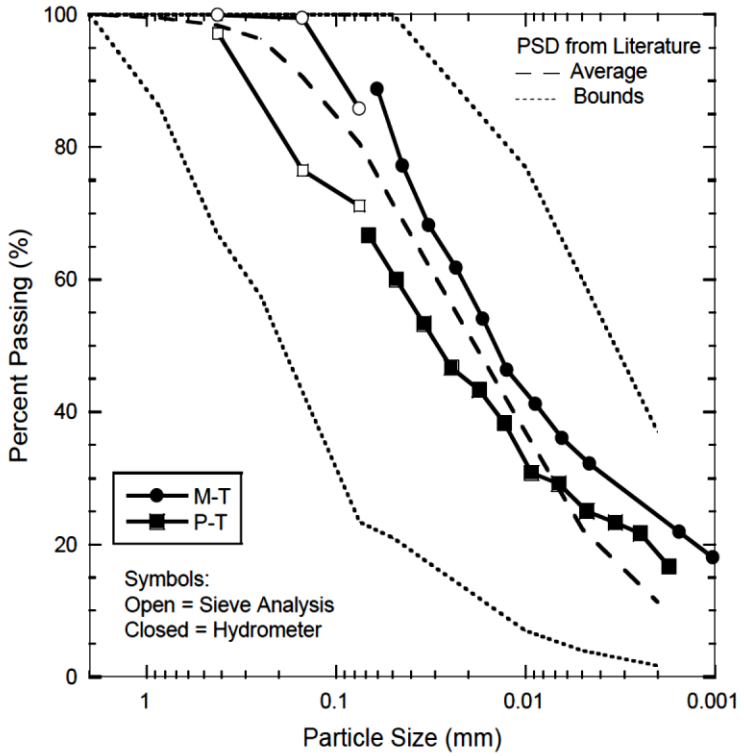

Figure 1.1 - Particle-size distributions (PSDs) for mine M tailings and mine P tailings based on mechanical sieve analysis and hydrometer. Dashed lines are the average PSD and upper and lower bounds of PSDs of mine tailings compiled from literature (after Gorakhki et al. 2019, adapted from Hamade 2017).

1.3. METHODS

The SWCCS were developed using pressure plate and hygrometer (chilled mirror) methods to measure suction for the M and P tailings. Filtered tailings specimens were prepared over a range of initial conditions. Initial dry densities (ρ_d, or dry unit weight, γ_d) corresponding to 80, 90, and 95% of the maximum dry density, $\rho_{d,max}$(or maximum dry unit weight, $\gamma_{d,max}$) were used. Initial

gravimetric water contents (w) of optimum and +5% wet of optimum water content were used. Details of the specimen preparation and test methods are provided in the following sub sections.

1.3.1. Specimen preparation

The air-dried filtered tailings were pulverized using a rubber hammer and then passed through a sieve #4 (Figure 1.2) to homogenize. After adding a target amount of water, tailings samples were mixed thoroughly and then sealed in a plastic container for 24 h. After 24 h, tailings were again mixed, passed through a #4 sieve, and then compacted. Filtered tailings with adjusted water content were compacted (using a metal hand tamper) to a target dry density inside rings with a 63.5-mm diameter and 20.0-mm height (Figure 1.3) for pressure plate testing.

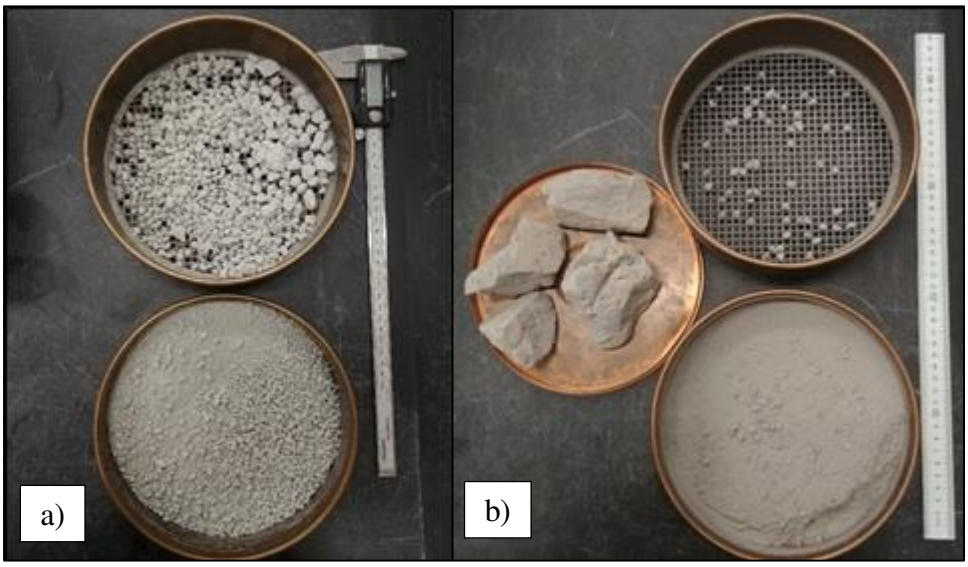

Figure 1.2 – As received tailings pulverized and passed through a #4 sieve: a) A mine M tailings; b) a mine P tailings.

After compaction, specimens used for drying pressure plate tests were sealed between rigid porous plates to prevent swelling and immersed in de-aired de-ionized water (DIW) for at least 48 h to saturate (Figure 1.4). The top and the bottom of the specimens were covered with filter paper to prevent fines migration. Wetting pressure plate test specimens were used as compacted.

Figure 1.3 - A pressure plate specimen compacted inside a ring.

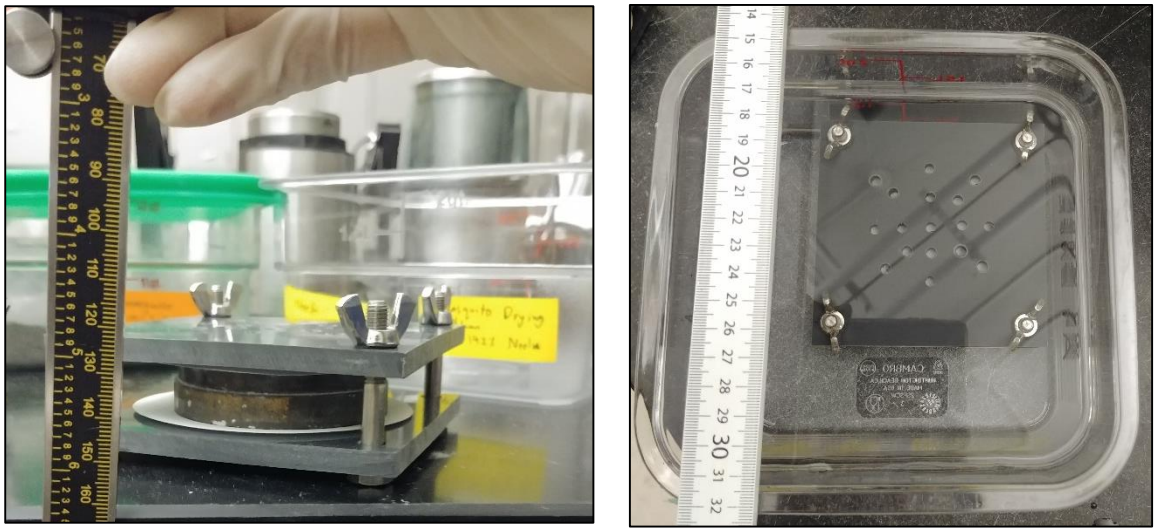

Figure 1.4 - A specimen prepared for and undergoing saturation for a drying pressure plate test.

1.3.2. Pressure plate test

2.2.3.2. Drying pressure plate test

The procedure detailed by Wang and Benson (2004) (Method B ASTM D6836; ASTM 2016) was followed for pressure plate tests in this study with the following deviations. The pressure plate test setup was installed above a high precision scale *OHAUS Model: AX422/E*. The outflow tubing of the pressure-plate cell was inserted into a 125-L volumetric beaker. The top of the beaker was covered with parafilm. Two small holes were cut into the parafilm, one for the outflow tubing of the pressure plate cell and another slit for air to leave the beaker. The beaker was filled with de-aired DIW such that the tip of the outflow tubing was always below the water surface in the beaker. The beaker was placed on the scale and changes in the mass of expelled water were recorded by the built-in software (*SPDC Data Collection*) of the scale (Fig. 1.5).

The axis translation technique (Lu and Likos 2004, Fredlund et al. 2012) was used. Positive air pressure was applied to the specimen translating the reference pore air pressure (atmospheric pressure increase) and resulting in a negative pore water pressure by an equal amount assuming incompressible soil solids and water. The positive air pressures applied in drying pressure plate tests were 14, 28, 55, 110, 221, and 441 kPa. The thickness, diameter, and gravimetric water content of the specimen were measured at termination. Figure 1.6 shows a terminated pressure plate test.

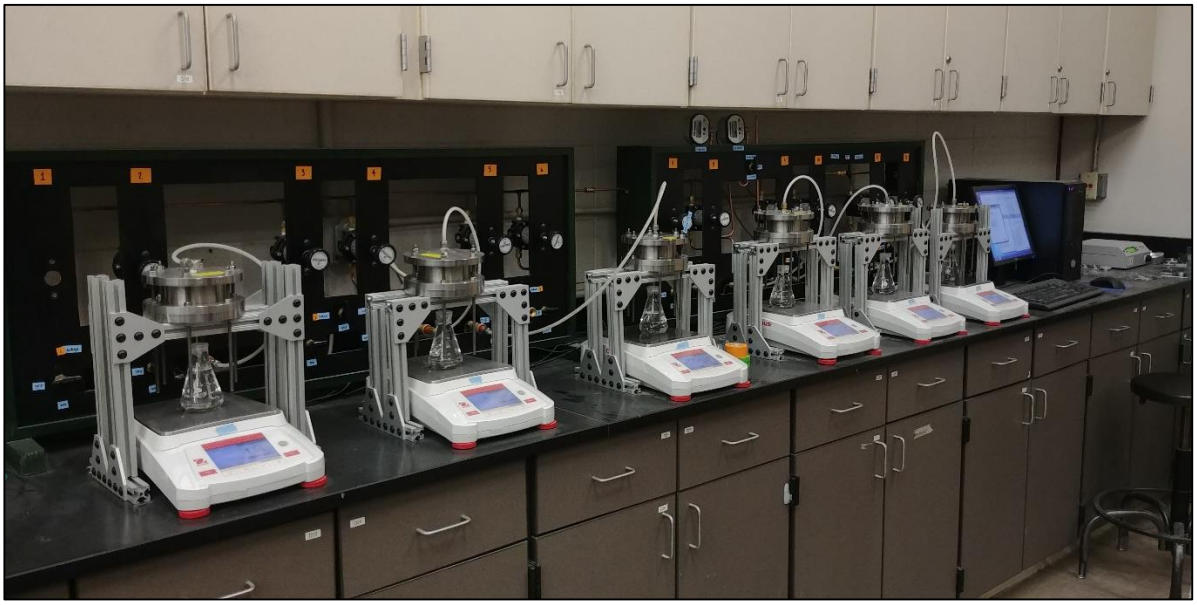

Figure 1.5 - Running pressure plate tests.

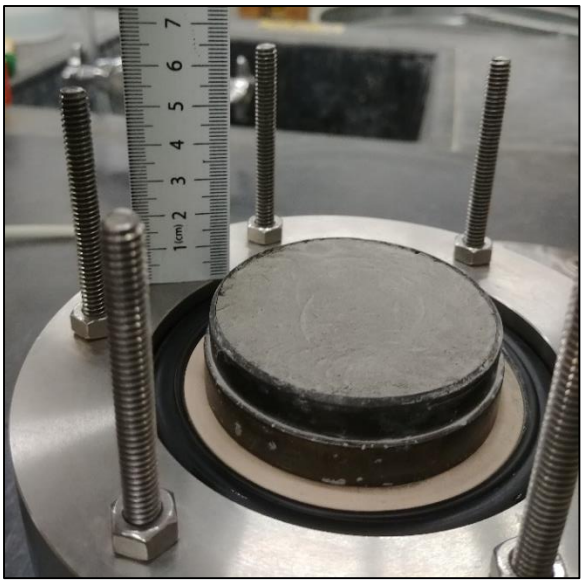

Figure 1.6 - A specimen (P tailings, 95%$\gamma_{d,max}$, w_{opt}) after the termination of a drying pressure plate test.

1.2.3.2. Wetting pressure plate test

The procedure for wetting pressure plate tests was similar to that of drying pressure plate tests with the following differences. In the wetting pressure plate tests, specimens were not saturated initially. Thus, for the wetting test, the compacted specimen was initially dried by axis translation (in a pressure plate) from the as-compacted condition to the water content corresponding to a suction slightly less than 500 kPa, and then tested by a stepwise decrease in matric suction (stepwise wetting). 500 kPa was the air entry value (AEV) of the high air entry (HAE) ceramic disk used in the pressure plates. The applied air pressures in the wetting pressure plate tests were 441, 221, 110, 55, 28, 14, and 1.3 kPa, respectively. The final stage was not atmospheric (0 kPa) because specimens were under -1.3 kPa pore water pressure (1.3 kPa matric suction) due to the configuration of the pressure plate apparatus.

The imbibed water at equilibrium was measured for each stepwise pressure decrease. Because the specimens in wetting tests were not initially saturated, air bubbles appeared in the bottom tubing of the cell on occasion. As the air pressure on the specimen decreases, cavitation occurs, and dissolved air inside water is released. Whenever air bubbles were observed in the outflow tubing, the test was stopped, the specimen was removed, the removed specimen was installed inside a new pressure plate apparatus with a newly saturated HEA disk, and the test was restarted. This procedure was repeated until no air bubbles were observed inside outflow tubing until the end of the test. Overall, the duration of a successful wetting pressure plate test (30 d) was approximately double the time needed to perform a drying test (16 d).

1.3.3. Chilled mirror hygrometer test

The pressure plate tests provided matric suction data to no more than 441 kPa due to the air entry value of the HAE ceramic disks used (i.e., 500 kPa). Thus, hygrometer tests were performed to measure higher suctions of up to 289,000 kPa for this study. The procedures provided in the manual of the hygrometer apparatus (*WP4C - Dewpoint PotentiaMeter*) and Method D of ASTM D6836 (ASTM 2016) were followed. Note that the suctions measured by the hygrometer are total suctions, whereas those measured using the pressure plates were matric suctions (negative matric potential).

Hygrometer tests were performed following each of the drying pressure plate tests. After the termination of a drying pressure plate test, a piece of the final specimen was cut and then nipped/crushed manually for hygrometry testing (Fig. 1.7).

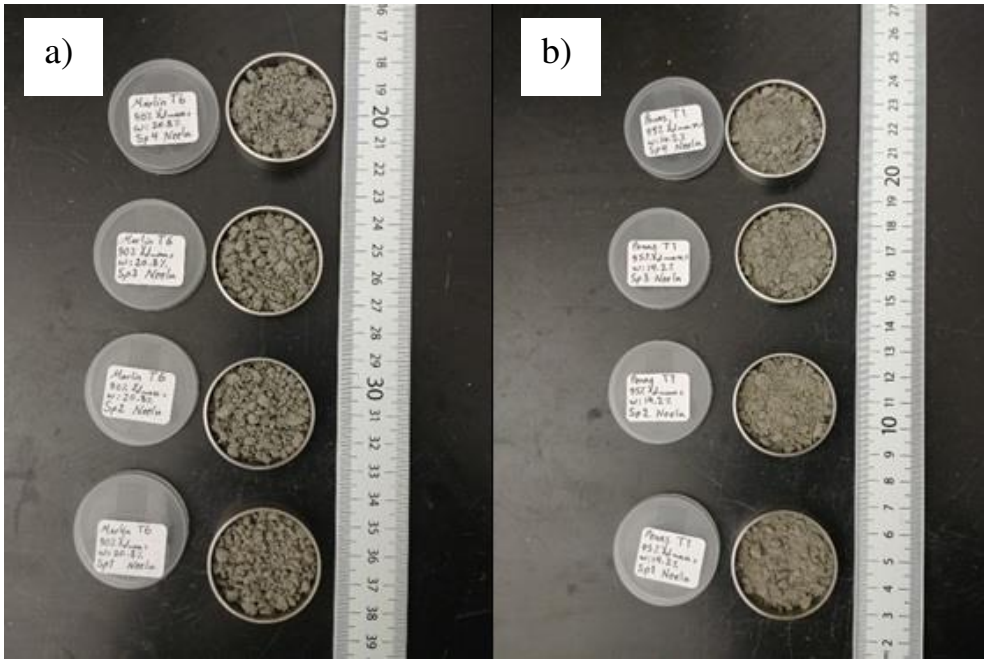

Figure 1.7 - Hygrometer test samples from a) M tailings, and b) P tailings.

1.3.4. Shrinkage curve test

The degree of saturation and volumetric water content are potentially affected by the shrinkage/swelling of tailings. Because direct measurement of the volume of tailings specimens in pressure plate tests is not feasible, shrinkage curve tests were performed. The shrinkage of tailings specimens was apparent after the termination of pressure plate tests. Separate shrinkage curve tests were performed to get relationships between gravimetric water content (w) and void ratio (e) during drying to correct volumetric water content (θ) data. The following equation was used to correct void ratio for shrinkage (Fredlund et al. 1996, Fredlund 2000, Fredlund et al. 2002, Fredlund and Houston 2013):

$$e(w) = a_{sh}\left[\frac{w^{c_{sh}}}{b_{sh}{}^{c_{sh}} + 1}\right]^{\frac{1}{c_{sh}}} \tag{1.1}$$

where a_{sh} is the minimum shrinkage limit void ratio (e_{min}), b_{sh} is the slope of the line of tangency (e.g., e/w when drying from saturated condition), and c_{sh} is the curvature of the shrinkage curve. Equation 1.1 was also used to account for the swelling of the specimens during wetting tests.

Shrinkage curves were measured following the procedure detailed by Fredlund and Houston (2013) with the following deviations. Sample preparation and saturation for shrinkage curve tests were the same as those of a drying pressure plate test. However, rings used for shrinkage curve tests had an average diameter of 41.0 mm and height of 12.0 mm. Similar to drying pressure plate tests, specimens were sealed between porous plates to prevent swelling and immersed in de-aired DIW for at least 48 h prior to testing. The specimens were removed from the hydration plates and placed on a piece of parafilm which was slightly greased to prevent adhesion of tailings to the surface and left to air dry. The dimensions and weights of specimens were measured periodically

until no considerable changes were recorded (measurement increments were based on observed trends). For most tests, measuring the diameter and thickness of the specimens was not initially possible because the moist specimens were too soft. Figure 1.8 illustrates the changes in dimensions of a shrinkage curve test specimen.

The results of shrinkage curve tests on M and P tailings are presented in Figure 1.9. Horizontal relationships shown in some data at high water contents were due to specimens being too soft to be measured by a caliper, and thus volume change could not be accurately quantified. Fitted parameters to Equation 1.1 are presented in Table 1.2, and the resulting fitted models are included in Figure 1.9. The e_{min} from tests on P tailings were generally lower than those from M tailings due to different particle gradations and clay contents of the tailings tested. Denser placement of filtered tailings ultimately resulted in lower shrinkage limit void ratio comparing to specimens with a looser initial condition. Moreover, specimens prepared wet of optimum water content (before being immersed in water) generally reached lower shrinkage limit void ratio and underwent more shrinkage than specimens with the same degree of compaction (same initial ρ_d) but prepared with optimum water content. M tailings were more deformable when prepared with higher initial water content than P tailings. The shrinkage curve test on the M tailings with 80% compaction was the only test which had the same shrinkage limit void ratio for both optimum and wet of optimum water content.

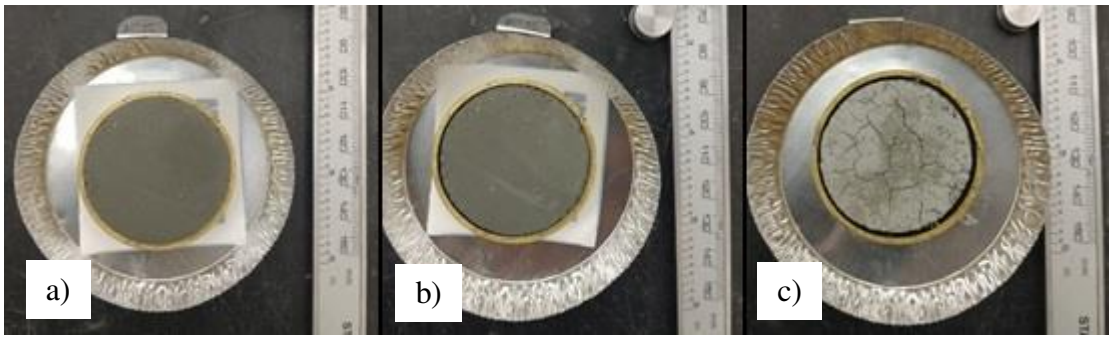

Figure 1.8 - Effect of shrinkage on specimen dimensions in shrinkage curve test (specimen is drying from a to c).

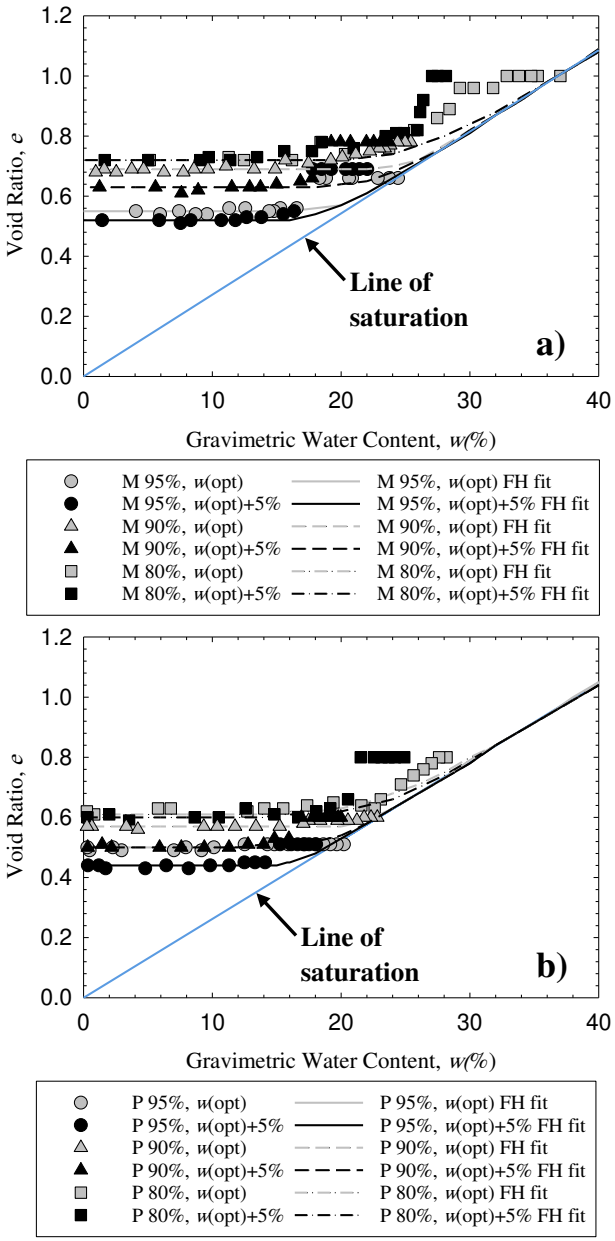

Figure 1.9 - Shrinkage curves (Fredlund and Houston 2013) for several samples from a) M tailings and b) P tailings.
(Notes: M = M tailings. P = P tailings. FH = Fredlund and Houston (2013). 95% = 95%$\gamma_{d,\ max}$. w(opt) = optimum water content which is 15.8% and 14.2% for M and P tailings, respectively).

Table 1.2 - the parameters of shrinkage curve equation proposed by (Fredlund et al. 1996, 2002, Fredlund and Houston 2013) fitted to data from shrinkage curve tests on M and P tailings.
a_{sh} = minimum void ratio. b_{sh} = slope of the line of tangency. c_{sh} = curvature of the shrinkage curve. MSE = mean squared error from fitted curves. M = M tailings. P = P tailings, *w*(opt) = optimum water content.

	95% compaction *w*(opt)		95% compaction *w*(opt)+5%		90% compaction *w*(opt)		90% compaction *w*(opt)+5%		80% compaction *w*(opt)		80% compaction *w*(opt)+5%	
	M	P	M	P	M	P	M	P	M	P	M	P
a_{sh}	0.55	0.50	0.52	0.44	0.69	0.57	0.63	0.50	0.72	0.61	0.72	0.60
b_{sh}	20.16	18.91	19.05	16.67	25.32	21.72	23.29	19.33	26.55	23.50	26.52	23.15
c_{sh}	13.04	37.97	9.836	12.96	18.08	23.22	12.68	13.18	9.726	7.756	9.617	9.548
MSE	3.6×10^{-2}	1.4×10^{-3}	9.8×10^{-2}	1.6×10^{-2}	4.1×10^{-2}	2.3×10^{-3}	1.2×10^{-1}	3.4×10^{-2}	8.0×10^{-2}	1.2×10^{-2}	1.9×10^{-1}	1.2×10^{-1}

1.3.5. Data analysis

At the termination of pressure plate tests, the final water content and dimensions were measured, and specimen masses for each of the previous steps were back calculated. Mass recordings from the pressure plate and hygrometer tests were then input into Eq. 1.1, and shrinkage parameters were optimized by minimization of the sum of squared error between measured and predicted data.

Equations describing the SWCC from van Genuchten (1980) and Fredlund and Xing (1994) were used to fit the measured SWCC data (corrected for shrinkage using previously described methods). These models were fit to experimental data by minimizing the sum of squared

error between measured and predicted data. The van Genuchten (1980) equation was used for data from M and P tailings:

$$\theta = \theta_r + (\theta_s - \theta_r)\left[\frac{1}{1 + (\alpha\psi)^n}\right]^m \quad (1.2)$$

where θ_r is the residual volumetric water content, θ_s is the saturated volumetric water content, α (inversely related to the air entry value), n (controls the slope of the SWCC) and m are fitting parameters (for the purposes of this study, $m = 1 - n^{-1}$).

To check the reproducibility of data from drying tests, replicate tests were performed on samples of M and P tailings prepared at 95% compaction and optimum water content, and the resulting SWCCs are shown in Figure 1.10. The similarity of the SWCC parameters in the modeled van Genuchten (1980) fits is apparent in Table 1.3, along with the goodness of fit (mean squared error = MSE). Data from replicates had close agreement illustrating general reproducibility of the SWCC plus shrinkage curve methods used in this study.

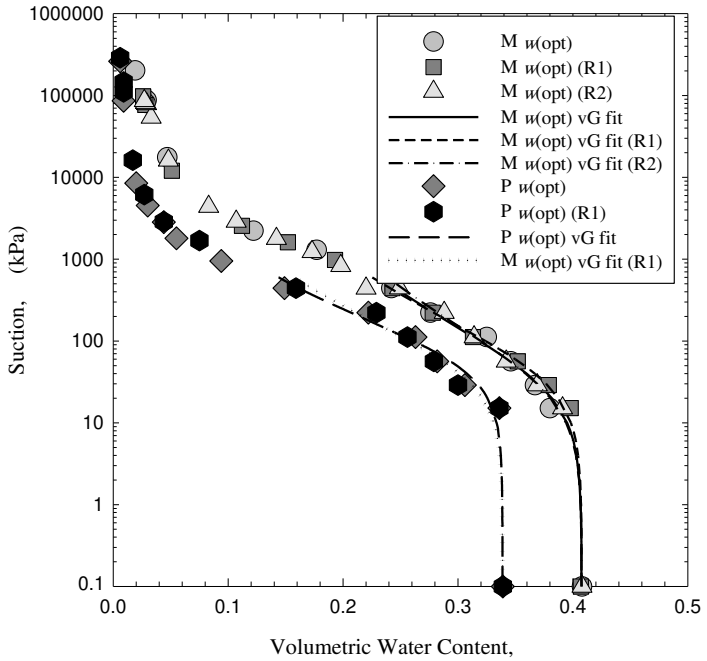

Figure 1.10 - The results from replicate tests performed on M and P tailings with the initial conditions of 95% compaction and optimum water content.
(Notes: M = M tailings. P = P tailings. FH = Fredlund and Houston (2013). 95% = 95%$\gamma_{d,\ max}$. w(opt) = optimum water content which is 15.8% and 14.2% for M and P tailings, respectively.)

Table 1.3 - van Genuchten parameters (van Genuchten 1980) from replicate drying SWCC tests on mine M and P tailings, with the consideration of the specimen shrinkage. θ_r = residual volumetric water content. θ_s = saturated volumetric water content. α, *n*, and *m* are fitting parameters ($m = 1 - n^{-1}$). R = replicate. MSE = mean squared error from fitted curves. M = M tailings. P = P tailings.
Specimens are 95% compacted with optimum water content at preparation.

Parameter	M	M-R1	M-R2	P	P-R1
θ_r	0.0192	0.0200	0.0200	0.0045	0.0062
θ_s	0.4075	0.4075	0.4075	0.3388	0.3388
α (kPa^{-1})	0.0273	0.0196	0.0303	0.0128	0.0172
n	1.2135	1.2542	1.1954	1.4211	1.3322
m	0.1759	0.2027	0.1635	0.2963	0.2494
MSE	3.6×10^{-5}	1.1×10^{-5}	1.2×10^{-5}	1.1×10^{-4}	1.2×10^{-4}

Measured SWCC data (corrected for shrinkage) were also fit using the relationship defined in Fredlund and Xing (1994) and Fredlund et al. (1994) as follows:

$$\theta = \left[1 - \frac{\ln\left(1 + \frac{\psi}{\psi_r}\right)}{\ln\left(1 + \frac{1{,}000{,}000}{\psi_r}\right)}\right] \frac{\theta_s}{\left(\ln\left(e + \left(\frac{\psi}{a}\right)^n\right)\right)^m} \tag{1.3}$$

where ψ is suction, ψ_r is the suction corresponding to the residual volumetric water content (1500 to 3000 kPa recommended by Fredlund and Zing (1994)), *e* is the Napier number (2.718), *a* is related to the air entry value, *n* is a parameter that controls the slope at the inflection point in the SWCC, and *m* is a parameter that is related to the residual water content.

1.2. RESULTS

1.4.1. Drying SWCC tests results

The results from drying SWCC tests on M tailings and P tailings are shown in Figures 1.11. Table 1.4 provides van Genuchten (1980) fitting parameters of models shown in Figure 1.11 along with the goodness of fit (MSE). The θ_r values in Table 1.4 were assigned based on the highest reading from chilled mirror tests for a fully air-dried condition.

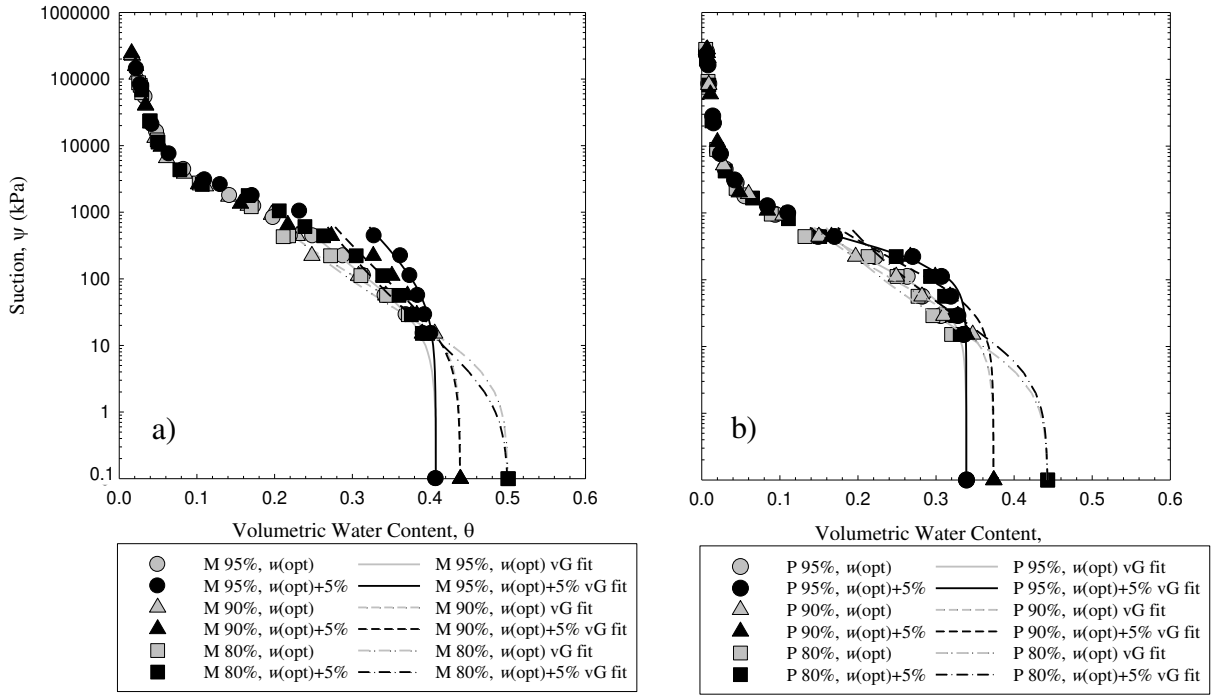

Figure 1.11 - Results from drying SWCC tests on a) M tailings and b) P tailings.
M: mine M tailings. P: mine P tailings. vG: van Genuchten. 95%: 95% compaction (95%$\gamma_{d,\,max}$). *w*(opt): optimum water content which is 15.8% and 14.2% for M and P tailings, respectively.

Table 1.4 - van Genuchten parameters (van Genuchten 1980) from drying SWCC tests on M and P tailings, with the consideration of the specimen shrinkage.
θ_r = residual volumetric water content. θ_s = saturated volumetric water content. α, *n*, and *m* are fitting parameters ($m = 1 - n^{-1}$). MSE = mean squared error from fitted curves. M = M tailings. P = P tailings, *w*(opt) = optimum water content.

	95% compaction *w*(opt)		95% compaction *w*(opt)+5%		90% compaction *w*(opt)		90% compaction *w*(opt)+5%		80% compaction *w*(opt)		80% compaction *w*(opt)+5%	
	M	P	M	P	M	P	M	P	M	P	M	P
θ_r	0.019	0.004	0.020	0.004	0.017	0.004	0.010	0.006	0.020	0.004	0.020	0.004
θ_s	0.407	0.339	0.407	0.339	0.439	0.374	0.439	0.374	0.501	0.443	0.501	0.443
α*	0.027	0.013	0.011	0.004	0.039	0.031	0.066	0.014	0.155	0.189	0.410	0.157
n	1.213	1.421	1.125	2.010	1.250	1.333	1.128	1.366	1.189	1.220	1.119	1.189
m	0.176	0.296	0.111	0.502	0.200	0.250	0.113	0.268	0.159	0.181	0.106	0.159
MSE	3.6×10^{-5}	1.1×10^{-4}	1.9×10^{-5}	5.8×10^{-5}	3.9×10^{-5}	4.1×10^{-5}	1.3×10^{-4}	4.0×10^{-4}	1.2×10^{-4}	4×10^{-4}	1.0×10^{-4}	7.5×10^{-4}

* in 1/kPa.

As expected, different placement conditions (viz. different initial gravimetric water content and dry density) of filtered tailings did not produce the same SWCC for either tailings tested. Experimental data from both M and P tailings consistently followed the same trend. Looser specimens contained more water at saturation ($\theta_{80\%} > \theta_{90\%} > \theta_{95\%}$) due to higher void ratio. When suction was applied, denser specimens tended to release less moisture. For example, an 80% compacted specimen released more water under 14 kPa suction than a specimen with 90% or 95% compaction. As suction increased, denser specimens maintained more moisture until suction surpassed 1000 kPa ($\theta_{95\%} > \theta_{90\%} > \theta_{80\%}$). If two specimens from the same tailings had similar dry

density, the specimen with higher initial water content (before being immersed) released less moisture under similar increases in suction comparing to specimens of the same tailings compacted at lower water content. At 1000 kPa, however, water content data from tailings with any initial dry density or gravimetric water content overlapped. M tailings maintained more moisture even under high suction (≥1000 kPa) comparing to P tailings consistent with the higher clay-size content and Atterberg limits of M tailings.

Fitted van Genuchten models in Figure 1.11 are extended to no more than 600 kPa as the model (Equation 1.2) could not fit a curve to all the SWCC data from a tailings specimen; this limitation of the van Genuchten model to fit the filtered tailings tested in this study is discussed further in the Discussion section of this chapter.

1.4.2. Wetting SWCC tests results

The results of wetting SWCC tests on M and P tailings are shown in Figures 1.12. Table 1.5 provides van Genuchten (1980) fitting parameters of models shown in Figures 1.12 along with the goodness of fit (MSE). As noted in the preceding section, the van Genuchten (1980) models were only fit to suctions below 600 kPa.

For M tailings, looser specimens placed wet of optimum water content adsorbed less moisture under matric suctions of 443 to 15 kPa than denser specimens with the same as-compacted water content. However, the trend in water adsorption was the opposite when tailings were compacted at optimum water content. For matric suctions below 15 kPa, however, denser specimens tended to imbibe less moisture. None of the wetting tests on M tailings reached saturation at termination. Complete saturation was not possible without returning the specimen to a suction less than 1.3 kPa. For tests on P tailings, however, denser specimens wet of optimum water content imbibed more moisture throughout the wetting tests (matric suctions 443 to 0 kPa)

than looser specimens with the same as-compacted water content. Four tests on P tailings with 95 and 90% compaction and optimum and wet of optimum water content resulted in fully saturated specimens at the termination.

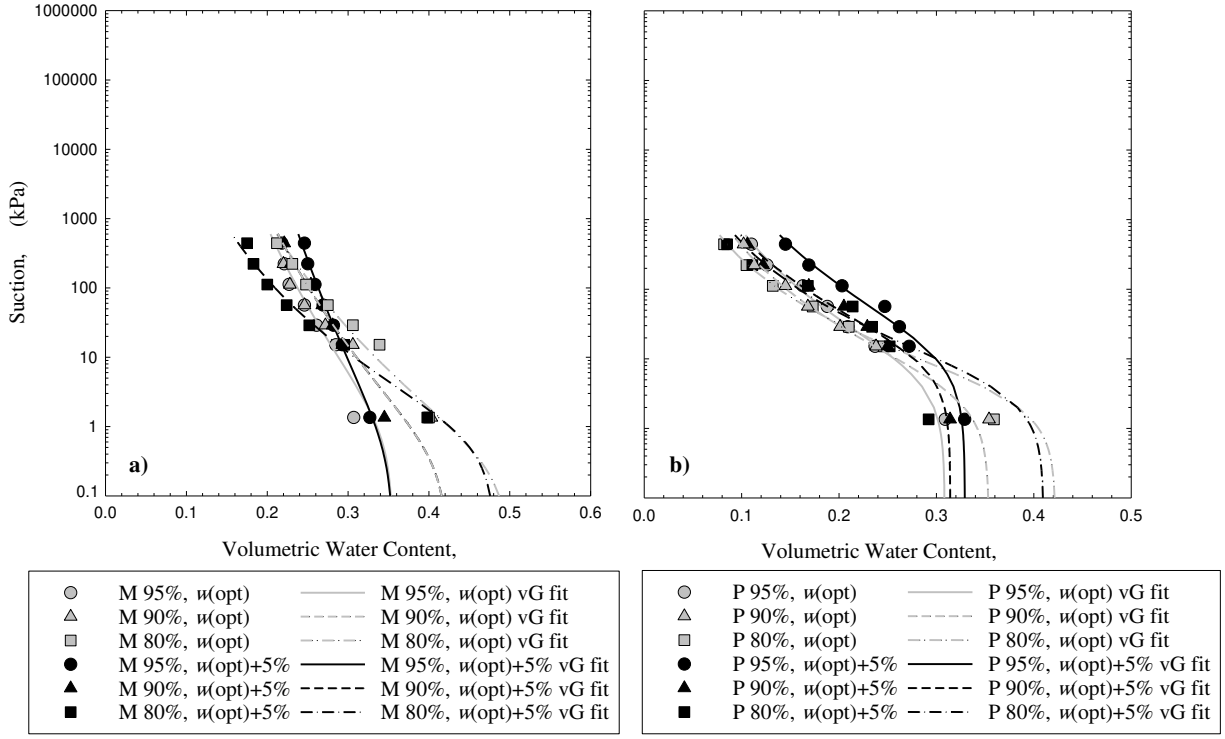

Figure 1.12 - Results from wetting SWCC tests on (a) M tailings and (b) P tailings.
Models are generated using the method described by van Genuchten (1980). M: M tailings. P: P tailings. vG: van Genuchten. 95%: 95% compaction (95%$\gamma_{d,\,max}$). *w*(opt): optimum water content which is 15.8% and 14.2% for M and P tailings, respectively.

Table 1.5 - van Genuchten parameters (van Genuchten 1980) from wetting SWCC tests on M and P tailings, with the consideration of the specimen shrinkage.
θ_r = residual volumetric water content. θ_s = saturated volumetric water content. α, *n*, and *m* are fitting parameters ($m = 1 - n^{-1}$). MSE = mean squared error from fitted curves. M = M tailings. P = P tailings, *w*(opt) = optimum water content.

	95% compaction *w*(opt)		95% compaction *w*(opt)+5%		90% compaction *w*(opt)		90% compaction *w*(opt)+5%		80% compaction *w*(opt)		80% compaction *w*(opt)+5%	
	M	P	M	P	M	P	M	P	M	P	M	P
θ_r	0.019	0.004	0.020	0.004	0.016	0.004	0.010	0.006	0.012	0.004	0.020	0.004
θ_s	0.355	0.308	0.355	0.329	0.429	0.354	0.423	0.314	0.500	0.422	0.481	0.410
α*	1.015	0.141	2.106	0.072	0.919	0.252	2.680	0.078	3.428	0.280	1.239	0.215
n	1.093	1.251	1.060	1.234	1.141	1.278	1.096	1.312	1.117	1.341	1.185	1.313
m	0.0852	0.201	0.057	0.190	0.123	0.218	0.088	0.238	0.105	0.254	0.156	0.238
MSE	3.0×10^{-5}	2.4×10^{-5}	6.5×10^{-6}	6.7×10^{-5}	3.1×10^{-2}	7.7×10^{-6}	2.2×10^{-5}	5.6×10^{-5}	1.1×10^{-4}	1.5×10^{-5}	4.7×10^{-5}	2.5×10^{-4}

* in 1/kPa.

1.3. DISCUSSION

1.5.1. Comparison of van Genuchten (1980) and Fredlund and Xing (1994) SWCCs

van Genuchten (1980) model is often used for quantifying moisture distribution in unsaturated soils and is supported by commercially available software for unsaturated flow such as HYDRUS 1/2/3D and FLAC3D. The main focus of this chapter and following chapters, which use results from this chapter, is the van Genuchten (1980) equation. However, as explained earlier in the Results section, the van Genuchten (1980) equation could not fit the unsaturated data of the

tailings tested in this study satisfyingly across the full range of suctions measured (Fig. 1.11) – although the van Genuchten (1980) equation is able to provide a satisfactory fit when constrained to suctions less than 600 kPa, the range of relevance in the following chapters, and a range over which the van Genucthten (1980) model provided a visually representative fit to the data. However, I also explored if the Fredlund and Xing (1994) model, supported in the 2/3D SoilVision Suite, provided a better fit across the full range of data. If the Fredlund and Xing (1994) model provided a substantially better fit, this could guide future unsaturated research on filtered tailings.

An exemplar comparison of the Fredlund and Xing (1994) model and van Genucthen (1980) model fits is provided in Figure 1.13. Both equations are only fit to data from drying tests on M and P tailings with initial 95% compaction and optimum water content prior to being immersed. The Fredlund and Xing (1994) method provides a lower MSE than the van Genuchten (1980) model when fit to the full range of SWCC data.

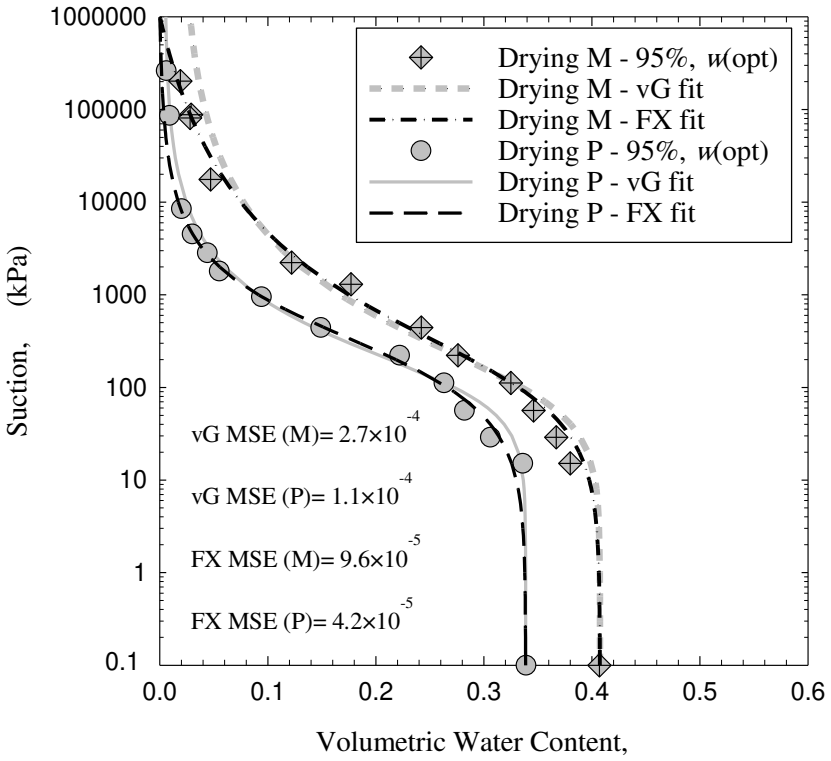

Figure 1.13 - The comparison of results from models fitted to all drying SWCC test data.
MSE = mean squared error from fitted curves. M = M tailings. P = P tailings. vG: vanGenuchten (1980). FX: Fredlund & and Xing (1994). 95%: 95% compaction (95%$\gamma_{d,\,max}$). *w*(opt): optimum water content which is 15.8% and 14.2% for M and P tailings, respectively.

Fitted drying SWCCs using the Fredlund and Xing (1994) model (Equation 1.3) are shown in Figure 1.14 and the resulting fitted parameters are provided in Table 1.6; the data shown in Figure 1.14 correspond to those fit with the van Genuchten (1980) model in Figures 1.11 and 1.12. As seen in Figure 1.14, data fitted with either the Fredlund and Xing (1994) [or the van Genuchten (1980) models as shown in Figures 1.11 and 1.12] did not capture well the full range of experimental data from tests on specimens with initial compaction at 80 and 90%. These results illustrate that neither the van Genucthten (1980) nor the Fredlund and Xing (1994) models provided a complete representation of the unsaturated characteristics of the filtered tailings tested in this study.

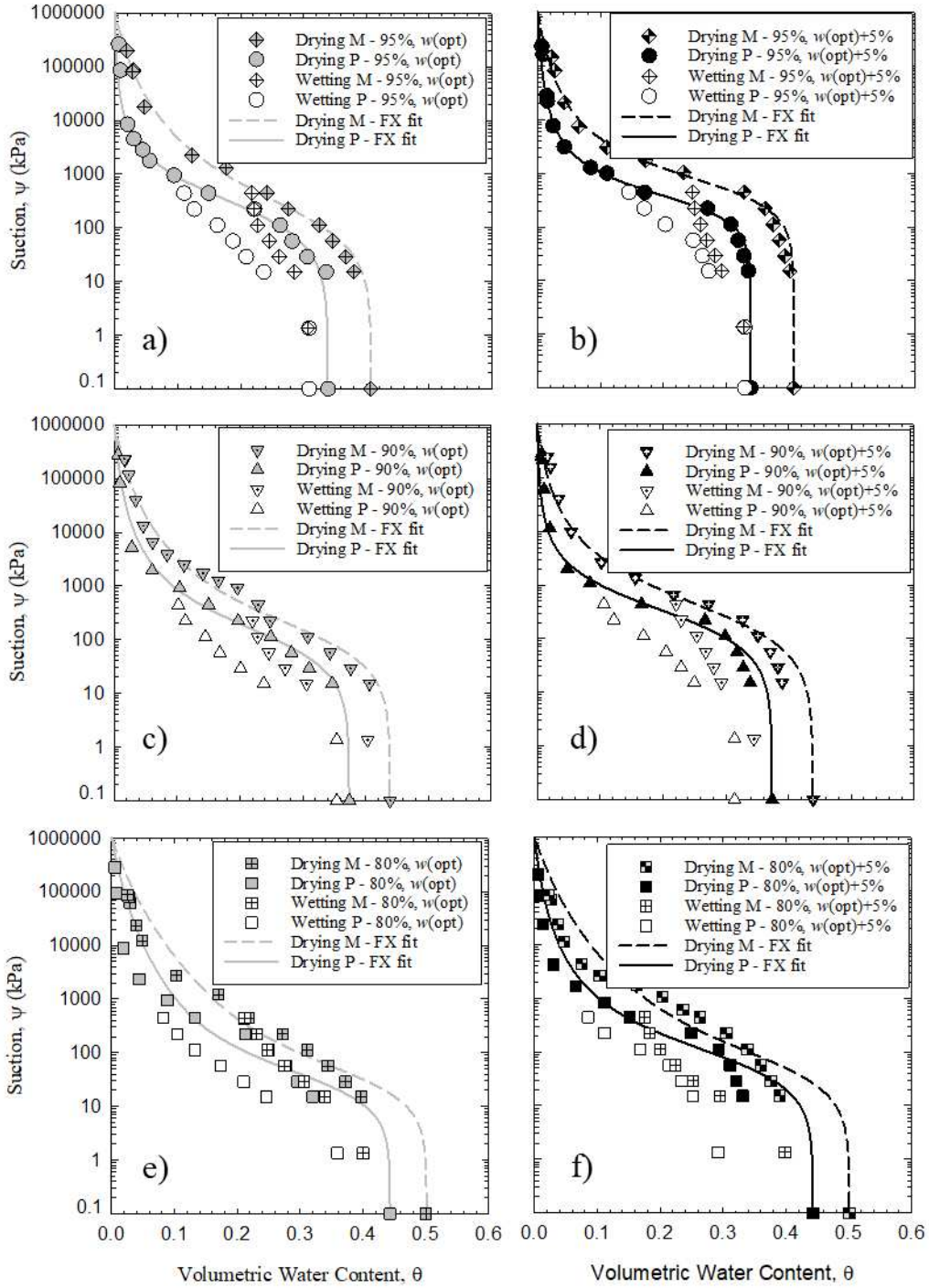

Figure 1.14 - The comparison of the drying and wetting SWCC test results performed on M and P tailings (24 tests in total).

Models are generated using the method described by Fredlund & Xing (1994). M: M tailings. P: P tailings. FX: Fredlund & Xing (1994). 95%: 95% compaction (95%$\gamma_{d,\ max}$). *w*(opt): optimum water content which is 15.8% and 14.2% for M and P tailings, respectively.

Table 1.6 - Fredlund-Xing parameters (Fredlund & Xing 1994) from drying SWCC tests on M and P tailings, with the consideration of the specimen shrinkage.
ψ_r = suction (1500 ~ 3000 kPa) corresponding to the residual water content (θ_r). θ_s = saturated volumetric water content. a, *n*, and *m* are fitting parameters. MSE = mean squared error from fitted curves. M = M tailings. P = P tailings, *w*(opt) = optimum water content.

	95% compaction *w*(opt)		95% compaction *w*(opt)+5%		90% compaction *w*(opt)		90% compaction *w*(opt)+5%		80% compaction *w*(opt)		80% compaction *w*(opt)+5%	
	M	P	M	P	M	P	M	P	M	P	M	P
ψ_r*	2977	1500	1500	1500	3000	1500	1500	1500	1500	1500	1500	1500
θ_s	0.407	0.339	0.407	0.339	0.439	0.374	0.439	0.374	0.501	0.443	0.501	0.443
a*	142	280	500	288	99.7	92.1	243	299	26.1	23.1	44.0	62.9
n	1.004	1.012	1.526	1.704	1.073	1.099	0.981	1.069	1.290	1.338	1.191	1.176
m	0.959	2.000	0.950	1.286	1.000	1.268	0.999	2.000	0.674	0.854	0.762	1.160
MSE	9.6×10^{-5}	4.2×10^{-5}	1.0×10^{-4}	3.71×10^{-5}	2.9×10^{-4}	1.1×10^{-4}	3.4×10^{-4}	1.9×10^{-4}	6.67×10^{-4}	1.1×10^{-3}	1.39×10^{-3}	1.2×10^{-3}

* in kPa.

1.5.2. Comparison of tests results and generated SWCCs

Wetting and drying data and drying SWCCs fit using the van Genuchten (1980) model are compared for a given placement condition in Figure 1.15. Figure 1.15 illustrates that the SWCC of filtered tailings is dependent on the placement condition (water content and compaction), viz., the initial gravimetric water content and dry density of the tailings appreciably influence the SWCCs. In drying tests, loose specimens with an initial 80% degree of compaction contained

higher volumes of water at saturation via larger pores comparing to denser specimens with initial 90 or 95% compaction.

When a suction of 14 kPa was applied the AEV of both filtered tailings was exceeded, and the largest pores were drained (Figs 1.11 and 1.15). A pronounced desaturation of both tailings started at approximately the plastic limit of each tailings (20.9 for M tailings and 19.6 for P tailings). These data show a pronounced desaturation independent of the initial condition (placement condition) of filtered tailings; however, the volume of moisture released appears to be controlled by the initial gravimetric water content and dry density of the filtered tailings.

As expected, denser specimens (90% and 95% compacted initially) retained more water due to the higher matric suction of smaller pores. As shown in Figure 1.16, this behavior appears between degrees of saturation between 90 to 40%, known as the two-phase zone or the transition zone (Fredlund et al. 2012). For suctions above 1000 kPa, water contents (w or θ) yield an almost identical curve (Figure 1.11). In other words, at suctions above 1000 kPa, filtered tailings have the same water retention characteristics independent of the placement condition.

Wetting test results (Figs 1.15 and 1.16) illustrate hysteresis with all initial conditions (ρ_d and w). All wetting tests specimens did not reach the same point of saturation observed in the corresponding drying tests when returned to atmospheric conditions (zero suction). Shrinkage varied based on initial placement conditions. M tailings, due to higher clay-size content and Atterberg limits, experienced more shrinkage, up to 9% for dense specimens and up to 16% in loose specimens. P tailings, experienced shrinkage up to 6% for dense specimens and up to 12% in loose specimens. This behavior illustrates that atmospheric drying may be an effective way to decrease the void ratio of filtered tailings after placement independent of initial compaction.

Hysteresis predominately occurred between suctions of 10 to 110 kPa (Fig. 1.15a to 1.15f). Pham et al. (2002, 2003a,b) used the difference between the hysteresis loops at the inflection points as the primary indicator of the magnitude of hysteresis. In this study, a wetting test started when the specimen was at equilibrium under 443 kPa matric suction. Once the matric suction was decreased to 222 kPa by reducing the applied positive air pressure, smaller pores at the boundary and in contact with the saturated HAE disk absorbed water. The imbibition continued until the wetting front reached large pores with entrapped air bubbles. Denser tailings adsorbed more water due to the existence of a higher number of smaller pores. In contrast, loose tailings (80% compaction) reached equilibrium faster due to the existence of more large pores. As suction was reduced sequentially more air bubbles were contained within the more loosely placed tailings with more larger pores.

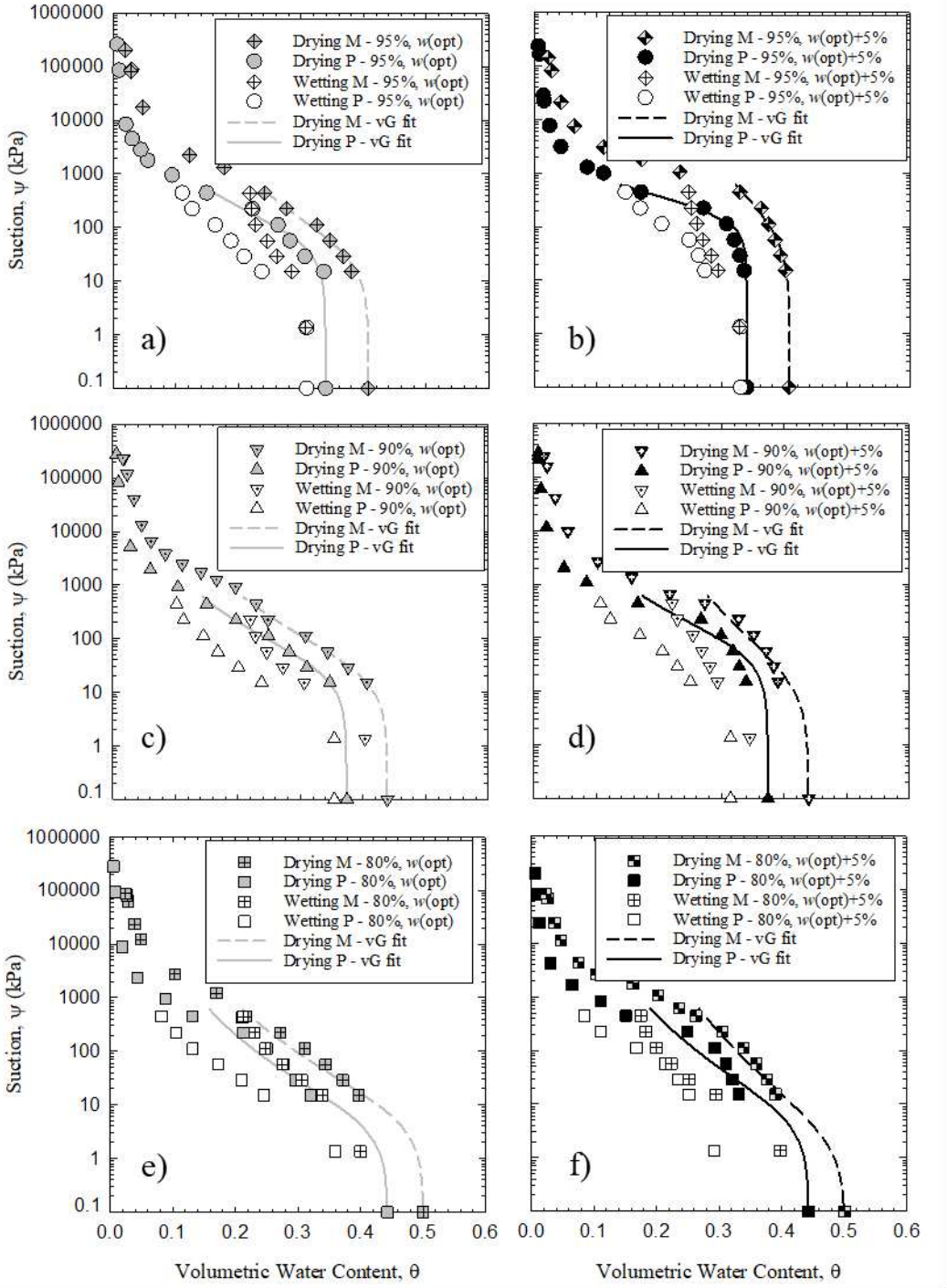

Figure 1.15 - The comparison of the drying and wetting SWCC test results performed on M and P tailings (24 tests in total).
M: M tailings. P: P tailings. vG: van Genuchten. 95%: 95% compaction (95%$\gamma_{d,\,max}$). *w*(opt): optimum water content which is 15.8% and 14.2% for M and P tailings, respectively.

Volumatic water content SWCCs corrected for shrinkage, are translated to degrees of saturation as a function of suction in Figure 1.16. Oxygen flow stops when saturation is at a range of 80% to 90% (Bussière et al. 2003); prevention of oxygen ingress is one of three methods to minimizing ARD in filtered tailings (the others being preventing, or minimizing percolation from the filtered tailings, and the final being removing reactive mineral phases prior to placement or providing/having sufficient buffering capacity in situ). Specimens with higher initial gravimetric water content from both tailings maintained higher degrees of saturation under high suctions. For example, M tailings with initial water content of +5% wet of optimum (Fig. 1.16b) was 80% saturated under 443 kPa suction, whereas M tailings with the same initial dry density but with optimum water content (Fig. 1.16a) was 59% saturated under 443 kPa. This observation illustrates the importance of understanding the tailings fabric that develops at different initial compaction conditions, particularly when keeping the stack near saturation is necessary to minimize oxygen flow and minimize ARD.

Figure 1.16 also illustrates that as the filtered tailings are more compacted initially, higher suctions are required to drain the tailings to degrees of saturation less than 80%. Again, due to the higher clay-size content of M tailings, M tailings maintained near saturated conditions (more than 80% saturation degree) under higher suctions (up to 443 kPa) in comparison to P tailings (Fig. 1.16). Thus, although tailings with a higher clay content are likely to be more difficult to filter, these tailings will be relatively more effective in maintaining conditions of saturation greater than 80%.

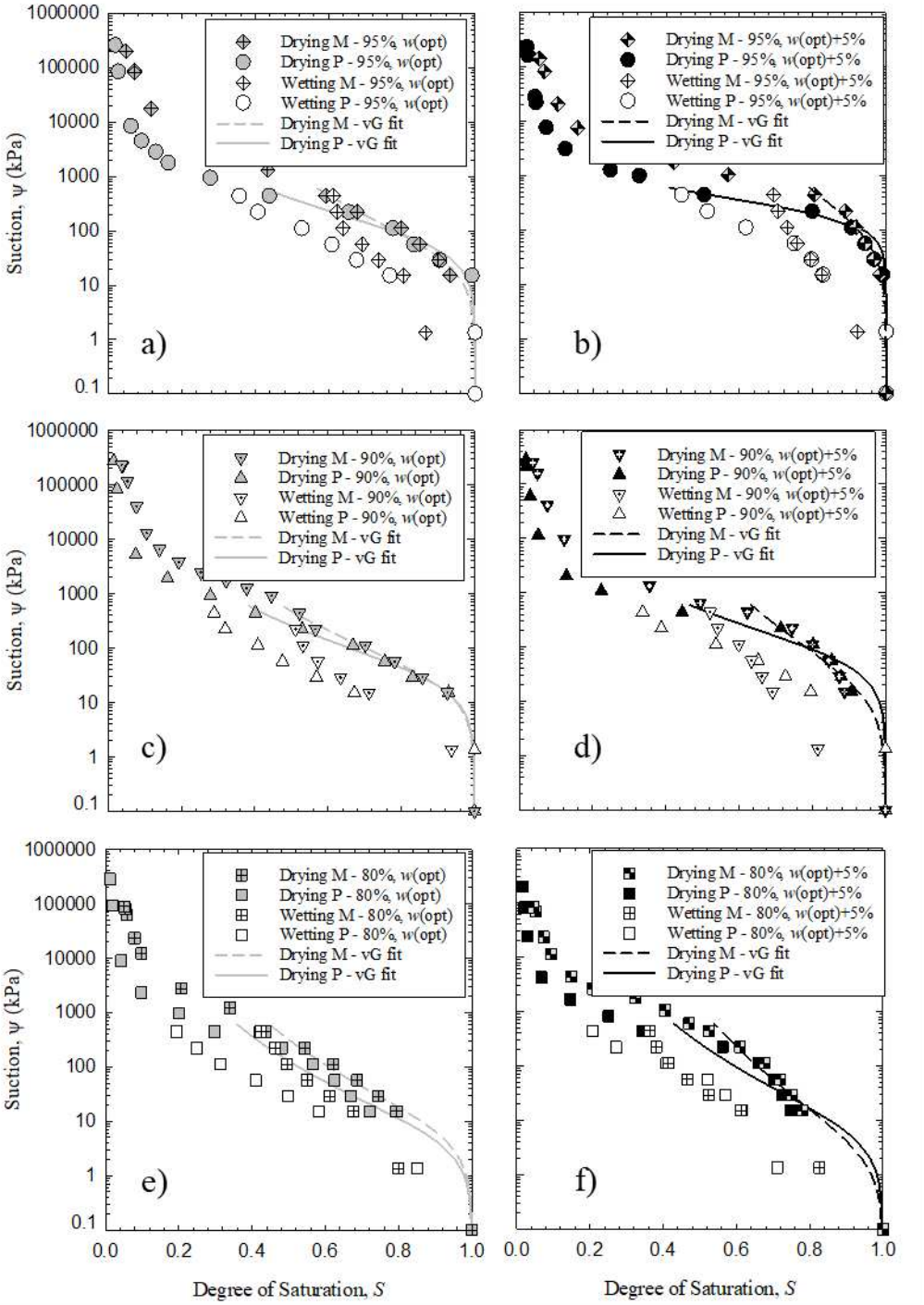

Figure 1.16 - Graphs of S as a function of ψ from the drying and wetting SWCC tests performed on M and P tailings (24 tests in total).

Models are generated using the method described by van Genuchten (1980). M: M tailings. P: P tailings. vG: van Genuchten. 95%: 95% compaction (95%$\gamma_{d,\,max}$). w(opt): optimum water content which is 15.8% and 14.2% for M and P tailings, respectively.

1.5.3. Fitting parameters evaluation

van Genuchten (1980) parameters from drying tests on M and P tailings are compared based on the initial dry densities of the specimens in Figure 1.17. van Genuchten (1980) parameters from replicate drying tests on M and P tailings are included in Figure 1.17. For tests on specimens with the same initial gravimetric water content, the α decreased with increasing initial dry density (Fig. 1.17a). A decrease in α corresponds to an increase in AEV. Regarding the effect of initial gravimetric water content on α, filtered tailings showed similar values of α when two samples with the same as-placed dry density but different initial gravimetric water contents are compared except for the test on M tailings with initial 80% compaction and +5% wet of optimum water content. For tests on specimens with the same initial water content, the parameter *n* increased with increasing dry density (Fig. 1.17b). Higher *n* values indicate faster drainage of water from filtered tailings with increased suction whilst lower *n* values (the lower bound of *n* is 1) indicate filtered tailings can maintain moisture at higher suctions without drainage. The rise in *n* values was more apparent in +5% wet of optimum tests on P tailings. When comparing filtered tailings with the same initial dry density but different initial water content, the parameters *n* did not show an identical trend. In general, M tailings, if placed wet of optimum, tended to have lower *n* values. Of note, parameter *m* follows the same trends as those of parameter *n* due to the fixed calculation method of parameter *m*. More tests on a variety of tailings are required to confirm the observed patterns.

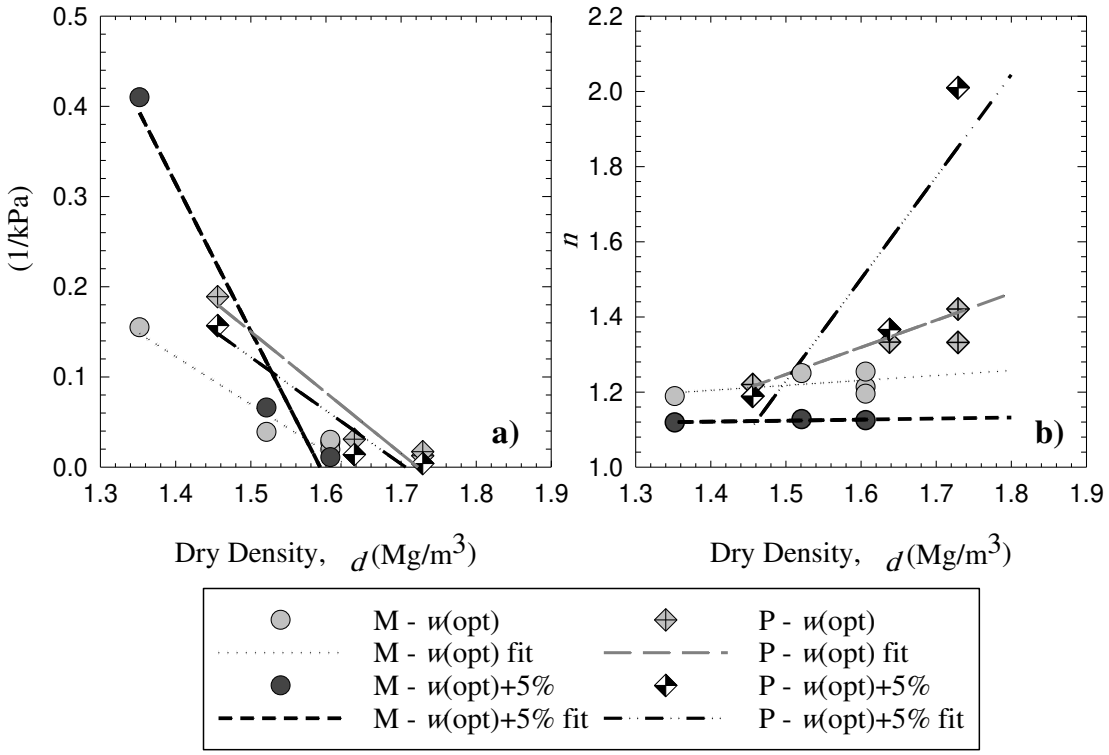

Figure 1.17 - Evaluation of the changes of van Genuchten (1980) fitting parameters with regards to changes in ρ_d, for drying SWCC tests performed at optimum water content and +5% wet of optimum. M: M tailings. P: P tailings. *w*(opt): optimum water content which is 15.8% and 14.2% for M and P tailings, respectively.

van Genuchten (1980) parameters from wetting tests on M and P tailings are compared based on the initial dry density of the specimens in Figure 1.18. Unlike drying tests, there is not a coherent pattern across the results. The parameter α followed the same pattern described for Figure 1.17 for dry tests except for the tests performed on M tailings with +5% wet of optimum water content. The parameter α increased with increasing initial dry density of the specimens for the tests performed on M tailings with +5% wet of optimum water content (Fig 1.18a). Parameter *n* decreased with increasing initial dry density (Figs 1.18b and 1.18c), which could be interpreted as dense filtered tailings adsorbing and maintaining more moisture under high suctions comparing to loosely placed filtered tailings. More tests on a variety of tailings are required to confirm the observed patterns.

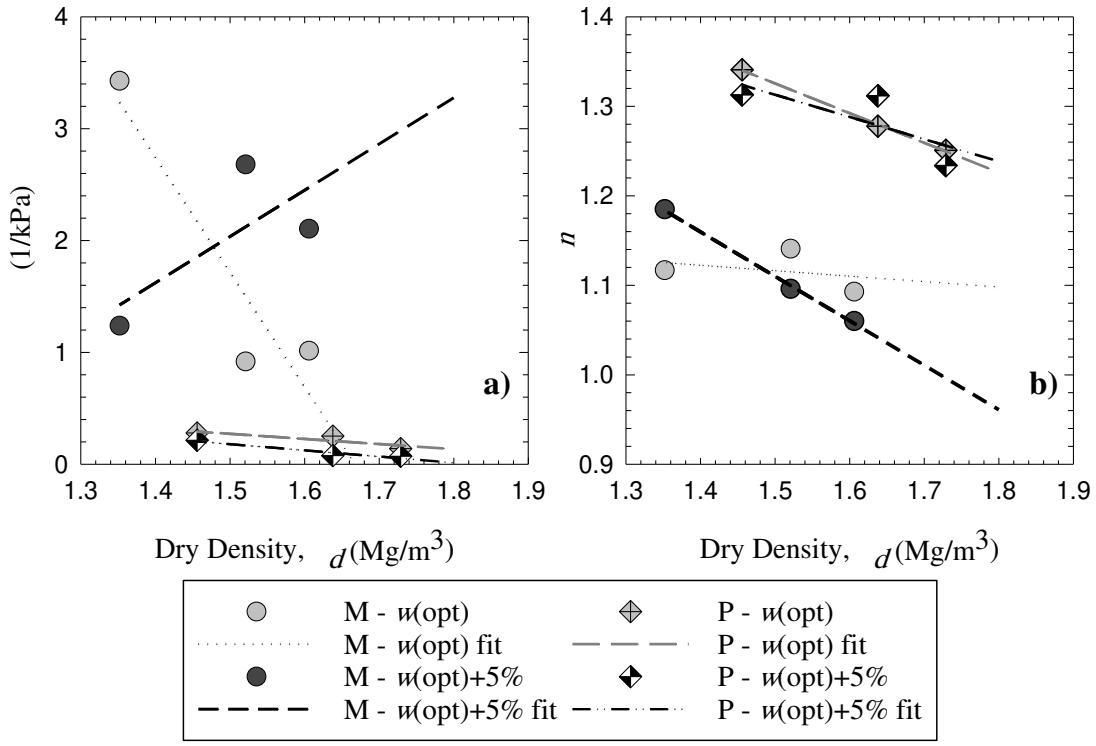

Figure 1.18 - Evaluation of the changes of van Genuchten (1980) fitting parameters with regards to changes in ρ_d, for wetting SWCC tests performed at optimum water content and +5% wet of optimum. M: M tailings. P: P tailings. *w*(opt): optimum water content which is 15.8% and 14.2% for M and P tailings, respectively.

Fredlund and Xing (1994) parameters from drying tests on M and P tailings are compared based in initial dry density in Figure 1.19. The parameter *a* increased when tailings were placed with higher dry density (Fig. 1.19a), meaning denser filtered tailings had higher AEVs, as expected. Moreover, filtered tailings placed wet of optimum water content had higher *a* values than those with the same initial dry density but with initial optimum water content. The trend for parameter *n* was not unique; in general, when the initial dry density increased, *n* seemed to be increasing for tests performed on specimens wet of optimum but decreased for tests performed on specimens prepared at optimum water content (Fig. 1.19b). Lower *n* values indicated filtered tailings could maintain moisture at higher suctions without drainage. The parameter *m* increased when the initial dry density increased (Fig. 1.19c). Higher *m* values can be interpreted that mean

filtered tailings will maintain more moisture under dryer conditions (all else being equal). More tests on a variety of tailings are required to confirm the trends observed Figures 1.17 to 1.19. In this study, wetting SWCCs are not generated using the Fredlund and Xing (1994) method (as the main focus is on the van Genuchten (1980) method) and thus no comparison is provided for the representing parameters. More tests on a variety of tailings are required to confirm the observed patterns.

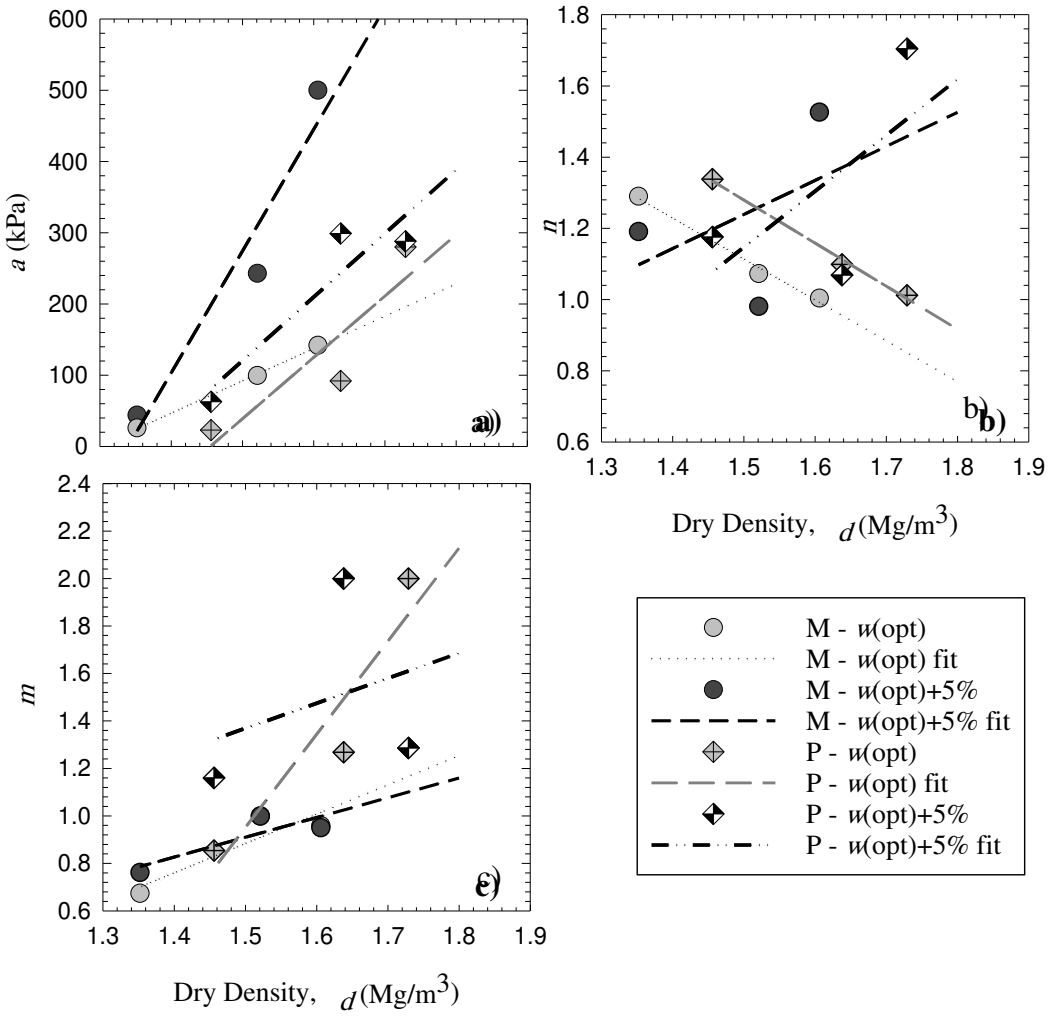

Figure 1.19 - Evaluation of the changes of Fredlund & Xing (1994) fitting parameters with regards to changes in ρ_d, for drying SWCC tests performed at optimum water content and +5% wet of optimum. M: M tailings. P: P tailings. *w*(opt): optimum water content which is 15.8% and 14.2% for M and P tailings, respectively.

Finally, shrinkage curve parameters (Fredlund et al. 1996, 2002; Fredlund and Houston 2013) are compared in Figure 1.20 based on the initial ρ_d of tailings. Parameters a_{sh} and b_{sh} decrease when the initial ρ_d increases (Figs. 1.20a and 1.20b), viz., filtered tailings if initially placed dense, will end up in lower void ratios at residual water contents but do not necessarily undergo higher levels of shrinkage. The parameter c_{sh}, however, increases with increasing ρ_d (Fig. 1.20c). Higher c_{sh} values indicate greater shrinkage potential. More tests on a variety of tailings are required to confirm the observed patterns.

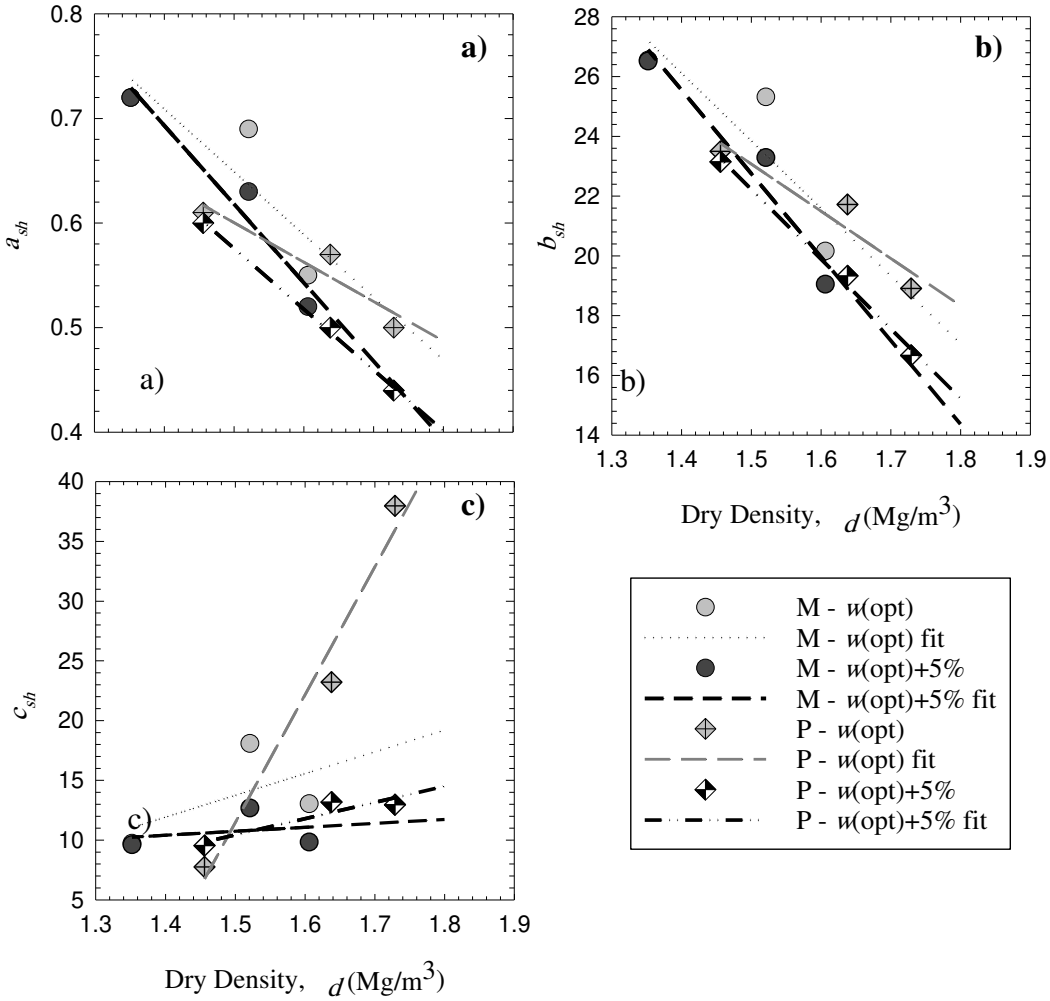

Figure 1.20 - Evaluation of the changes of fitting parameters of shrinkage curves (Fredlund & Houston 2013) with regards to changes in ρ_d, for tests performed at optimum water content and +5% wet of optimum.
M: M tailings. P: P tailings. *w*(opt): optimum water content which is 15.8% and 14.2% for M and P tailings, respectively.

1.4. SUMMARY AND CONCLUSION

Drying and wetting SWCCs were generated by performing a series of tests on two different filtered tailings from precious metal mines. The initial dry densities of the specimens were 80%, 90%, and 95% of the maximum dry density of the tailings, and the initial water content were optimum and +5% wet of the optimum. The results and interpretations provided in this study can provide a basis of understanding for the distribution of water in filtered tailings stacks designed with varying placement conditions. Conclusions from this study are provided subsequently.

- Unsaturated behavior of filtered tailings studied in this research are strongly influenced by the placement condition (initial w and ρ_d) of filtered tailings. According to the results from this study, the SWCCs of filtered tailings can be expected to evolve as a filtered tailings stack is built and tailings are compressed.
- The SWCC fitting parameters from Fredlund and Xing (1994) and van Genuchten (1980) models illustrated expected trends when the same filtered tailings with various initial water content and dry density were compared. In general, highly compacted ($\geq$ 90% $\rho_{d,max}$) filtered tailings maintain more moisture and higher degrees of saturation under suctions ranging from 15 to 600 kPa, when compared to loosely placed (80% $\rho_{d,max}$) filtered tailings. Similarly, filtered tailings compacted wet of optimum maintained more water under suctions ranging from 15 to 600 kPa compared with filtered tailings compacted at optimum water content.
- The van Genuchten (1980) model provided poor fits at suctions higher than ~600 kPa for drying tests. In addition, both van Genuchten (1980) and Fredlund and Xing (1994) SWCCs poorly represented experimental data from tests on filtered tailings with initial compactions of 80 and 90%.

- A distinct desaturation of both tailings tested in this study started at the plastic limit of each tailings. The plastic limit of these tailings (i.e., 20.9 for M tailings and 19.6 for P tailings) were approximately representatives of the suctions equal to air entry values of the tailings for each test.
- Findings from this study illustrate the effects of placement conditions on the unsaturated characteristics of filtered tailings and the pore fluid flow within filtered tailings stacks. To make predictive models, consideration of as-placed water content of filtered tailings and the levels of compression/consolidation as a tailings stack is built and compression occurs is critical. Unsaturated model parameter trend data, coupled with compression data, could be used for this purpose.

Chapter 2. Generation of positive excess pore water pressure in unsaturated filtered tailings during undrained compression

2.1. INTRODUCTION

Mining and beneficiation of minerals generate large quantities of mineral byproducts, principally in the form of tailings and waste rock. Conventional tailings facilities use slurry deposition of tailings with solid contents ranging from 15 to 60% (Davies 2018, ICOLD 2018), resulting in loose fabrics after placement, and low strength that has resulted in recent flow-type failures (Mt. Polley mine in 2014, Samarco Mariana mine in 2015, and Córrego do Feijão mine in 2019; Morgenstern et al. 2015, Petticrew et al. 2015, Morgenstern et al. 2016; Fonseca do Carmo et al. 2017, Robertson et al. 2019). Slurry deposition of tailings also creates long times for consolidation necessitating long-term management of inherently weak materials.

To potentially eliminate flow-type failures from the time of placement, tailings must be sufficiently dewatered prior to placement such that the resultant tailings are sufficiently dense to stay below the critical state line as they are subsequently compressed. Filtration is an increasingly used method of separating solid phase from liquid (at smaller scale facilities; Wang et al. 2014), and the resulting filtered tailings are unsaturated material with high solids content (> 85%) that are managed like an earth fill (Lupo and Hall 2010). Filtered tailings are placed via dumping or conveyor to form a tailings stack. Filtered tailings are envisioned as potential solutions to the possible geotechnical instability of slurry-deposited tailings but are not a perfect solution.

Two major shortcomings of filtered tailings are cost and potential for geochemical instability (e.g., acid rock drainage) if not correctly implemented. In addition, tailings filtration at a large scale has historically not been technically or economically practical. However, this is

shifting with increasing technological advancements by filter manufacturers and industry pressures to prevent potential geotechnical failures. To minimize costs and maximize throughput, a maximally viable filtered tailings pile will be placed as wet as possible to minimize dewatering, and not compacted. However, the generation of positive excess pore water pressure in unsaturated filtered tailings can potentially prevent sufficiently dense placement and the achievement of geotechnical performance. Further investigation is required to enable the optimized construction of filtered tailings stacks; this is the topic of this study.

The unsaturated nature of filtered tailings makes analysis more complicated than saturated or dry analyses used conventionally for tailings systems. Air-water mixtures in the soil are compressible, and the magnitude of pore air and pore water pressure generation during undrained loading are a function of the compressibility of the air-water mixture as well as the compressibility of the soil structure (Fredlund et al. 2012). The soil-water system in an unsaturated soil is no longer an equivalent continuum medium (Lu and Likos 2006). In an unsaturated soil, describing the state of stress from a macroscopic or boundary-level perspective is challenging because pore pressure is no longer a neutral stress and splits into several microscopic interparticle forces acting within the vicinity of the grain contacts (Lu and Likos 2006). Mixing across scales is not consistent with continuum mechanics (Burland 1965, Fredlund and Morgenstern 1977, Zhang and Lu 2020). Lu and Likos (2006), Lu et al. (2010), and Zhang and Lu (2020) introduced and refined the term "suction stress" or "suction stress characteristic curve, SSCC" to define a macroscopic effective stress in unsaturated soils, σ':

$$\sigma' = \sigma - u_a - \sigma^s \tag{2.1}$$

where σ is total stress, u_a is gauge air pressure, and σ^s is suction stress (negative). Suction stress is a macroscopic stress, which accounts for van der Waals forces, electrical double-layer forces,

cementation forces, surface tension (capillary) forces, and forces arising from negative pore water pressure in an unsaturated soil (Lu and Likos 2006). Suction stress is used as a way of extending Bishop's (1959) effective stress and generalizing Terzaghi's (1936) effective stress under both saturated and unsaturated conditions (Zhang and Lu 2020). As shown in Equation 2.1, σ^s acts to increase σ' in unsaturated soils, i.e., since $\sigma^s < 0$.

Aghazamani et al. (2021) showed unsaturated filtered tailings, when incrementally loaded, generated positive excess pore pressure under some conditions. Subtracting excess pore pressure (u_e) from the right of Equation 2.1 results in Equation 2.2:

$$\sigma' = \sigma - u_a - \sigma^s - u_e \tag{2.2}$$

In cases of undrained 1D loading (or K_0-loading, where K_0 is the coefficient of at-rest earth pressure) and using Equation 2.2, σ' can be estimated for filtered tailings during stack construction. Via knowledge of σ' of filtered tailings placed under specific conditions (density, water content), the dilative or contractive behavior of tailings under loading can be assessed.

The generated excess pore pressure in Equation 2.2 must be at a macroscopic scale consistent with the other terms in the equation. When the volume of voids in filtered tailings under K_0-loading reduces, there should be an increase in the pore air pressure according to Boyle's law. However, pressure transducers are designed to measure macroscopic changes in pore pressure (air and/or water). If changes in pore air pressure are microscopic, such as when the air phase is discontinues near saturation, the pressure transducer will not capture increased pore air pressures. The configuration of test setups used for compression tests also impacts the induced pressure readings (Dunn 1965, Matyas and Radhakrishna 1968, Barden et al. 1969, Compton 1970, Fredlund 1973). Fredlund and Morgenstern (1977) and Fredlund (2000) used a modified Antaeus

odometer for their K_0-loading tests and applied axis translation technique (Lu and Likos 2004, Fredlund et al. 2012) to preset matric suction. In the study by Aghazamani et al. (2021) and this research, the suction was not controlled, when performing K_0-loading tests and only one pore pressure transducer was attached to the bottom of the specimen in the apparatus. In both setups from Fredlund and Morgenstern (1977) and this study, air and water are separated via a high air entry (HAE) disk; however, dissolved air eventually diffuses through the water in the disk. In the K_0-loading tests performed by Fredlund and Morgenstern (1977) air could also diffuse from the chamber, when the specimen was being back pressured in saturated tests or when the air was regulated in unsaturated tests. Thus, the volume of diffused air could be higher than those of tests performed by Aghazamani et al. (2021) or of this study.

Results from Aghazamani et al. (2021) and this study show that the pressure transducer does not read the generation of u_e until a certain degree of saturation is reached. Critically, generation of u_e after a certain degree of saturation can become a hinderance in further stacking of filtered tailings preventing tailings densification. This observation also implies that changes in excess pore water pressure are in macroscopic level and can be considered as u_e.

In this study, instead of controlling suction, experimental data from drying and wetting soil water characteristic curve (SWCC) provided in Chapter 1 are used to estimate σ^s and therefore to estimate σ' of a soil/tailings with a given as-placed condition. Suction affects both σ' and the pre-consolidation stress (i.e., yield stress) in unsaturated soils (Khalili and Khabbaz 1996). The shift in the pre-consolidation stress or softening/hardening of soil skeleton with suction may cause widely different volumetric changes in initially identical soil samples (Khalili and Khabbaz 1996). Experimental evidence indicates the angle of internal friction (φ') increases only slightly with increasing suction (Drumright 1989, Escario & Saez 1989). The value of φ' may be assumed

constant for suction values less than 600 kPa, which is commonly observed in geotechnical engineering practice (Khalili and Khabbaz 1996).

The objectives of this chapter are to investigate i) the possibility of generation of u_e, and ii) the potential dilative or contractive behavior of filtered tailings during undrained loading. The initial behavior of unsaturated tailings under undrained K_0-loading is evaluated, and the impact of as-placement conditions and the degree of saturation on the generation of u_e is assessed. Undrained compression tests were performed on initially unsaturated filtered tailings from two precious metal mines using a modified rigid-wall permeameter with controlled vertical stress. Specimens were prepared with different initial dry densities and gravimetric water contents (standard Proctor optimum and wet of optimum). Confirmatory compression and consolidation tests were also performed on the same material to investigate the possible convergence of experimental compression data. Finally, σ' is calculated using σ^s to enable the development of stress paths so that the location of stress paths can be determined relative to the critical state line (i.e., to forecast development of contractive or dilative behavior types during shear). Results from this study can be used to understand the compression behavior of filtered tailings, the potential need for initial compaction, and to guide future assessment of filtered tailings placement water contents.

2.2.BACKGROUND

Equation 2.3 introduced by Lu et al. (2010) provides an estimation for σ^s (Song 2014) based on suction and degree of saturation experimental data. According to Lu et al. (2010), there is a relationship between σ^s and the degree of saturation of the soil, such that:

$$\sigma^s = -(u_a - u_w)S_e \tag{2.3}$$

where u_w is pore water pressure, S_e is the effective saturation or the ratio of free water volume to the total available volume such that: $S_e \equiv \frac{S-S_r}{1-S_r}$, and S_r is residual saturation. Of note, Lu et al. (2010) used the $S_e \equiv \frac{S-S_r}{1-S_r}$ formulation to define effective saturation, while Corey (1994) and Chiu and Shackelford (1998) recommend $S_e \equiv \frac{S-S_r}{S_m-S_r}$. In the latter equation, S_m is the maximum field saturation. Maximum saturation is considered equal to one for drying soils, whereas for wetting soils, S_m cannot reach one (without immersion) and must be measured. Bicalho et al. (2000) also showed that disregarding S_m at higher degrees of saturation leads to an overestimation of relative hydraulic conductivities in an infiltration (wetting) process. Of note, a method of directly measuring σ^s is defined by Dong and Lu (2017); however, this method is burdensome and not used in this study; future work should explore implementation of this method for tailings.

To estimate σ^s for a range of saturation (S) data, a model is needed. Lu et al. (2010) provide a model for σ^s versus matric suction in which σ^s reaches infinity at extremely low S (< 0.001). However, Dong and Lu (2017) and Zhang and Lu (2020) prove that depending on the soil, σ^s reaches a specific threshold at low S. This maximum σ^s is shown to be as low as zero in Esperance sand or as high as 1 MPa in Denver bentonite (Zhang and Lu 2020). Zhang and Lu (2018) postulate that adsorptive water content depends on soil mass and not on the void ratio or porosity. The following equation from Zhang and Lu (2020) redefines a model for σ^s based on w:

$$\sigma^s(w) = \sigma^S{}_{ads}(w) + \sigma^S{}_{cap}(w)$$

$$= f_{ads}(w)\sigma^s{}_{dry} + \frac{-f_{cap}(w)}{\alpha^{SS}}\frac{w}{w_s}\left[\left(\frac{w}{w_s}\right)^{n^{SS}/1-n^{SS}} - 1\right]^{1/n^{SS}}, \quad (2.4)$$

$$f_{ads}(w) = \frac{1}{2}\left[1 - erf\left(\beta\frac{w - w_{tran}^{SS}}{w_{tran}^{SS}}\right)\right],$$

$$f_{cap}(w) = \frac{1}{2}\left[1 + erf\left(4\frac{w - w_{tran}^{SS}}{w}\right)\right]$$

where $\sigma^S{}_{ads}(w)$ refers to adsorptive stresses caused by electromagnetic fields of van der Waals, double-layer, surface, and cation hydration as a function of *w*, and $\sigma^S{}_{cap}(w)$ refers to capillary pressure as a function of *w*, $\sigma^s{}_{dry}$ (σ^s at a *w* corresponding to an oven-dry condition) is a soil property independent of *w* or matric suction (ψ), which combines the effects of contact area and mineral properties on σ^s, β is a dimensionless parameter representing the strength of adsorptive suction stress, which depends on soil types and soil fabrics, w_{tran}^{SS} is a transitional *w* from adsorptive to the capillary regime, w_s is *w* at saturation, and α^{SS} and n^{SS} are fitting parameters. Adsorptive stresses do not have a major effect on σ^s when a filtered tailings stack is maintained near saturation (e.g., during construction), and thus, in this study, only capillary pressure will contribute to σ^s.

2.3. MATERIALS AND METHODS

2.3.1. Materials

Filtered tailings from two confidential precious metal mines, mine M and mine P (same material in Chapter 1), were used in this study (Fig. 2.1). Geotechnical characterization of mine M

and mine P filtered tailings (referred to as M tailings and P tailings henceforth) are described in Gorakhki et al. (2019) and are summarized in Table 1.1. Characteristics of the tailings include mechanical sieve and hydrometer (ASTM D422; ASTM 2007), Atterberg limits (ASTM D4318; ASTM 2014), specific gravity (ASTM D854; ASTM 2014), and standard-Proctor-effort compaction (ASTM D698; ASTM 2014).

The particle-size distributions (PSDs) for M tailings and P tailings are shown in Figure 1.1, along with an average, upper-bound, and lower-bound PSD based on a compilation from literature for other mine tailings (Gorakhki et al. 2019). Based on Table 1.1 and Figure 1.1, tailings from both mines are comparable to average tailings properties. The higher fines content and clay-size content (particle size < 0.002 mm) of M tailings compared with P tailings and closer to the upper bound for tailings from the literature coincided with higher plasticity (plastic index and liquid limit) and illustrate that M tailings are more clayey than the average tailings.

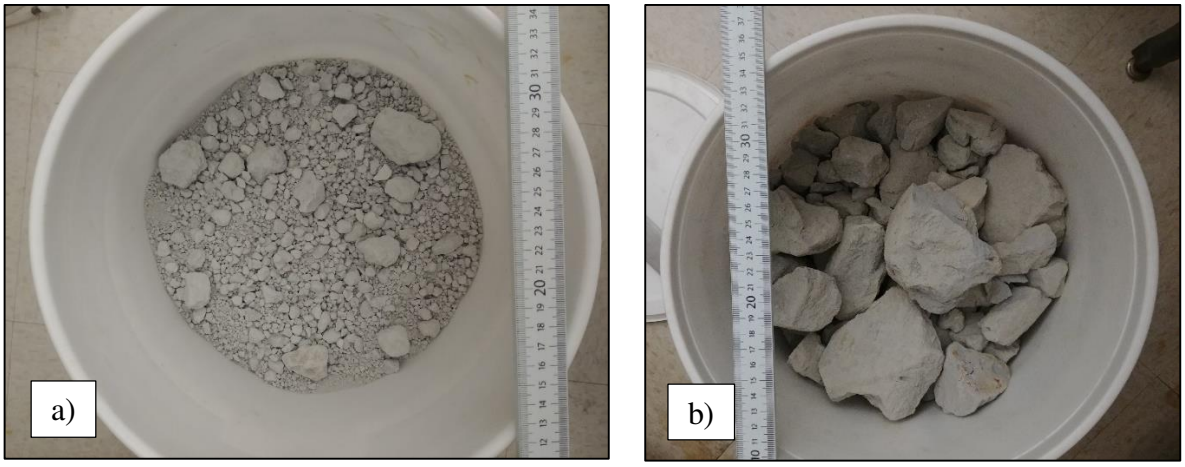

Figure 2.1 - Filtered tailings used in this study. a) A sample from mine M, b) a sample from mine P.

2.3.2. Specimen preparation

The air-dried filtered tailings were pulverized using a rubber hammer and then passed through a sieve #4 (Figure 1.2) to homogenize. After adding the target amount of water, tailings samples were mixed thoroughly and then sealed in a plastic container for 24 h. After 24 h, filtered tailings were again mixed and passed through a sieve #4.

2.3.3. Undrained Large-Strain Compression Test

Undrained large-strain compression tests were conducted using a modified large-strain rigid-wall permeameter with controlled vertical stress (the unmodified permeameter is described in Daniel 1994 as an odeopermeameter), shown in Figure 2.2. A complete description of the test setup is provided in Appendix A1, and an early version of the method is explained in Appendix A2.

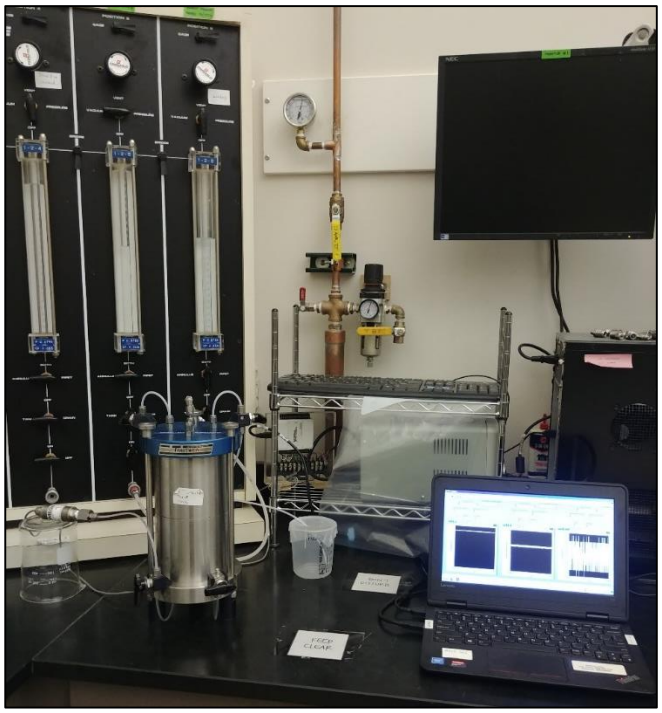

Figure 2.2 - Undrained large-strain compression apparatus while running a compression test

Cell modification included sealing a saturated 10-mm-thick high air-entry ceramic disk (500 kPa air-entry pressure) to the top of the base pedestal (Fig. 2.3), such that the specimen rested atop the high air entry disk. The role of the saturated disk was to measure positive excess pore water pressure within the specimen without contributing water to the specimen.

Figure 2.3 - The bottom plate of the compression apparatus containing a high air entry (HAE) ceramic disk.

Filtered tailings with adjusted water contents were compacted within the test cell which had an inside-diameter of 101.6 mm (Fig. 2.4). Specimens were compacted to an initial height of 25 mm. Compaction was performed on a rigid flat surface and the specimen and cell were subsequently moved to the permeameter base and placed atop the high air entry disk.

Figure 2.4 - A filter cake specimen getting compacted to the marked line of 25 mm inside the compression apparatus cell.

The initial target dry densities were 80%, 90%, and 95% of the maximum standard Proctor dry unit weight, and +0%, +2%, and +5% of the standard Proctor optimum water content. A filter paper was placed atop the high air entry disk before specimen placement to prevent fouling of the disk pores. Another filter paper and an unsaturated (hydrophobic) 3-mm-thick-porous plastic disk were placed above the specimen and overlain by the top piston. After closing the cell, the space above top piston was filled with water to apply a vertical total stress to specimens (Fig. 2.5).

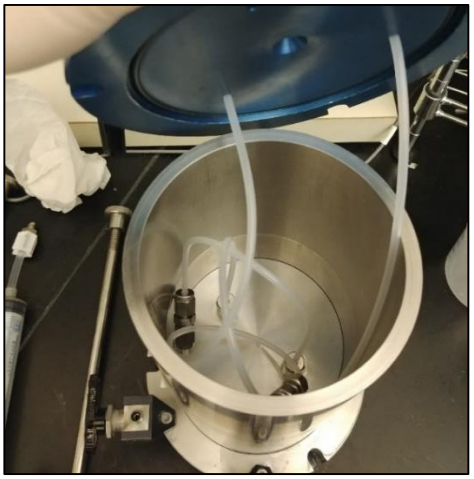

Figure 2.5 - The space inside compression apparatus top chamber, which will be filled with water connected to a pressure panel.

A pressure transducer (*OMEGA Model No: PX209G10V_0-30 psi*) was connected via a saturated line to the bottom of the high air entry disk. To control the vertical stress applied to the specimen, water above the top piston was pressurized incrementally using a pressure panel in steps to apply a total vertical stress to the specimen. Specimen volume change was monitored by measuring inflow to the reservoir above the top piston. The total stress applied in the compression tests were 14, 34, 69, 103, 138, 172, 207, 241, 276, 310, 345, 379, 414, 448, 483, 517, 552, and 586 kPa. The upper bound is governed by the capacity of the pressure panel used to apply total vertical stress. One top (air) valve of the cell was kept open for approximately 10-20 min after applying the first load step of 14 kPa (2 psi). The temporary opening of the valve was to let air between the specimen and the piston out and thus assuring the piston cell was in intimate contact with the specimen. After 10-20 min, all outflow valves were closed and remained closed throughout the undrained test (i.e., neither air nor water could leave the cell). Time intervals between each load increment were approximately 24 h. At the end of the test, the specimen was unloaded, during which the volume change was recorded. The test was then terminated after approximately 20 mins, when the generated excess pore pressure (if any) had been dissipated. The thickness of the specimen at the end of each load step was back calculated using the final specimen measurements after test termination. A specimen after the termination is shown in Figure 2.6.

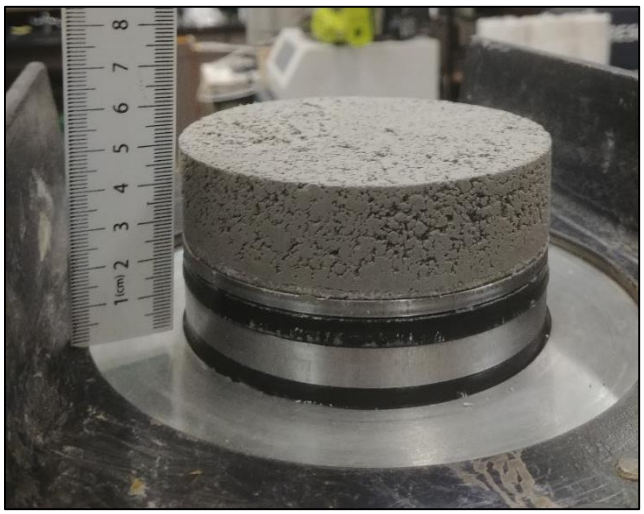

Figure 2.6 - A mine M specimen extruded out of a compression apparatus cell at termination.

Undrained compression tests on M and P tailings are listed in Table 2.2 and Table 2.3, respectively. The specimens were targeted to have initial degrees of compaction of 80, 90, and 95%, but the length of the test cell impacted the accuracy of compaction and resulted in the values reported in Tables 2.2 and 2.3. A less than 1% loss of moisture during compaction of some of the specimens is also shown in Tables 2.2 and 2.3.

2.3.4. GeoJac Consolidation and Undrained Compression

Confirmatory tests were performed via Sigma-1 ICON GeoJac apparatus manufactured by *Trautwein Soil Testing Equipment Company* to investigate whether compression data would merge under higher vertical loads, viz. initial conditions cease to matter at higher stresses and conventional oedometer tests can be used to predict consolidation under large vertical stresses. The initial target dry densities were 80% and 95% of the maximum standard Proctor dry unit weight, and +0% and +5% of the standard Proctor optimum water content. The specimens were compacted inside stainless-steel rings with 63.5 mm inside diameter and 25.4 mm height. For

unsaturated undrained compression tests, the top and bottom of the ring were covered with plastic wrap to minimize evaporative water loss. The covered ring was then placed atop a porous stone and overlain by another porous stone inside the cell of the apparatus. For the saturated consolidation tests, the rings were not covered with plastic wrap, and the cell containing the specimen was inundated with water at the beginning of the test.

The consolidation tests were performed on samples with an initial target dry density of 95% of the maximum standard Proctor dry unit weight, and standard Proctor optimum water content. The total stress applied in the compression/consolidation tests were 14, 34, 69, 103, 138, 172, 207, 575, 766, 1532, 2394, and 14 kPa. The upper bound is governed by the capacity of the load cell of the apparatus. Time intervals between each load increment were 24 h, except for the first (1 h), second (3 h), and the last (1 h) load steps due to the limitation of the apparatus in maintaining low vertical loads. The initial thickness of the specimen at the end of each load step was back calculated using the final specimen measurements after test termination.

As can be seen in Figure 2.7, the data from compression and consolidation tests on each of mine M and mine P tailings tended to merge under higher loads (more than 1500 kPa). Because the apparatus used in the confirmatory compression tests was not as water-tight as the modified rigid-wall permeameter, specimen moisture was reduced slightly by the end of tests. The initial applied load (14 kPa) is affected by the swelling pressure of the specimen. Thus, the values recorded by the apparatus load-cell and reported by the built-in software (Fig. 2.7) are less than the initially programmed vertical load (14 kPa). Plots of combined results from the undrained large-strain compression tests and unsaturated and saturated confirmatory tests are provided in Appendix A3 and indicate general agreement between both test methods.

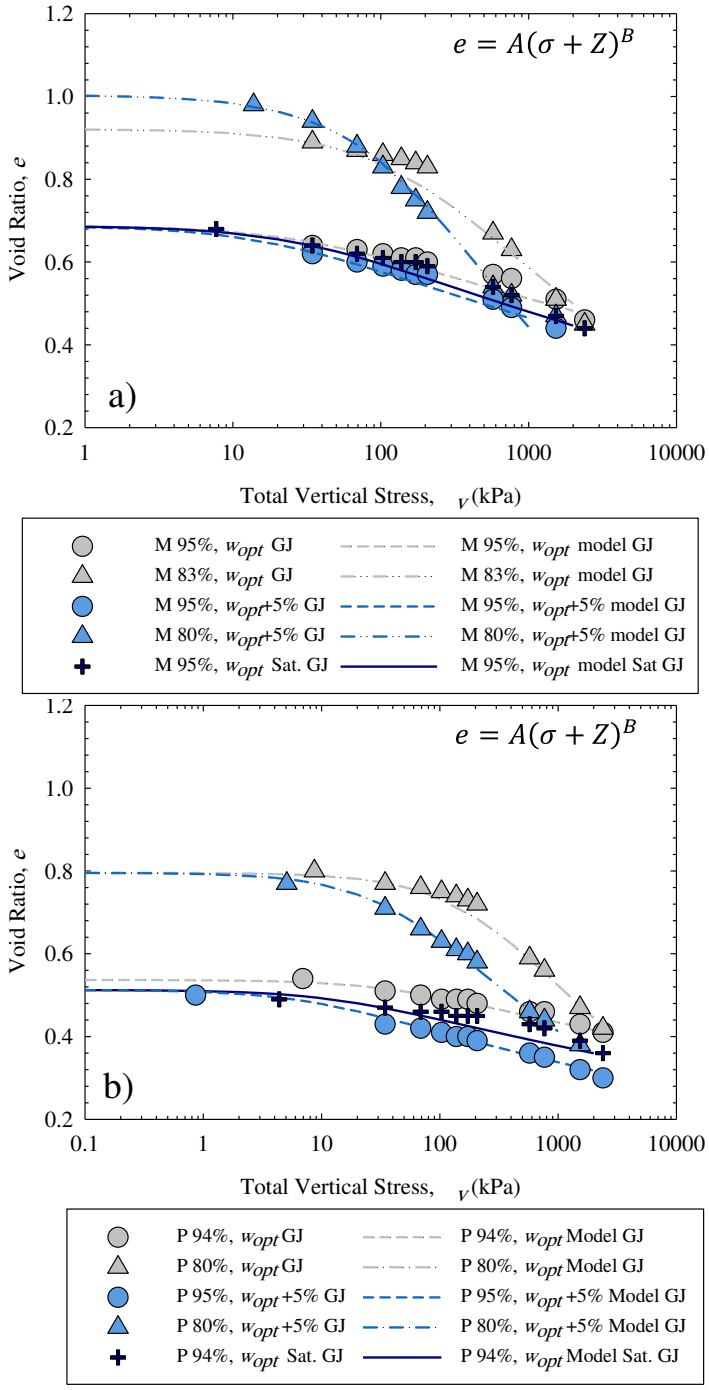

Figure 2.7 - a) Results from a saturated consolidation and four unsaturated undrained compression confirmatory tests on M tailings; and b) on P tailings.
Tests identified in the legend include the percent of maximum dry unit weight and water content relative to optimum water content (w_{opt}), which is 15.8% for M and 14.2% for P tailings. $e = A(\sigma + Z)^B$, a constitutive relationship by Liu and Znidarčić (1991).

2.3.5. Data Analysis

Results from large-strain compression tests were combined with the results from SWCCs from Chapter 1 to assess the influence of water distribution on the generation of u_e. Data from SWCCs from Chapter 1 were used to estimate σ^s for filtered tailings for a given initial as-placement condition. Subsequently, applied total vertical stress, measured u_e, and estimated σ^s were used to estimate σ′ of filtered tailings with specific initial as-placement conditions in the undrained compression tests.

Equation 2.4 was used to approximate σ^s. This model was fit to the σ^s data calculated via Equation 2.3 by minimizing the sum of squared error between calculated and fit values. The matric suction as a function of saturation were obtained from drying and wetting SWCC tests described in Chapter 1 on the same filtered tailings with similar as-placement conditions (w and ρ_d). The S_e corresponding to gravimetric water contents in the generated σ^s models (Eq. 2.4) were obtained by phase relationships. If there had not been sufficient data to complete phase relationships, the model proposed by Fredlund and Houston (2013) for the degree of saturation could be used to estimate S_e. The resulting models of $\sigma^s(S_e)$ are used to estimate σ^s corresponding to each data point from the compression tests in the current chapter. There will be two different sets of σ^s data for each undrained compression test as σ^s varies in drying and wetting cycles. The two different sets of σ^s data are used to estimate σ′ for the undrained compression tests performed in this chapter for both drying and wetting cycles. Table 2.1 provides the drying and wetting SWCC tests from Chapter 1, which were matched to the undrained compression tests in this chapter to calculate σ^s.

Table 2.1 - Guide table on the matched soil water characteristic curves (SWCC) with the undrained compression tests (UCT) of this study.
M = M tailings. P = P tailings, *w*(opt) = optimum water content.

M tailings		P tailings	
SWCC	UCT	SWCC	UCT
95% compaction, *w*(opt)	95% compaction, *w*(opt) 95% compaction, *w*(opt)+1.3%	95% compaction, *w*(opt)	95% compaction, *w*(opt)-1.0%
95% compaction, *w*(opt)+5%	98% compaction, *w*(opt)+4.3% 97% compaction, *w*(opt)+4.4%	95% compaction, *w*(opt)+5%	94% compaction, *w*(opt)+5%
90% compaction, *w*(opt)	90% compaction, *w*(opt)	90% compaction, *w*(opt)	91% compaction, *w*(opt)
90% compaction, *w*(opt)+5%	90% compaction, *w*(opt)+3.8%	90% compaction, *w*(opt)+5%	92% compaction, *w*(opt)+4.3% 88% compaction, *w*(opt)+2.7%
80% compaction, *w*(opt)	80% compaction, *w*(opt)	80% compaction, *w*(opt)	80% compaction, *w*(opt)
80% compaction, *w*(opt)+5%	83% compaction, *w*(opt)+5% 80% compaction, *w*(opt)+5%	80% compaction, *w*(opt)+5%	80% compaction, *w*(opt)+5%

Note: SWCCs are obtained from Chapter 1.

Stress paths were identified for the undrained compression tests on P tailings to investigate the possibility of dilative/contractive behavior or brittle/ductile failure. The critical state line (CSL) was available for P tailings from Borja and Bareither (2020) and thus the logp′ versus void ratio (*e*) data were plotted for this material only. From Borja and Bareither (2020) the φ′ was 33° and

K_0 was $1 - \sin(33) = 0.45$ assuming normally consolidated tailings in the laboratory. Although, the latter assumption cannot be simply made for field conditions. Equation 2.5 by Borja and Bareither (2020) is the CSL for mine P tailings for a range of p' less than 500 kPa.

$$e = 0.80177 - (0.11283 \times \log(p')), \tag{2.5}$$

$$p' = \frac{\sigma' - K_0 \times \sigma'}{2}$$

2.4. RESULTS

2.4.1. Undrained compression tests results

Compression results from 16 tests on M and P filtered tailings are presented in Figure 2.8. Compression data were fitted to constitutive models for *e* versus applied total vertical stress. Large-strain *e* versus stress constitutive relationship described by Liu and Znidarčić (1991) was used, i.e., $e = A(\sigma + Z)^B$, where A, B, and Z are fitting parameters; A has units of stress^{-B}, B is dimensionless and always negative, and Z has units of stress, and σ is the applied vertical stress. As shown in Figure 2.9, specimens initially compacted wet of optimum underwent greater compression compared to specimens with the same degree of compaction but at optimum water content. The higher moisture content (lower capillary suction) of the specimens made tailings clods softer, such that the specimen could be more readily compressed (Fredlund et al. 2012). I hypothesize the presence of air in the tubing connecting the specimen to the closed valves (Fig. 2.2 and Appendix A1) to be the reason for a small degree of volume change occurring after saturation of a given tailings specimen was achieved.

Table 2.2 - List of performed undrained compression tests on M tailings.

Test No.	Gravimetric water content	Initial compaction	Excess pore pressure generated?	Initial degree of saturation (%)	Final degree of saturation (%)	Critical degree of saturation [a] (%)
1	w_{opt} [b]	95% $\gamma_{d,max}$ [c]	No	62	78	NA [d]
2	w_{opt}	90% $\gamma_{d,max}$	No	54	73	NA
3	w_{opt}	80% $\gamma_{d,max}$	No	43	67	NA
4	w_{opt}+1.3%	95% $\gamma_{d,max}$	Yes	68	91	NA
5	w_{opt}+3.8%	90% $\gamma_{d,max}$	Yes	68	97	92
6	w_{opt}+4.3%	98% $\gamma_{d,max}$	Yes	79	100	80
7	w_{opt}+4.4%	97% $\gamma_{d,max}$	Yes	80	100	80
8	w_{opt}+5%	83% $\gamma_{d,max}$	Yes	62	92	78
9	w_{opt}+5%	80% $\gamma_{d,max}$	Yes	56	100	79

[(a)] At which the ratio of positive excess pore pressure over total vertical stress is ≥ 0.1, [(b)] w_{opt}: Optimum water content which is 15.8% for M tailings, [(c)] $\gamma_{d,max}$: Maximum dry unit weight which is 16.6 kN/m^3 for M tailings, [(d)] NA: Does not apply.

Table 2.3 - List of performed undrained compression tests on P tailings.

Test No.	Gravimetric water content	Initial compaction	Excess pore pressure generated?	Initial degree of saturation (%)	Final degree of saturation (%)	Critical degree of saturation [a] (%)
1	w_{opt} [b] -1%	95% $\gamma_{d,max}$ [c]	Yes	62	78	NA [d]
2	w_{opt}	91% $\gamma_{d,max}$	Yes	65	100	100
3	w_{opt}	80% $\gamma_{d,max}$	No	47	73	NA
4	w_{opt}+2.7%	88% $\gamma_{d,max}$	Yes	69	93	NA
5	w_{opt}+4.3%	92% $\gamma_{d,max}$	Yes	87	100	94
6	w_{opt}+5%	94% $\gamma_{d,max}$	Yes	96	100	97
7	w_{opt}+5%	80% $\gamma_{d,max}$	Yes	65	100	94

[(a)] At which the ratio of positive excess pore pressure over total vertical stress is ≥ 0.1, [(b)] w_{opt}: Optimum water content which is 14.2% for P tailings, [(c)] $\gamma_{d,max}$: Maximum dry unit weight which is 17.8 kN/m^3 for P tailings, [(d)] NA: Does not apply.

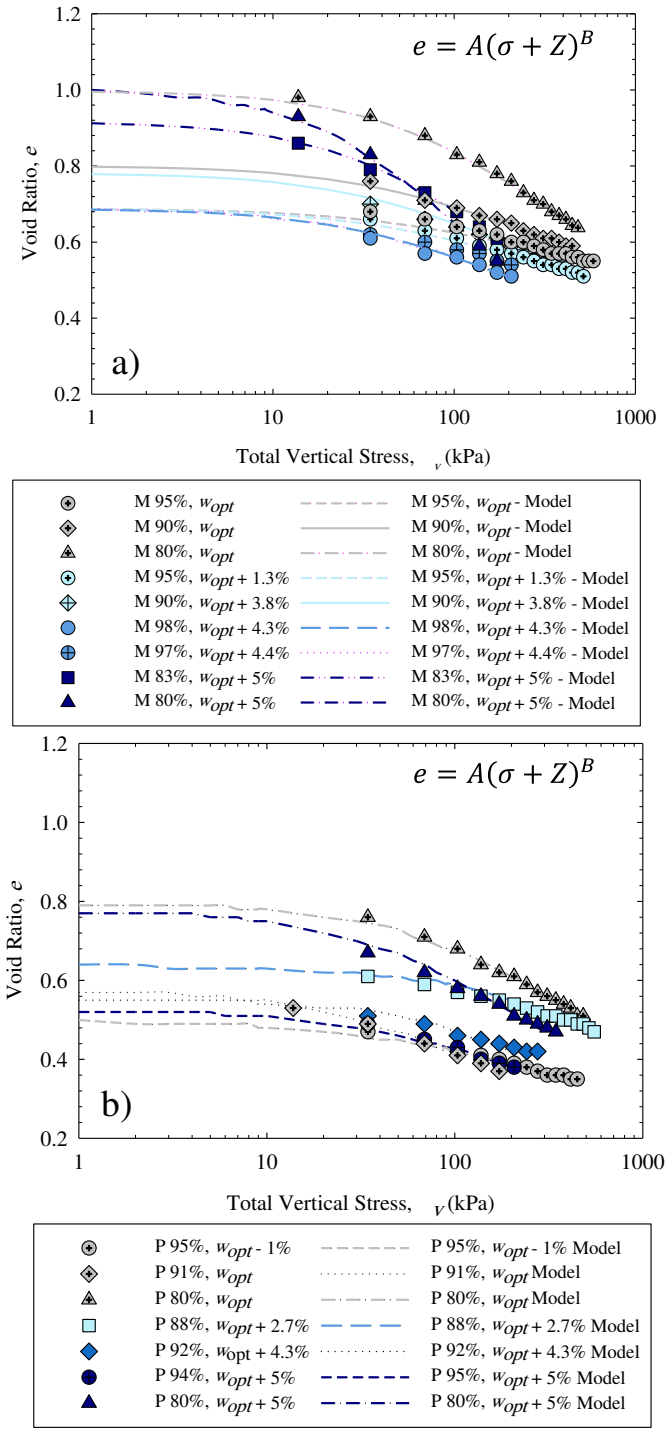

Figure 2.8 - Undrained compression test results on a) M filtered tailings; and b) P filtered tailings.
Tests identified in the legend include the percent of maximum dry unit weight and water content relative to optimum water content (w_{opt}), which is 15.8% for M and 14.2% for P tailings. $e = A(\sigma + Z)^B$, a constitutive relationship by Liu and Znidarčić (1991).

Values of u_e shown in Figure 2.9 are the maximum readings from the pressure transducer during each approximately 24-hour period. Appreciable u_e in this study is defined as when the ratio of u_e over applied total vertical stress (σ_v) was ≥ 0.1. The generation of appreciable u_e was not observed under the same total vertical stress (Fig. 2.9) for any of the tested material. For example, an M tailings specimen initially compacted to 80% of the maximum dry unit weight at +5% optimum water content generated an appreciable u_e of 33 kPa under 103 kPa total stress ($u_e/\sigma_v = 0.3$). Higher initial degree of compaction appears to have shifted the generation of appreciable u_e to greater applied total stress. For example, M tailings specimens with initial conditions of 97% maximum dry unit weight with +4.4% optimum water content and 98% maximum dry unit weight with +4.3% optimum water content generated u_e of 31 and 36 kPa, respectively, under a 207 kPa total stress (Fig. 2.9a). M tailings specimens prepared at optimum water contents did not generate appreciable u_e under vertical stresses as high as 586 kPa. P tailings specimens prepared at optimum water contents did not follow the same behavior as of M tailings (Fig. 2.9b).

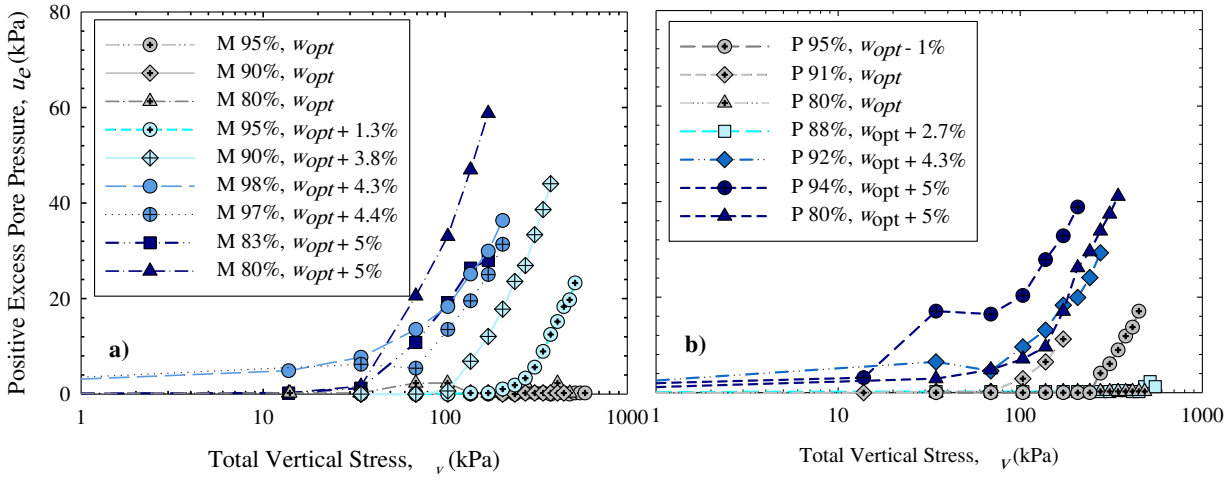

Figure 2.9 - Maximum generated positive excess pore pressure at each load step from undrained compression tests on a) M tailings; and b) P tailings.
Tests identified in the legend include the percent of maximum dry unit weight and water content relative to optimum water content (w_{opt}), which is 15.8% for M and 14.2% for P tailings.

The generation of u_e versus saturation is shown in Figure 2.10. Similar to Figure 2.9, the u_e shown in Figure 2.10 are the maximum readings from the pressure transducer over each 24-hr period. As shown in Figure 2.10, M and P tailings did not follow the same trend in the generation of u_e. Compression tests on M tailings demonstrated appreciable u_e started to be generated at approximately 80% saturation (Fig. 2.10a), whereas for P tailings the degree of saturation for generation of appreciable u_e was about 94% (Fig. 2.10b). This degree of saturation, labeled as the critical degree of saturation in Tables 2.2 and 2.3, represents the saturation when appreciable u_e was measured. In two tests on P tailings, u_e was generated when 80% saturation was reached. But the generated u_e had a ratio of u_e/σ_v slightly less than 0.1 and was dissipated to zero or near zero during the approximately 24 h period. The generated u_e (with $u_e/\sigma_v \geq 0.1$) did not fully dissipate after 24 h in any tests, instead the magnitude of generated u_e increased under subsequent load steps until 100% saturation of the specimen and continued increasing thereafter.

Based on the results from undrained compression tests on M and P tailings, higher initial degree of compaction reduced the magnitude of generated u_e, when the initial w was not more than +3% optimum water content (i.e., denser specimens compressed less, as expected). As seen in Tables 2.2 and 2.3, one M tailings specimen did not generate appreciable u_e until 91% saturation, and one P tailings specimen did not generate appreciable u_e even 93% saturation.

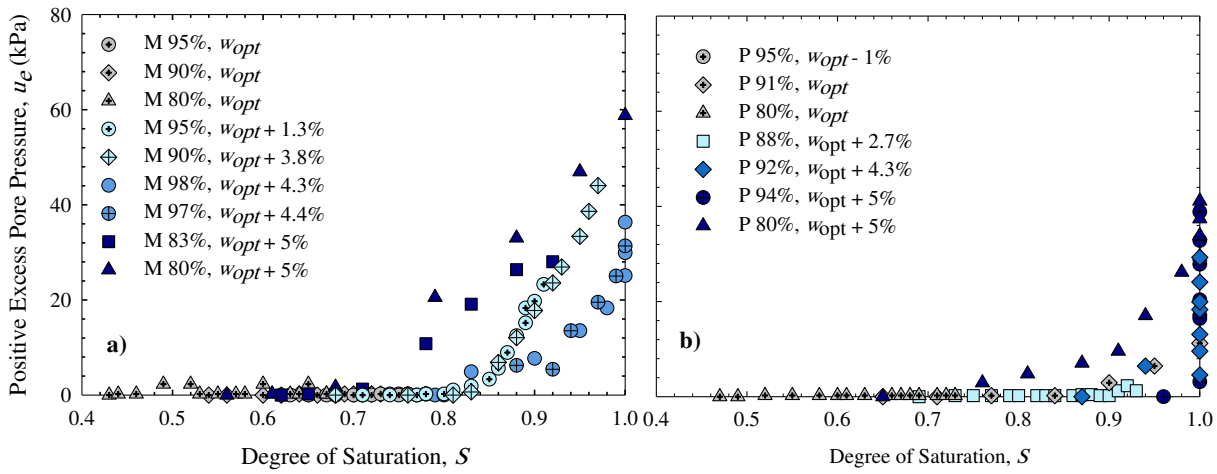

Figure 2.10 - Positive excess porewater pressure generation versus saturation from undrained compression tests on a) M tailings; and b) P tailings.
Tests identified in the legend include the percent of maximum dry unit weight and water content relative to optimum water content (w_{opt}), which is 15.8% for M and 14.2% for P tailings.

2.5. DISCUSSION

2.5.1. Generation of positive excess pore pressure under undrained K_0-loading

The results from the compression tests provide a framework to interpret the unsaturated excess porewater pressure generation of filtered tailings. For degrees of saturation approximately less than 70%, minimum to zero u_e was measured, despite the specimens compressing noticeably. The volume of air was sufficient to allow for deformation via compression and redistribution of the continuous air phase. Porewater did not generate an appreciable u_e because there was sufficient compressibility in the air phase to accommodate compression of the tailings skeleton [as well as additional (connected) air in the unsaturated porous plastic top disk and closed tubes]. In the field, under drained conditions, air would readily leave the filtered tailings. Low degrees of saturation also result in lower specimen compression (Fredlund et al. 2012), which is illustrated in Figure 2.8.

At degrees of saturation greater than approximately 70% but less than approximately 80%, the air phase became discontinuous. Excess pore water pressure is generated near 80% saturation, where the water phase is continuous, and the tailings are locally saturated. However, the generated excess porewater pressure dissipated by the time the next load was applied and did not reach the defined appreciable threshold. The compressibility of air is inversely proportional to absolute air pressure (Fredlund et al. 2012). Therefore, air compressibility decreases as the partial pressure of air inside the specimen increases. When a load is applied, air bubbles become entrapped in the water phase, the partial pressure of air in these bubbles increases (Boyle's law). However, the increased pressure is not appreciable, and the air bubbles are gradually dissolved in the water phase based on Henry's law. As summarized in Tables 2.2 and 2.3, tests in which the specimens did not reach approximately 80% saturation by the termination, did not generate appreciable positive excess porewater pressure.

At degrees of saturation close to or greater than 80%, the particle size distribution of tailings influences the u_e generation. For M tailings with higher clay-size content, appreciable u_e was generated. When a load was applied, the air pressure of occluded air bubbles increased, and these air bubbles began to dissolve. However, there was insufficient free air to accommodate all volume change, and a portion of the load was balanced in the water phase generating u_e. As for P tailings with the degree of saturation close to 80% but less than approximately 94%, the generated u_e increased close to the defined threshold, yet was dissipated to zero or low pressures during the 24 h period. After approximately 94%, P tailings shared the same behavior as that of M tailings. I believe this behavior results from the lower compressibility (more rigid structure) of the more silty P tailings

When the degree of saturation is above 90%, the air phase generally exists as occluded air bubbles and air flow is reduced to the diffusion of air through the pore-water (Matyas 1967) as well as dissolved air flow by advection (Fredlund et al. 2012).

2.5.2. Defining thresholds for the generation of excess pore pressure

In Figure 2.11, the ratio of induced pressure over the applied vertical load is graphed versus S and ρ_d, from the undrained compression tests on M and P tailings. In Figures 2.11a to 2.11d, the $u_e/\sigma_v = 0.1$ threshold is highlighted in red. As illustrated in Figures 2.11a and 2.11c, loose specimens (< 90% initial compaction), compacted wet of optimum water content, and dense specimens (≥ 90% initial compaction), compacted < 4% wet of optimum water content exhibited a smooth increase in the u_e ratio until a constant value was reached. In contrast, dense specimens compacted at more than +4% wet of standard Proctor optimum exhibited a sudden increase in the u_e ratio under lower loads (~34 kPa), which decreased to a constant ratio under higher loads in tests on M tailings. These ratios were not identical for all the tests on M tailings (Fig. 2.11a). Similar to M tailings, in tests on dense P tailings specimens compacted at more than +4% wet of optimum water content, an initial increase in the u_e ratio is followed by a decrease. However, the u_e ratio increases near saturation (Fig. 2.11c).

Thes u_e ratio shown in Figure 2.11 is not the Skempton pore pressure parameter B (Skempton 1954), which is used as an indication of saturation of specimens in isotropic triaxial tests. The (tangent) B-value is close to 1 when saturation is reached in isotropic triaxial tests. In contrast, in the K_0-loading tests performed in this study the (secant) u_e ratio never approached 1, even when specimens were at saturation. The measured u_e is also affected by the compressibility of the pore pressure measuring system, as well as the compressibility of the specimen (Casey 2014). As seen in Figure 2.2 and the schematic of the large-strain compression setup in Appendix

A1, there is tubing coming from the specimen upper boundary to closed valves. The air within the tubing and the porous plastic disk, and the body of the porous plastic disk can be compressed even after saturation, which can lead to a reduction in u_e ratio.

As shown in Figures 2.11b and 2.11d, the u_e ratio is much less for specimens with higher initial ρ_d and lower w. The applied σ_v on these specimens is mainly born by the tailings skeleton rather than water and thus less u_e is generated compared to tests on looser specimens with higher w. In other words, specimens compacted to 90% or more, with w less than +3% optimum water content do not generate appreciable u_e even at degrees of saturation above 80%. Given that all tests performed were undrained, the increase in the ρ_d of specimens was due to the reduction of the volume of air (compression and subsequent dissolution into water).

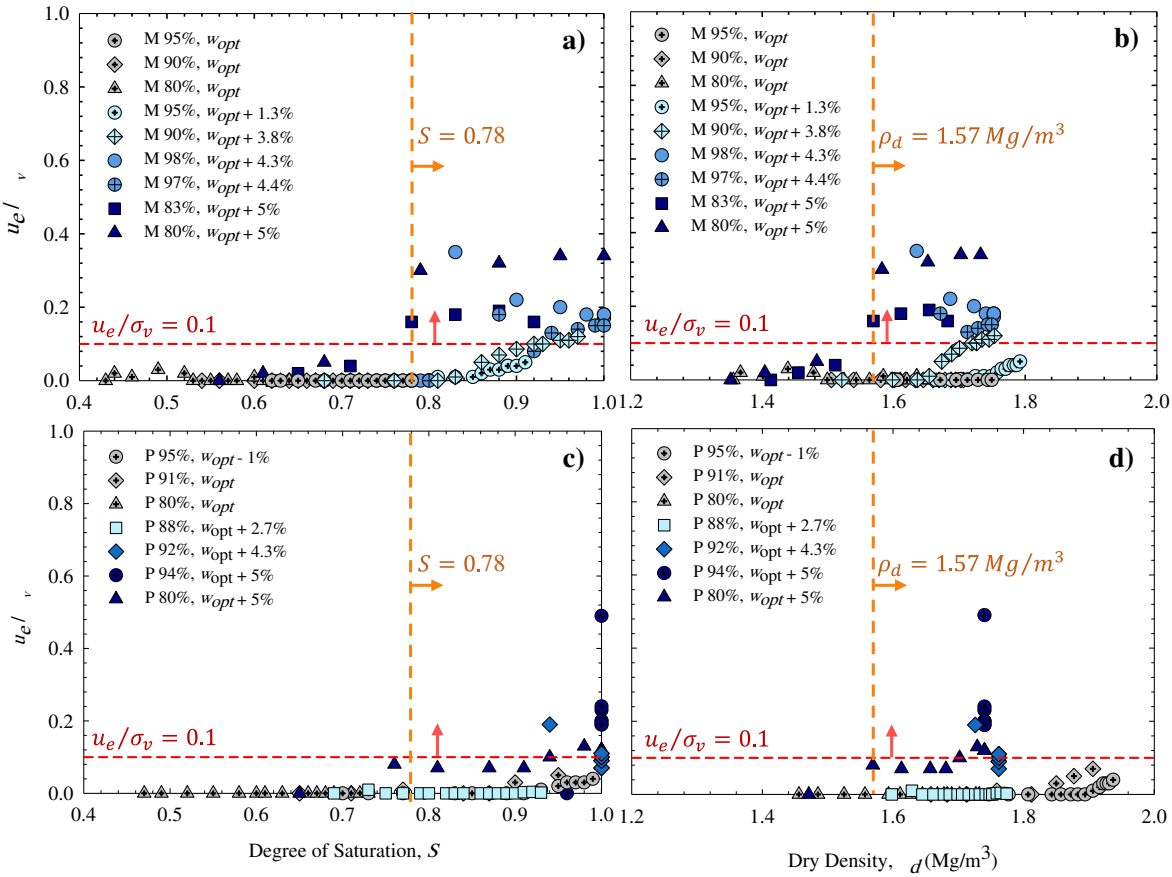

Figure 2.11 - The (secant) ratio of generated positive excess pore pressure over applied vertical stress versus saturation from K_0-loading undrained compression tests on:
a) M tailings; and c) P tailings. The (secant) ratio of generated positive excess pore pressure over applied vertical stress versus dry density from K_0-loading undrained compression tests on b) M tailings; and d) P tailings. Tests identified in the legend include the percent of maximum dry unit weight and water content relative to optimum water content (w_{opt}), which is 15.8% for M and 14.2% for P tailings.

Based on the results from the total 16 undrained compression tests performed on M and P tailings, some thresholds can be identified such that under specific circumstances a substantial u_e will be generated. These thresholds can be updated as more tests are performed on various tailings. As seen in Figure 2.11a, the lowest S at which a substantial u_e was generated and was not readily dissipated was 78% (~ 80%) for M tailings. Although for P tailings measurable u_e was generated at a slightly lower S, although this generated u_e was dissipated quickly (within hours) and the u_e ratio was low (Fig. 2.11c). Regarding the density of the filtered tailings, the lowest ρ_d at which a

substantial u_e was generated and was not readily dissipated was 1.57 Mg/m^3 (marked by an orange line in Figs. 2.11b and 2.11d). These thresholds by no means define a no-go zone and merely suggest critical areas where the practitioners and tailings engineers should be cautious, when dewatering filtered tailings and compacting and stacking at the field.

2.5.3. Suction stress contribution to the effective stress in unsaturated tailings

Suction stress characteristic curves for M and P tailings are presented in Figure 2.12. Curves were calculated using Equation 2.3 inputting matric suction and effective degree of saturation (S_e) data from pressure plate tests on M and P tailings. The pressure plate test method and results are reported in Chapter 1. Residual saturation of M and P tailings were 0.03 and 0.01, and the average S_m of M and P tailings from wetting tests were 0.941 and 0.940, respectively.

Figure 2.13 illustrates the relationship between σ^s and S_e for M and P tailings. Tables 2.4 and 2.5 provide fitting parameters of Zhang and Lu (2020) models shown in Figures 2.12 and 2.13 along with the goodness of fit (mean squared error = MSE). The Zhang and Lu (2020) models were fit to σ^s data resulted from matric suction data of SWCCs only. The Zhang and Lu (2020) model provided a better fit for wetting data in comparison to drying data (Fig. 2.13). However, this model could not represent the sudden loss of moisture (when drying) or the slow absorption of moisture (when wetting) under low capillary pressures.

M tailings with higher clay-size content exhibited higher σ^s, whether on a drying cycle or a wetting cycle, comparing to siltier P tailings. Loosely placed tailings exhibited much lower σ^s than dense (compacted ≥ 90%) tailings at the same S_e. Suction stress data for M and P tailings with different initial compaction tended to merge at very low S_e, representing highest values of σ^s.

As shown in Figures 2.13b and 2.13d, filtered tailing on a wetting cycle lost σ^s primarily when at near saturation (S_e > 80%). Filtered tailings on a drying cycle, however, maintain high σ^s (~100 kPa) until approximately $S_e \leq 85\%$ (Figs. 2.13a and 2.13c). Overall, σ^s resulting from drying cycles are much higher than those resulting from wetting cycles. Thus, considering σ^s from wetting cycles is conservative for stability analyses.

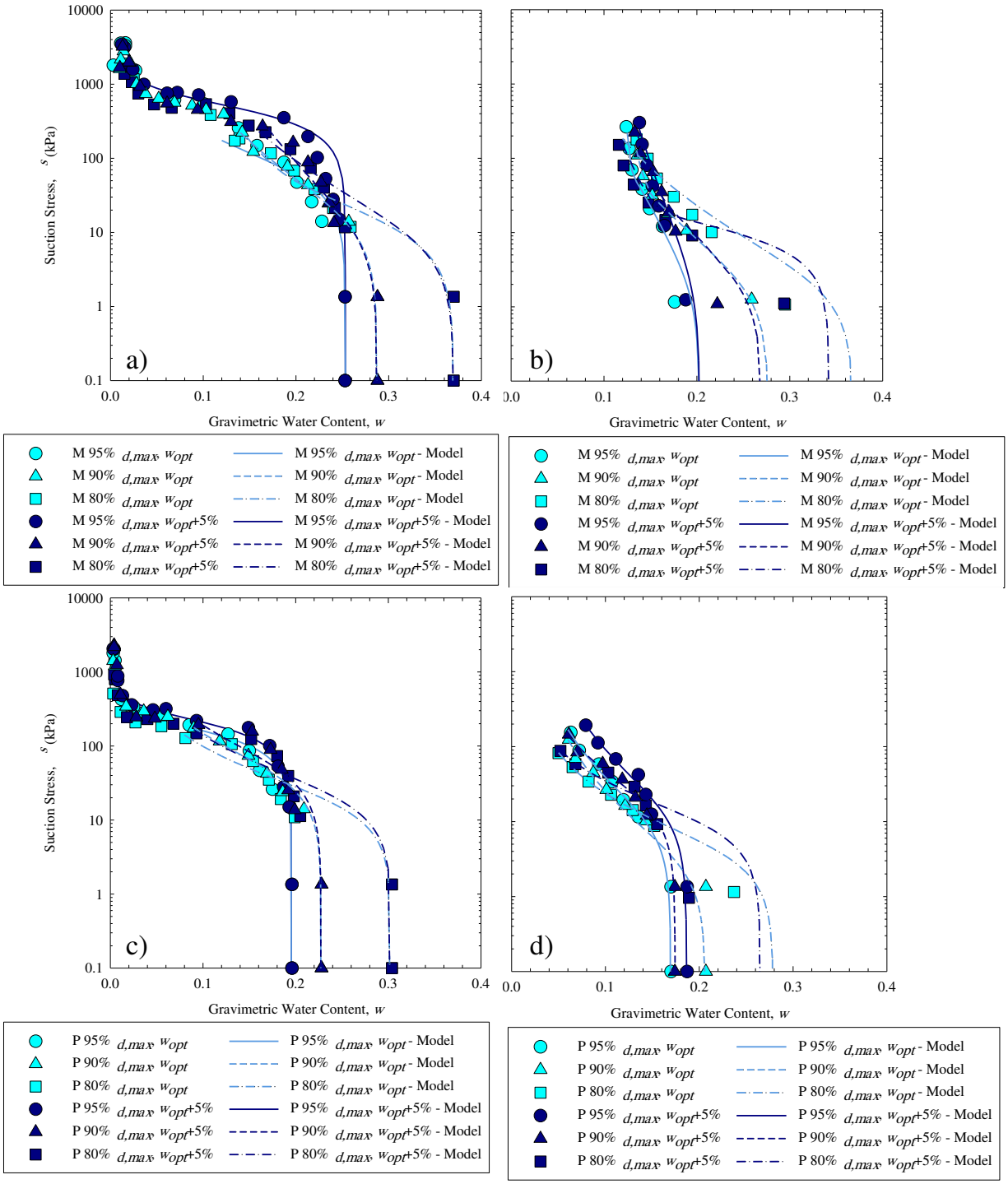

Figure 2.12 - Suction stress versus gravimetric water content from a) drying, and b) wetting soil water characteristic curves (SWCCs) of M tailings. Suction stress versus gravimetric water content from c) drying, and d) wetting soil water characteristic curves of P tailings.
Tests identified in the legend include the percent of maximum dry unit weight and water content relative to optimum water content (w_{opt}), which is 15.8% for M and 14.2% for P tailings. Data points are calculated using suction data from SWCCs. Models are generated using Zhang and Lu (2020) method.

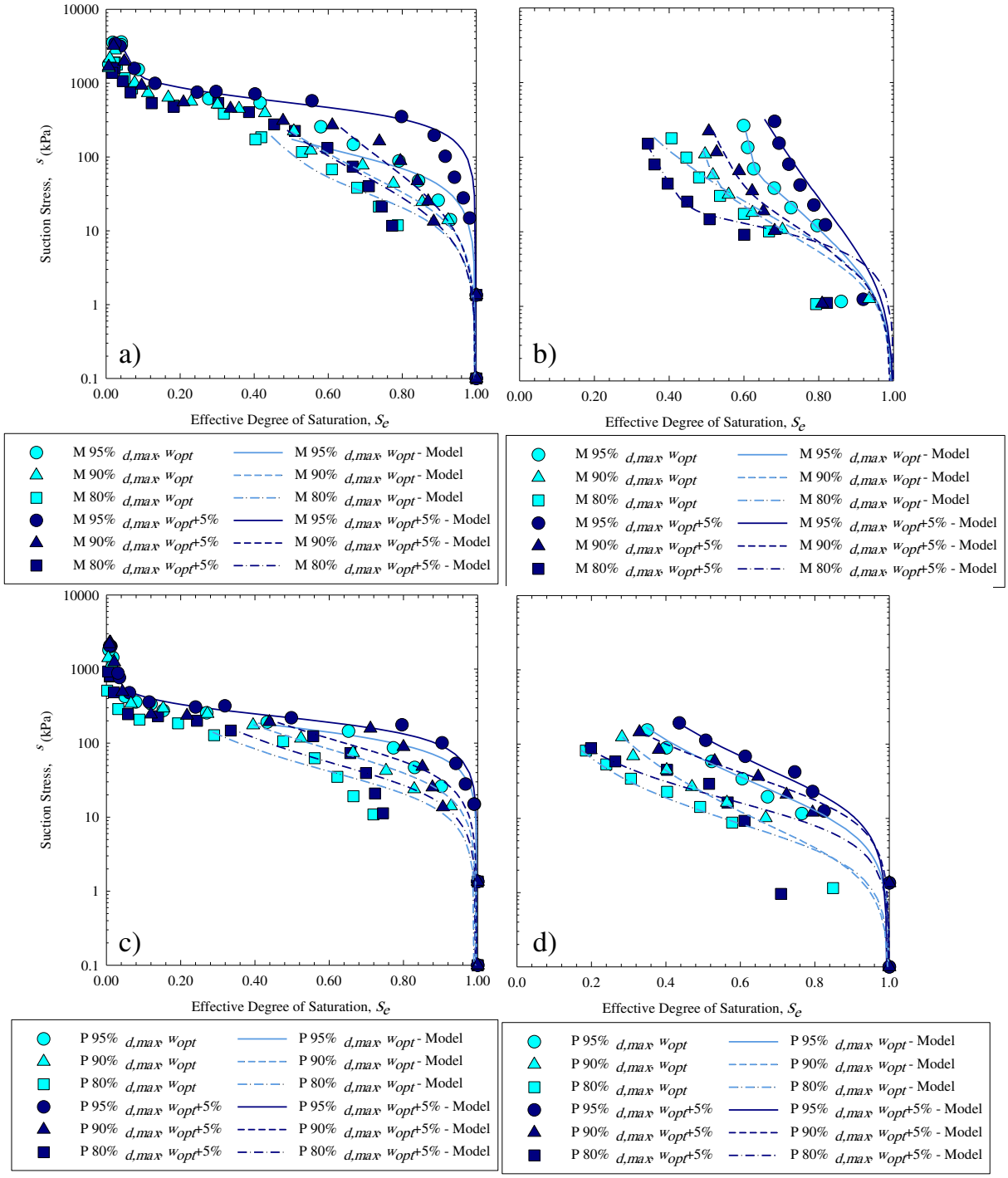

Figure 2.13 - Suction stress versus effective degree of saturation from a) drying, and b) wetting soil water characteristic curves (SWCCs) of M tailings. Suction stress versus effective degree of saturation from c) drying, and d) wetting soil water characteristic curves of P tailings.
Tests identified in the legend include the percent of maximum dry unit weight and water content relative to optimum water content (w_{opt}), which is 15.8% for M and 14.2% for P tailings. Data points are calculated using suction data from SWCCs. Models are adapted from Zhang and Lu (2020).

Table 2.4 - Fitting parameters for suction stress models based on drying soil water characteristic curves of M and P tailings.
M = M tailings. P = P tailings, *w*(opt) = optimum water content. σ_{dry}^{s}= suction stress corresponding to an oven-dry condition, β = represents the strength of adsorptive suction stress, ω_{tran}^{ss}= transitional *w* from adsorptive to the capillary regime, w_s = *w* at saturation, and α^{ss} and n^{ss} are fitting parameters. MSE = mean squared error from fitted curves.

	95% compaction *w*(opt)		95% compaction *w*(opt)+5%		90% compaction *w*(opt)		90% compaction *w*(opt)+5%		80% compaction *w*(opt)		80% compaction *w*(opt)+5%	
	M	P	M	P	M	P	M	P	M	P	M	P
σ_{dry}^{s}*	3614	2373	4940	2922	2796	1471	3300	2302	2122	800	2122	928
β	3.763	1.500	1.578	1.500	1.500	2.444	4.000	4.413	1.500	4.000	10.00	4.000
w_{tran}^{ss}	0.018	0.005	0.014	0.005	0.013	0.007	0.012	0.006	0.081	0.005	0.020	0.005
w_s	0.253	0.195	0.253	0.195	0.288	0.228	0.288	0.228	0.370	0.304	0.370	0.304
α^{ss}	0.016	0.007	0.002	0.005	0.068	0.025	0.100	0.020	0.092	0.057	0.123	0.048
n^{ss}	1.412	1.715	1.678	1.733	1.209	1.378	1.140	1.373	1.289	1.389	1.200	1.368
MSE	2100	360	3600	380	190	40	1000	1100	971	380	390	740

* in kPa.
Note: Fitting parameters are used in Zhang and Lu (2020) model for suction stress.

Table 2.5 - Fitting parameters for suction stress models based on wetting soil water characteristic curves of M and P tailings.
M = M tailings. P = P tailings, *w*(opt) = optimum water content. σ^s_{dry}= suction stress corresponding to an oven-dry condition, β = represents the strength of adsorptive suction stress, ω^{ss}_{tran}= transitional *w* from adsorptive to the capillary regime, w_s = *w* at saturation, and α^{SS} and n^{SS} are fitting parameters. MSE = mean squared error from fitted curves.

	95% compaction *w*(opt)		95% compaction *w*(opt)+5%		90% compaction *w*(opt)		90% compaction *w*(opt)+5%		80% compaction *w*(opt)		80% compaction *w*(opt)+5%	
	M	P	M	P	M	P	M	P	M	P	M	P
σ^s_{dry}*	3110	2000	3200	2922	2796	1471	3300	2302	2000	1000	2000	1000
β	18.40	4.000	3.357	1.500	7.298	3.900	4.435	3.900	10.00	4.000	2.294	2.738
w^{ss}_{tran}	0.117	0.035	0.025	0.005	0.114	0.012	0.107	0.012	0.020	0.012	0.084	0.008
w_s	0.203	0.170	0.203	0.187	0.278	0.206	0.270	0.174	0.369	0.279	0.342	0.265
α^{ss}	0.500	0.102	0.500	0.072	0.500	0.358	0.500	0.059	0.500	0.261	0.107	0.109
n^{ss}	1.107	1.267	1.074	1.245	1.178	1.246	1.160	1.334	1.199	1.358	1.500	1.417
MSE	3.82	40.5	1310	29.6	0.245	46.4	643	65.2	660	1.48	108	51.3

* in kPa.
Note: Fitting parameters are used in Zhang and Lu (2020) model for suction stress.

By generating models of σ^s for given initial conditions of filtered tailings (initial *w* and ρ_d), σ^s can be predicted at a given S_e. S_e were calculated using phase relationships. Using parameters summarized in Tables 2.4 and 2.5, corresponding σ^s were calculated via the obtained S_e data of undrained compression tests. σ^s data were then used to estimate σ' using Equation 2.2. Future studies should compare resulted σ' of this section with other methods of

measuring/estimating σ' of unsaturated tailings. Figures 2.14 and 2.15 illustrate σ^s, σ', σ_v, u_e for known S_e data from each of the 16 undrained compression tests on M and P tailings, respectively. In Figures 2.14a and 2.15a, σ^s were estimated from models based on drying and wetting SWCCs. Therefore, two different σ' were resulted for each of the compression data based on drying and wetting cycles (Figs. 2.14b and 2.15b). Because filtered tailings stacks are subject to atmospheric changes, wetting and drying of tailings, especially at the top layers, are inevitable. Thus, being aware that σ' is affected by drying and wetting cycles is essential to estimate the tailings strength and to evaluate the dilative and contractive behavior of tailings during shear.

σ^s data from drying and wetting cycles were an order of magnitude different at high degrees of saturation of tailings (Figs. 2.14a and 2.15a). Simms (2021) concluded that the substantial increase in total stress, followed by a large decrease in suction at higher saturations of filtered tailings stacks favors collapse. Confirmed in this study, σ^s differs when there is either a drying or a wetting cycle. However, Figures 2.14b and 2.15b show σ' has close values on drying and wetting cycles at effective degrees of saturation above 90% due to the generated u_e and the disappearance of the free air phase. For M tailings with higher clay-size content, the difference between drying σ^s and wetting σ^s were much more significant than for silty P tailings at high degrees of saturation ($75\% \leq S_e$). σ^s equals zero at complete saturation for both M and P tailings.

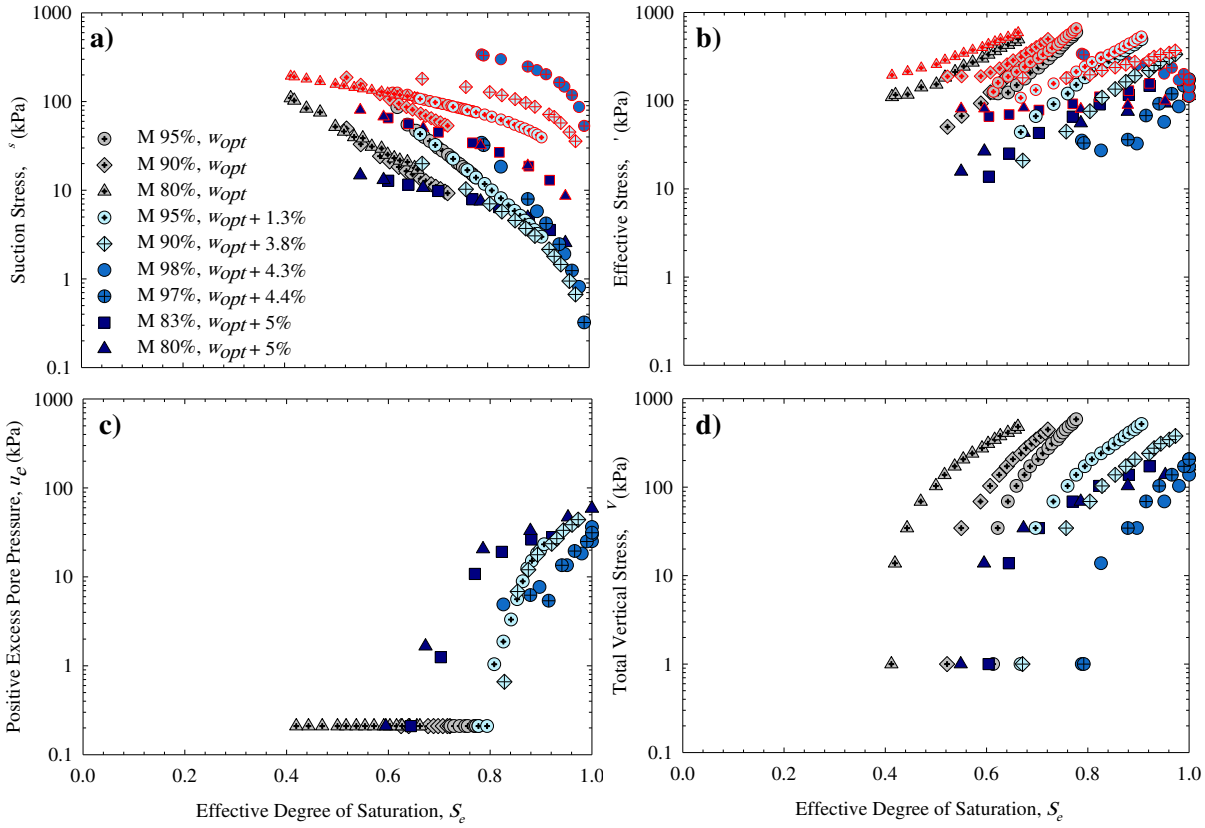

Figure 2.14 - a) Suction stress versus S_e, and b) σ′ versus S_e for M tailings. For (a) and (b) symbols if in red edge, represent data points resulted from drying soil water characteristic curves (SWCCs), and if in black edge, represent data points resulted from wetting SWCCs. c) u_e versus S_e. d) σ_v versus S_e.
All data points come from undrained compression tests. For (a) and (b) results from SWCC tests and undrained compression tests are combined. Tests identified in the legend include the percent of maximum dry unit weight and water content relative to optimum water content (w_{opt}), which is 15.8% for M tailings.

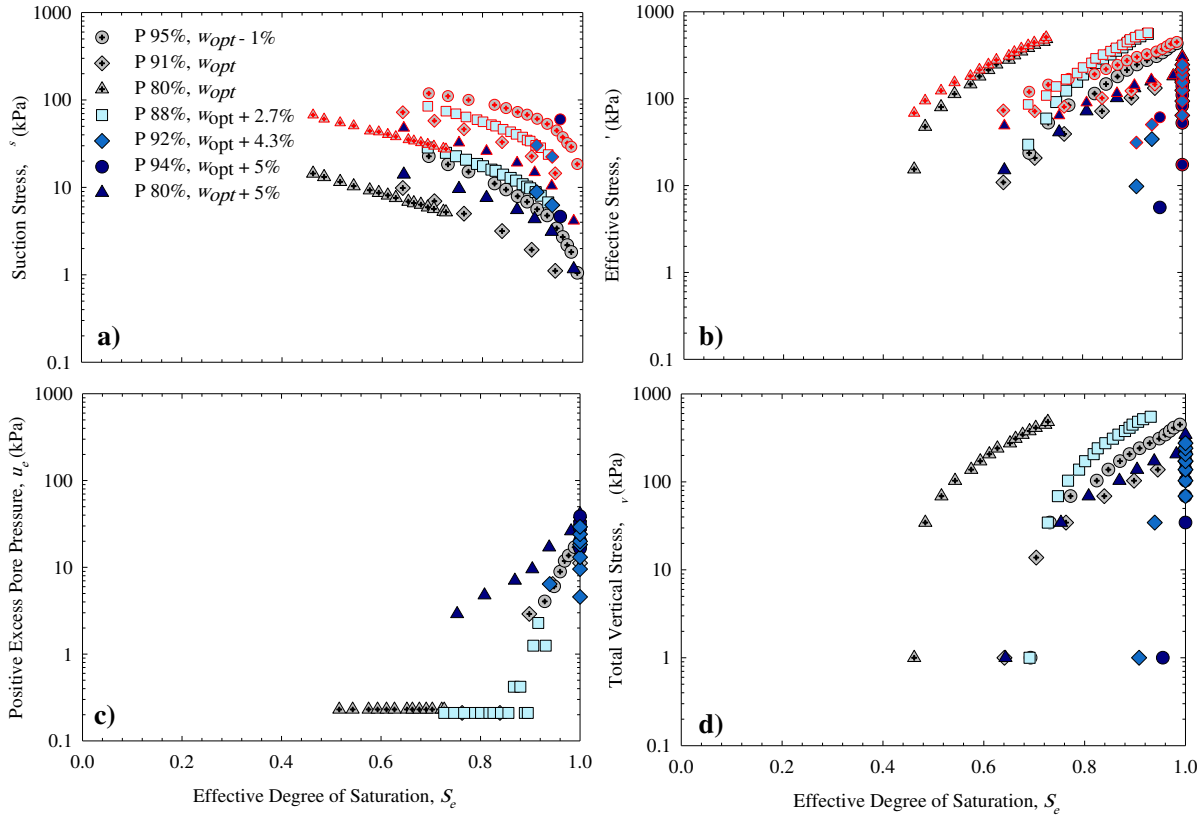

Figure 2.15 - a) Suction stress versus S_e, and b) σ′ versus S_e for P tailings. For (a) and (b) symbols if in red edge, represent data points resulted from drying soil water characteristic curves (SWCCs), and if in black edge, represent data points resulted from wetting SWCCs. c) u_e versus S_e. d) σ_v versus S_e. All data points come from undrained compression tests. For (a) and (b) results from SWCC tests and undrained compression tests are combined. Tests identified in the legend include the percent of maximum dry unit weight and water content relative to optimum water content (w_{opt}), which is 14.2% for P tailings.

2.5.4. Investigating the dilative or contractive behavior of filtered tailings

Stress paths using undrained compression data of P tailings are presented in Figure 2.16. The CSL by Borja and Bareither (2020) is also provided in Figure 2.16. Two different stress paths are provided for each of the seven undrained compression test using either of drying or wetting cycle data. According to Figure 2.16, stress paths stay below the CSL, illustrating potential dilative behavior during undrained shear. The two tests with 80% initial compaction and compacted to optimum and 5% wet of optimum w shift towards contractive behavior (located above CSL) but eventually end below the CSL (dilative). This observation supports that the geotechnical stability

of tailings stacks may be established at the initial phase of stacking filtered tailings. σ' data resulted from drying σ^s appeared to have higher potential for compression and thus contraction (Fig. 2.16a).

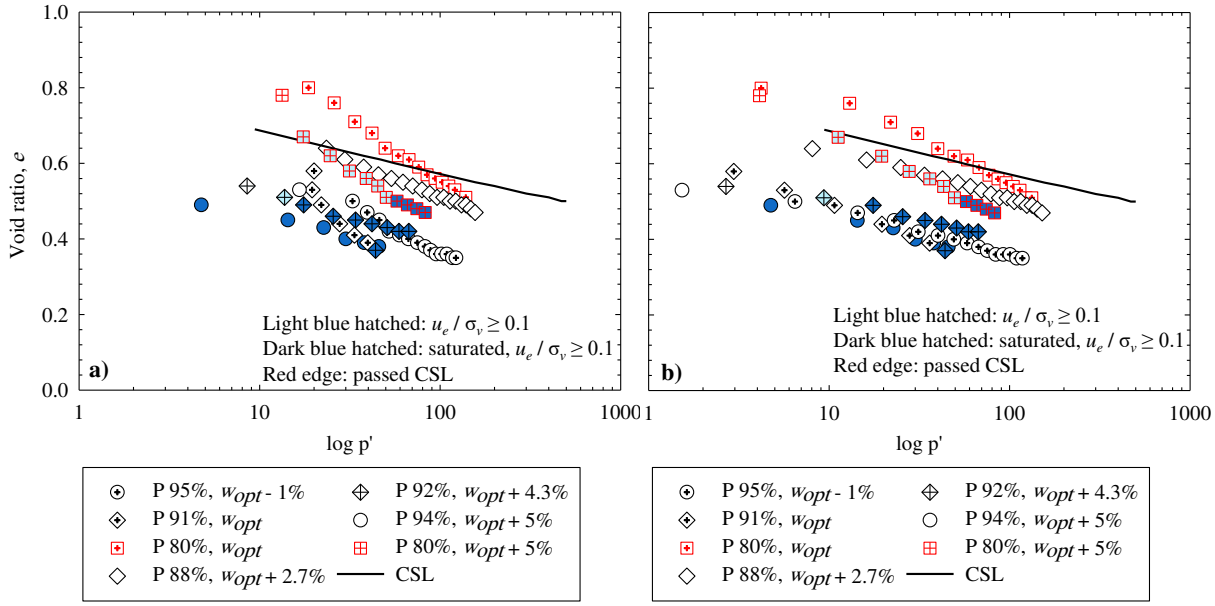

Figure 2.16 - Critical state line (CSL) and logp′ versus void ratio for P tailings. Effective stress is calculated using data from a) drying soil water characteristic curves (SWCCs); and b) wetting SWCCs. Total vertical stresses and void ratios come from undrained compression tests.
Tests identified in the legend include the percent of maximum dry unit weight and water content relative to optimum water content (w_{opt}), which is 14.2%. u_e is positive excess pore pressure. σ_v is the applied vertical stress.

2.6. SUMMARY AND CONCLUSIONS

16 undrained compression tests were performed on filtered tailings from two precious metal mines with various initial ρ_d and w. The w of these specimens ranged from optimum to +5% wet of optimum. The initial degree of compaction of the specimens ranged from 80 to 98% of the standard Proctor maximum dry unit weight. These tests were performed to investigate the possibility of generation of u_e under undrained loading, and to estimate σ' of unsaturated tailings so that the potential dilative or contractive behavior of filtered tailings during undrained loading

can be recognized. Future studies are required to compare calculated σ' of this study with other methods of measuring/estimating σ' of unsaturated tailings. The following conclusions are drawn from this study:

- Greater compression was observed in tests on specimens wet of optimum in comparison to tests on specimens with the same degree of compaction but at optimum water content.
- Appreciable positive excess porewater pressure was not observed under the same total vertical stress for different initial compacted states of the filtered tailings.
- Appreciable positive excess porewater pressure was consistently generated at saturations around 80% for specimens with more than +3% optimum water content and with 20% clay-size content, and at around 90% saturation for specimens with more than +3% optimum water content and with less than 20% clay-size content. The generated positive excess porewater pressure increased under subsequent loadings. In tests where no appreciable positive excess porewater pressure was observed, the specimens had not reached 78% saturation by the end of the test. In all tests, minimum or zero positive excess porewater pressure was generated at degrees of saturation less than 70%.
- Tests on specimens with ≥ 90% maximum dry density initial compaction and gravimetric water contents less than +3% wet of optimum resulted in the least amount of generated positive excess porewater pressure, even after reaching 80% saturation (viz., less compressible specimens generate less excess porewater pressure).
- The suction stress differs in drying and wetting cycles for the same degree of saturation. Filtered tailings tested in this study maintained suction stresses as high as ~100 kPa until approximately effective degrees of saturation ≤ 85% on a drying cycle. However, at

effective degrees of saturation above 90%, the resulting effective stresses from drying and wetting cycles were not considerably different due to the generated excess pore pressure and the shifting of free air to diffused air.

- This study shows a combination of soil water characteristic curves and compression results from undrained compression tests can guide tailings engineers to identify required levels of dewatering and compacting filtered tailings to attain geotechnically stable stacks. Generation of positive excess pore water pressure in unsaturated filtered tailings is a factor of the degree of saturation and compressibility of the as placed tailings. Drier tailings are less compressible for a given applied stress but have a lower degree of saturation. Wetter tailings are more compressible for a given applied stress but have a higher degree of saturation. Given that the goal of filtered tailings is to achieve a density sufficiently high (or void ratio sufficiently low) to preclude the possibility of flow liquefaction, placement must be a balance of factors to achieve success.

Chapter 3. Using water balance to minimize acid rock drainage of filtered and comingled tailings in different climatic type settings

3.1.INTRODUCTION

Mine waste in the form of tailings and waste rock is a currently unavoidable consequence of civilization. Tailings are fine residuum of milling and other mineral processing generated during the extraction of valuable metals. Waste rock are the rocks (and soils) extracted to access ore that does not have metal concentrations of economic interest. Waste rock dumps have a porous structure and often contain sulfide minerals, such that if the rock is exposed to oxygen and water, the rock will produce acid rock drainage, ARD (Munroe et al. 1999, Wickland and Wilson 2005, Wickland et al. 2006, Wickland et al. 2010).

Filtration is an increasingly practiced method of separating solid phase of tailings from liquid (Wang et al. 2014). Resulting filtered tailings, also known as "filter cake", when placed, are unsaturated materials with greater density and lower compressibility than slurry tailings (Lupo and Hall 2010). Filter cakes are then compacted to form a tailings stack. When potentially acid generating, PAG, material is present (e.g., sulfide minerals), filtered tailings stacks and waste rock piles, by nature of being unsaturated, may have an increased propensity for ARD, which requires leachate treatment in perpetuity (Munroe et al. 1999, Wickland and Wilson 2005, Akcil and Koldas 2006, Wickland et al. 2006, Bussière 2007, Wickland et al. 2010).

Over the past decades, tailings and waste rock management innovations have emerged to increase geotechnical and geochemical stability of filtered tailings and waste rock (Bolduc and Aubertin 2014, Ferdosi and James 2015, James et al 2017). Co-disposal of tailings and waste rock was initially proposed by Brawner (1978) and evolved over the last 20 years (Bussière 2007).

Table 3.1 provides a summary of common co-disposal methods based on Wickland et al. (2006) and Bussière (2007). The important factors differentiating each method are the blending and quantity of tailings and waste rock.

Table 3.1 - Methods of co-disposal of tailings and waste rock (Wickland et al. 2006, Bussière 2007).

Method	Description
Homogeneous mixture	Tailings and waste rock are blended to form a homogeneous mass (no specific mixture ratios)
Comingled	Alternating layers of tailings and waste rock
Tailings dominant blend	Waste rock is added to a tailings impoundment
Waste rock dominant blend	Tailings are added to a waste rock pile

The geochemical stability of an acid-generating filtered tailings or co-disposal stack can be controlled by limiting water infiltration in an arid or semiarid climate (Ghorakhki et al. 2020), thus minimizing the volume of ARD. Filtered tailings can be comingled with layers or zones of waste rock or any available coarse-grained material to improve the geochemical behavior of the stack, if designed correctly. In an arid climate, due to having minimum precipitation and high potential evapotranspiration filtered tailings and co-disposed tailings may provide the function of a water balance cover, minimizing or zeroing ARD fluxes (Ghorakhki et al. 2020).

In wet climates and climates with appreciable seasonal wet and dry cycling, however, we cannot solely rely upon limiting percolation via evapotranspiration to minimize ARD. Layers of filtered tailings should be maintained as wet as possible to prevent or impede ARD by limiting oxygen ingress but not placed too wet to affect the physical stability of the stack adversely (i.e., by preventing sufficient initial densities be achieved to create a dilative fabric during undrained shear). Water flow (viz., potential ARD flux) is also minimized via dense placement. Finally,

using capillary layers can enhance moisture retention and reduce water flow through commingled stacks.

When the degree of saturation is above 90%, the air phase generally exists as occluded air bubbles and airflow is reduced to the diffusion of air through the pore-water (Matyas 1967) as well as dissolved airflow by advection (Fredlund et al. 2012). As illustrated in Chapter 2 of this dissertation, at degrees of saturation greater than 80%, the air phase was no longer continuous.

Creative methods such as intentionally creating heterogeneity inside filtered tailings stacks can be used to achieve near saturation conditions. There is evidence that capillary barriers are effective in covers, when built correctly, for maintaining a saturated zone that reduces oxygen ingress into PAG waste rock piles (Bossé et al. 2013). Using existing numerical models (viz. HYDRUS 1D/2D) parameterized with field/lab-derived material parameters and soil water characteristic curves (SWCC), various scenarios (e.g., climates, as-placement conditions) for a heterogeneous stack of alternate layers of filtered tailings and coarse-grained soil can be investigated. Coarse-grained layers (e.g., waste rock or underflow tailings) can act as internal capillary barriers, maintaining or increasing the degree of saturation of filtered tailings layers and ultimately, keeping oxygen out of PAG zones/layers. Coarse-grained layers, thus, are used to enhance geochemical stability.

The objective of this chapter is to demonstrate that the hydrologic path to ARD reduction in a filtered tailings stack is climate driven. This study also explores the potential efficacy of internal capillary barriers in creating and maintaining near saturation conditions (to minimize ARD) when required by climatic conditions. Climate impacts and the efficacy of capillary barriers are investigated via numerical modeling with HYDRUS-2D. Numerous scenarios for two different filtered tailings from two precious metal mines (mine M and mine P tailings) were investigated.

The scenarios were varied in terms of the initial conditions of the filtered tailings and the climate of the site. The initial conditions include gravimetric water contents (w) of standard Proctor optimum and 5% wet of optimum and degrees of compaction of 95, 90, and 80% of the maximum dry density of tailings. Arid, hemiboreal, and extremely wet climates, as well as a no-climatic contribution (base case) condition were investigated. Compression and the resulting impact on saturated and unsaturated properties is not included in the investigations and the results are focused on a single lift of filtered tailings.

3.2. MATERIALS AND METHODS

3.2.1. Materials

Filtered tailings from two confidential precious metal mines, mine M and mine P (same material as in Chapters 1 and 2) were considered. Geotechnical characterization of mine M and mine P filtered tailings (referred to as M tailings and P tailings henceforth) are described in Gorakhki et al. (2019) and are summarized in Table 1.1. Characteristics of the tailings include mechanical sieve and hydrometer (ASTM D422; ASTM 2007), Atterberg limits (ASTM D4318; ASTM 2014), specific gravity (ASTM D854; ASTM 2014), and standard-Proctor-effort compaction (ASTM D698; ASTM 2014).

The particle-size distributions (PSDs) for M tailings and P tailings are shown in Figure 1.1, along with an average, upper-bound, and lower-bound PSD based on a compilation from literature for other mine tailings (Gorakhki et al. 2019). Based on Table 1.1 and Figure 1.1, tailings from both mines are comparable to average tailings properties. The higher fines content and clay-size content (particle size < 0.002 mm) of M tailings compared with P tailings and relatively closer to the upper bound for tailings from the literature coincided with higher plasticity (LL and PI) and

illustrate that M tailings are more clayey than the average tailings. SWCCs for M and P tailings were available from Chapter 2. However, since PSDs and SWCCs for underflow tailings or waste rock coming from the same mines were not available, sand from Rosetta Model within HYDRUS-2D was considered as the internal capillary barrier in this research.

3.2.2. Site conditions

Three different climates were investigated in this study: Tucson-AZ as an example arid climate (hot desert; Köppen *BWh*), Bozeman-MT as an example hemiboreal climate (dry continental; Köppen *Dfb*), and Juneau-AK as an example wet climate (on transition zone between humid continental and oceanic climates (Köppen *Dfb*/*Cfb*/*Cfc*)). Apart from the previously mentioned climates, models without climatic inputs were also investigated as a base case without the influence of climate-driven effects. For the three climates simulate, climatic data from 2020 were used. Assembled climate input data are provided in Appendix A4.

3.2.3. Numerical modeling

The HYDRUS-2D program by PC-Progress was used in this study. HYDRUS numerically solves the Richards equation for saturated-unsaturated water flow and convection-dispersion type equations for heat transport (Mendoza et al. 1991). The heat transport equation considers movement by conduction as well as convection with flowing water. In this study, only water flow and heat transfer packages were used. In seasons with high precipitation rates, surface ponding and rapid infiltration occur, which lead to sharp changes in the water contents of the simulated filtered tailings layer. Spatial discretization using finite element mesh in HYDRUS-2D allowed handling such issues to some extent, (HYDRUS-1D does not provide this option and thus was not used for this study). HYDRUS does not handle processes of freezing and thawing, however, when heat transport is simulated simultaneously with water flow, snow accumulation on top of the soil

surface can be simulated. The HYDRUS code assumes that when the air temperature is below -2°C all precipitation is in the form of snow. When the air temperature is above +2°C all precipitation is in the form of liquid, while a linear transition is used between the two limiting temperatures (-2,2°C). To prevent numerical instabilities, the melted snow and/or the ponded water leaves the system as runoff in case the low hydraulic conductivity of the soil/tailings layer hinders infiltration. Although SWCCs from wetting tests were available for the material used in this study, only drying SWCCs were considered because the HYDRUS does not allow for the inclusion of hysteretic SWCC parameters. Vegetation (root water uptake) and thus transpiration was not considered in any of the models (i.e., tailings stacks were assumed to be bare). Of note, HYDRUS does not account for compression/consolidation of soil layers through time. Thus, this chapter is focused on a single surficial lift of filtered tailings. Future work may consider the effect of compressing using the data provided in the preceding chapters.

3.2.3.1. Flow and heat transport modeling

Schematics of the two types of columns modeled in this study are presented in Figure 3.1. The column on the right includes a layer of filtered tailings only, which is compared to a column of filtered tailings placed atop a capillary layer of sand on the left of Figure 3.1. The observation nodes shown in Figure 3.1 were used to generate output files at specific depths of tailings and sand layers. An observation node was insert at the depth of 20 cm representing near the surface condition, another at the depth of 130 cm (of a tailings column of 260 cm) representing the middle, and another at the depth of 250 cm representing either the near-bottom of the tailings column or the area of tailings most-directly impacted by the capillary layer. Two more observation nodes were insert at the top and bottom area of the 100-cm capillary layer. However, results from the two observation nodes within the capillary layer are not presented in this study because water flow,

when appreciable, flushes out of the sandy layer rapidly. The van Genuchten (1980) method was chosen as the soil hydraulic model.

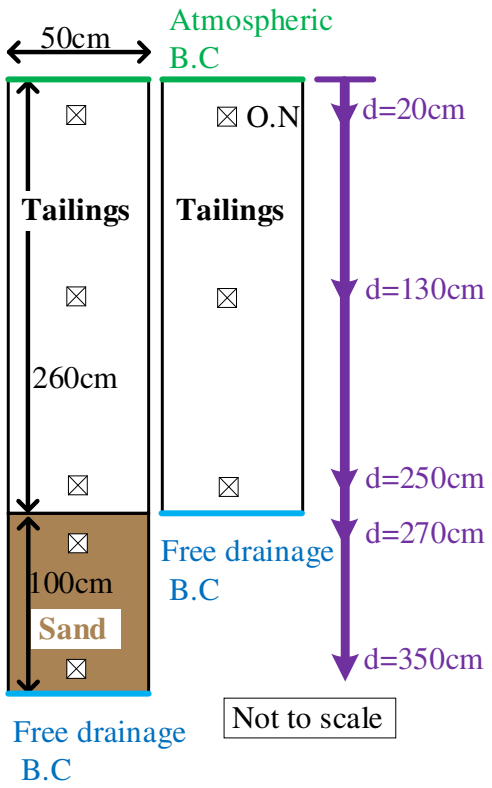

Figure 3.1 - Schematics of modeled filtered tailings columns in HYDRUS-2D.
The column on the left consists of a layer of tailings above an internal capillary layer of sand. Depths of the observation nodes in each column are also presented. The boundaries on the sides are set to no-flux boundary conditions. BC: Boundary condition. ON: Observation node. d: Depth from the ground surface.

The SWCCs parameters of M and P tailings were obtained from Chapter 1 (Table 1.4) for tailings with optimum standard proctor water content and 5% wet of optimum water content and with degrees of compaction of 95, 90, and 80% of maximum dry unit weights of tailings (Fig. 1.11). The constitutive model by Somogyi (1979) was fit to experimental saturated hydraulic

conductivity (K_s) data measured by Gorakhki et al. (2019) for various dry densities of M and P tailings (Eq. 3.1). The SWCC and saturated hydraulic conductivity of sand were assumed based on the values available within the HYDRUS program and are provided in Appendix A4.

$$K = Ce^D \tag{3.1}$$

where C is a fitting parameter with units of length per time and D is a dimensionless fitting parameter. Knowing the initial void ratio of the tailings, the saturated hydraulic conductivity of each of the simulated filtered tailings columns was calculated. The C and D parameters for M and P tailings are provided in the Appendix A4. Saturated hydraulic conductivities of M and P tailings are provided in Table 3.2, which are for void ratios corresponding to 95, 90, and 80% compacted tailings. Saturated hydraulic conductivity of sand was assumed constant in all simulations.

Table 3.2 - Saturated hydraulic conductivities (K_{sat}) of mine M and P tailings and the sand layer used in the models in this study.
K_{sat} of tailings were calculated using initial void ratios (e) of as-compacted tailings provided herein.

Compaction	95%	90%	80%
M tailings			
e	0.69	0.78	1.00
K_{sat} (m/s)	2.7×10^{-9}	8.0×10^{-9}	7.6×10^{-8}
P tailings			
e	0.51	0.60	0.80
K_{sat} (m/s)	2.3×10^{-9}	7.4×10^{-9}	5.9×10^{-8}
Sand*			
K_{sat} (m/s)	8.2×10^{-5}	8.2×10^{-5}	8.2×10^{-5}

*Sand layer is considered invariant.

HYDRUS models were run for 10 years or until steady-state conditions were achieved to assess immediate (transient) and long-term behavior.

3.2.3.2. Initial conditions

The solution of Richards' equation requires knowledge of the initial distribution of the volumetric water content or the pressure head within the flow domain. The initial conditions used for M and P tailings were the as-compacted volumetric water contents (θ) for each case. The as-compacted volumetric water contents are calculated based on the initial water content and initial degrees of compaction of M and P tailings. The initial condition used for sand (capillary layer) was slightly above the residual volumetric water content of sand. The initial temperatures considered for the arid, hemiboreal, and wet, climates corresponded to Jan. 1, 2020, as the first day of a 365-day climatic dataset (viz. one full year). The temperature data were obtained from the National Centers for Environmental Information website (*www.ncdc.noaa.gov*). Initial conditions entered into the flow and heat transport packages of the program are summarized in Table 3.3.

Table 3.3 - Initial conditions entered to the model.
Initial conditions used for tailings were the as-compacted volumetric water contents, and the initial condition used for sand (capillary layer) was slightly above the residual volumetric water content of sand. w_i: Initial gravimetric water content. w_{opt}: Optimum standard proctor water content which is 15.8% and 14.2% for M and P tailings, respectively.

Compaction	95%	90%	80%	95%	90%	80%
w_i		w_{opt}			w_{opt} + 5%	
M tailings θ (initial condition)	0.254	0.241	0.214	0.335	0.317	0.282
P tailings θ (initial condition)	0.246	0.233	0.207	0.333	0.315	0.280
Sand* θ (initial condition)	0.05	0.05	0.05	0.05	0.05	0.05

*Sand layer is considered not compacted, i.e., the initial condition of sand layer is constant for all models.

3.2.3.3. Boundary conditions

For the flow model, the top of the filtered tailings layer (at the ground surface) was set to an atmospheric boundary condition (Fig. 3.1). The atmospheric boundary condition required the knowledge of precipitation and temperature data (obtained from *www.ncdc.noaa.gov*) and evaporation data (obtained from Western Region Climatic Center, *wrcc.dri.edu*). Complete daily rainfall, snowfall (if any), and temperature data (year 2020) were available for all three locations. Daily pan evaporation data (year 2020) were also available for the hemiboreal climate, whereas monthly pan evaporation data had to be divided into daily evaporation for arid and wet climates due to lack of daily data. The bottom of simulated columns (Fig. 3.1) was set to free drainage (or unit vertical hydraulic gradient) boundary condition. The free drainage boundary condition is used as a bottom outflow boundary condition for situations where the water table is situated far below the domain of interest. This type of boundary condition represents tailings stack in the field, as groundwater table is anticipated to be far below the first lift of tailings. The left and right boundaries were set to no-flux boundary conditions.

For the heat transport model, boundary conditions for the top and bottom of the simulated columns (Fig. 3.1) were set to third type (mixed type) boundary condition, and the other boundaries set to no flux. The third type boundary condition is mass conservative, meaning, when water flux is zero or directed out of the region, third-type boundary conditions for heat movement are automatically switched from a Dirichlet (temporary type with specified values) to a Neumann (second type with known flux) boundary condition.

3.2.4. Data Analysis

HYDRUS generates output files throughout the modeling period at the location of observation nodes. Three observation nodes were set in the tailings layers at the depths of

approximately 20, 130, and 250 cm from the ground surface (Fig. 3.1). HYDRUS stopped working when large volumes of water entered the domain, and the hydraulic conductivity of tailings was too low for the wetting front to progress downward. This issue resulted in sharp differences between the moisture content of adjacent nodes and prevented the program from continuing computations. Therefore, some models presented in this study have incomplete results.

The volumetric water content data extracted from observation nodes were used to calculate the degrees of saturation (*S*) at specific depths through time. The saturation versus time results were compared for all scenarios investigated in this study so that the efficacy of initial compaction and initial water content of tailings, and installation of internal capillary layers could be assessed. To have a comprehensive assessment, unsaturated hydraulic conductivity of filtered tailings for the various initial degrees of compaction and water content were calculated using van Genuchten (1980) method. Equations 3.2 or 3.3 (van Genuchten 1980) can be used to correct the saturated hydraulic conductivity based on the SWCC (from Chapter 1).

$$K_r = \frac{[1-(\alpha\psi)^{n-1}[1+(\alpha\psi)^n]^{-m}]^2}{[1+(\alpha\psi)^n]^{mP}}, \quad P=-2 \tag{3.2}$$

$$K_r = \left(\frac{\theta-\theta_r}{\theta_s-\theta_r}\right)^P \left[1-\left(1-\left(\frac{\theta-\theta_r}{\theta_s-\theta_r}\right)^{\frac{1}{m}}\right)^m\right]^2, \quad P=-2 \tag{3.3}$$

where K_r is the relative hydraulic conductivity, and *P* is a fitting parameter, usually considered -2 for fine soils. Fitting parameters to Equations 3.2 and 3.3 are the same as those of Equation 1.2. The K_r is multiplied by saturated hydraulic conductivity gives unsaturated hydraulic conductivity.

Infiltration from the top boundary and the cumulative flux from the bottom boundary were compared so that a better understanding of wetting front movement and seepage could be achieved. These output files were obtained at the end of the one-year simulation as a short-term assessment,

and at the end of the ten-year modeling as the long-term assessment. For the sake of brevity, cumulative flux outputs were divided by cumulative infiltration to provide a percentage for the contribution of tailings layers in absorbing and maintaining moisture. In other words, whether external water would turn into seepage or stay within tailings layers was evaluated.

3.3. RESULTS

3.3.1. Changes to of the degree of saturation of tailings stacks

3.3.1.1. No climatic input

Baseline simulation results from simulations of M tailings with no climatic inputs are presented in Figure 3.2. Graphs on the left of Figure 3.2 show changes of the degree of saturation of a 260-cm column of M tailings through 10 years of modeling, whereas graphs on the right show changes of the degree of saturation of a 260-cm column of M tailings placed above a 100-cm internal capillary layer of sand. As can be seen, there was effectively no difference in the degree of saturation of M tailings due to drain down or if an underlying capillary layer was included. The higher clay-size content and lower unsaturated hydraulic conductivity of M tailings maintained the degree of saturation at the as-placed condition. In other words, M tailing with initial saturation of more than 80% will maintain an oxygen ingress limiting condition in the absence of atmospheric effects. Because no external stress, viz. no atmospheric changes, were applied to the domain, the degree of saturation was also independent of the depth of the tailings.

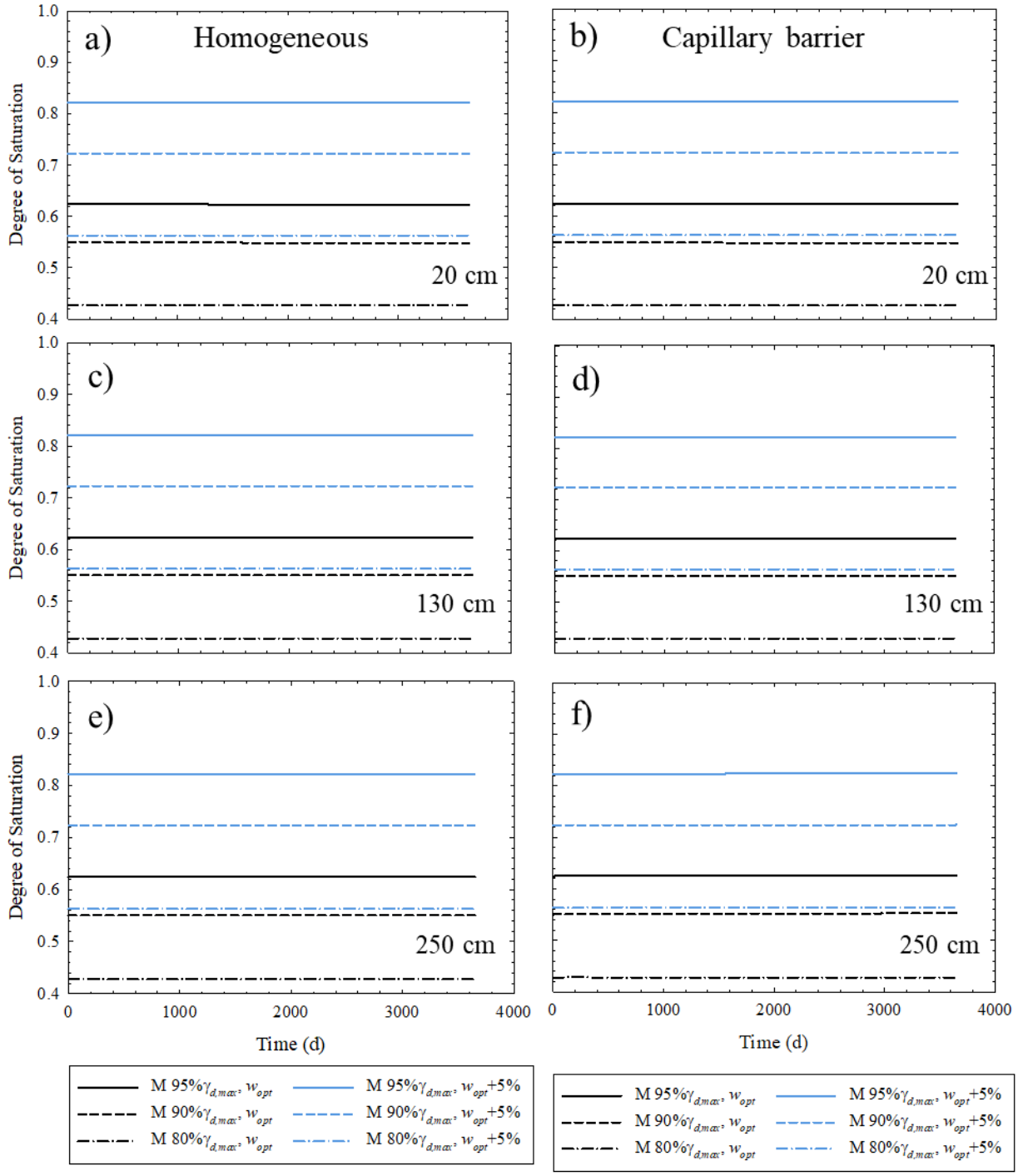

Figure 3.2 - Changes to the degree of saturation based on HYDRUS 2D outputs without considering a specific climatic condition for a 260-cm column of M tailings at the depth of (a) 20 cm, (c) 130 cm, and (e) 250 cm from ground surface, and for a column of 260-cm M tailings atop a 100-cm sandy capillary layer at the depth of (b) 20 cm, (d) 130 cm, and (f) 250 cm from ground surface. w_{opt}: Optimum water content which is 15.8%.

Baseline simulation results of P tailings with no climatic inputs are presented in Figure 3.3.

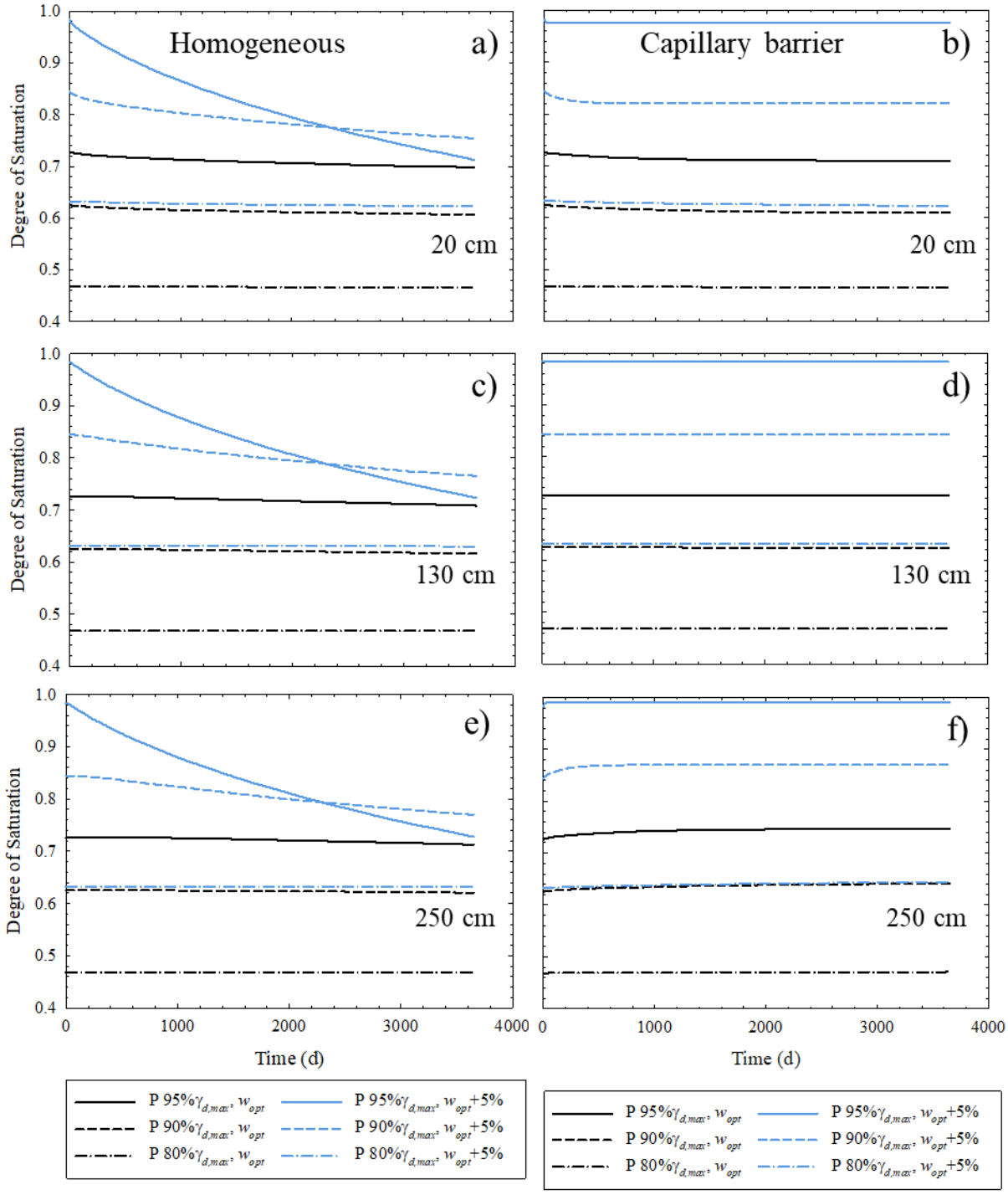

Figure 3.3 - Changes to the degree of saturation based on HYDRUS 2D outputs without considering a specific climatic condition for a 260-cm column of P tailings at the depth of (a) 20 cm, (c) 130 cm, and (e) 250 cm from ground surface, and for a column of 260-cm P tailings atop a 100-cm sandy capillary layer at the depth of (b) 20 cm, (d) 130 cm, and (f) 250 cm from ground surface. w_{opt}: Optimum water content which is 14.2%.

The capillary layer prevented substantial drain down of more in silty P tailings, which occurred without the capillary barrier, for dense P tailings (≥ 90% initial compaction) with +5% wet of optimum Proctor water content. Internal capillary barriers enabled the maintenance of a high degree of saturation (98%) for 10 years, when P tailings were initially placed dense (95% compaction) and wet of optimum water content. At shallower locations within the P tailings, the internal capillary layer slightly increased the degree of saturation, when the initial degree of saturation was approximately between 62% and 84% (independent of the initial degree of compaction). This increase, however, was not sufficient to reach saturation degrees above 80%.

3.3.1.2. Arid climate

Simulation results for M tailings considering an arid climate are presented in Figure 3.4. Similar to Figure 3.2, M tailings layers showed the same levels of *S* independent of the inclusion of a capillary layer. The relatively higher evaporation and temperature of the arid climate outweighed the minimum precipitation of this climate – this was particularly evident at depths shallower than 20 cm. At 20 cm depth, loosely placed tailings (80% compaction), whether compacted to optimum or wet of optimum water content exhibited a minor increase in the degree of saturation due to the easier infiltration of precipitation. The higher clay-size content and lower hydraulic conductivity of M tailings prevented the saturation to appreciably change. Additional discussion of the water balance of this condition is described later in this chapter.

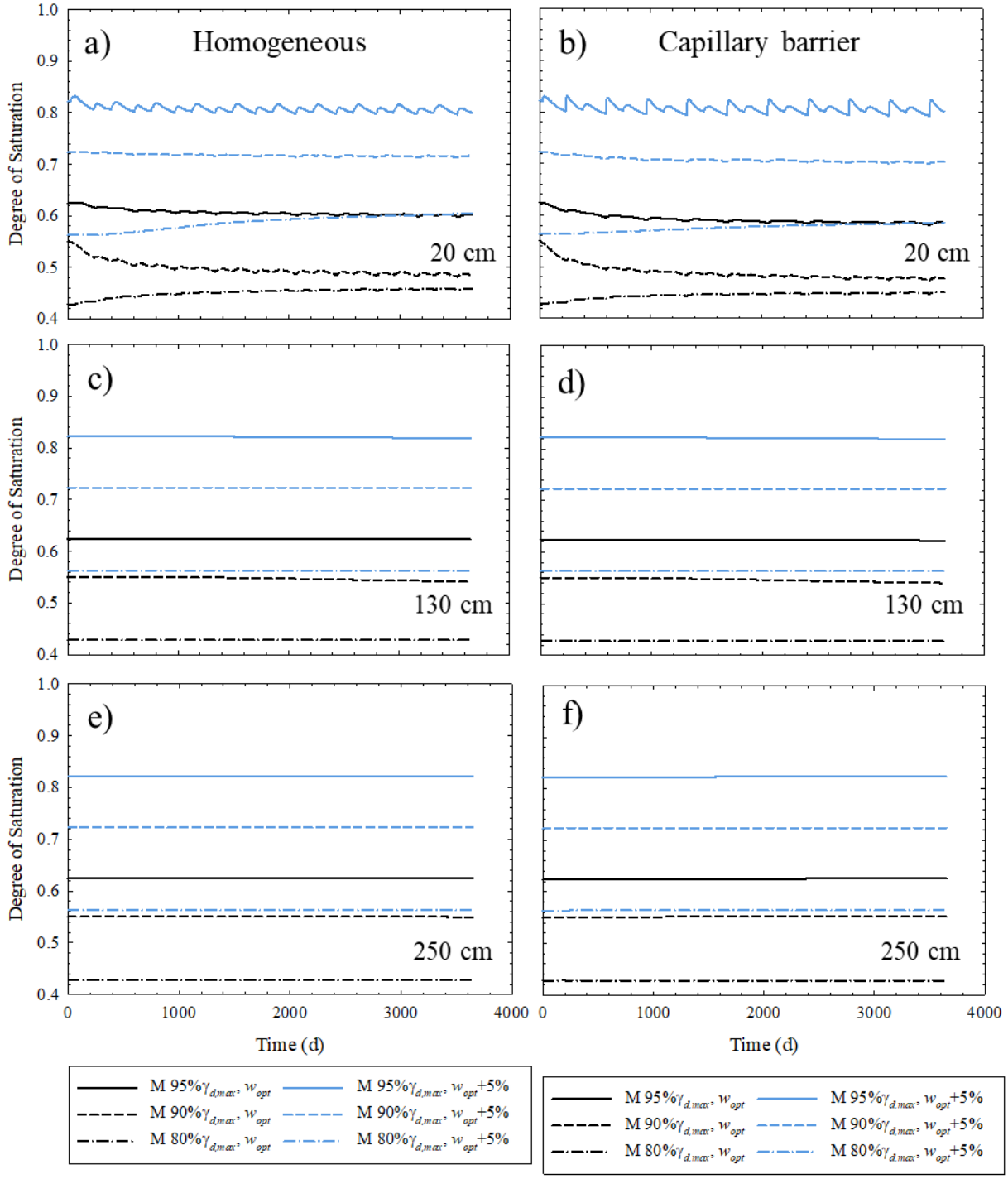

Figure 3.4 - Changes to the degree of saturation based on HYDRUS 2D outputs arid climatic condition for a 260-cm column of M tailings at the depth of (a) 20 cm, (c) 130 cm, and (e) 250 cm from ground surface, and for a column of 260-cm M tailings atop a 100-cm sandy capillary layer at the depth of (b) 20 cm, (d) 130 cm, and (f) 250 cm from ground surface. w_{opt}: Optimum water content which is 15.8%.

Simulation results of P tailings considering an arid climate are presented in Figure 3.5. Following the pattern of Figure 3.4, the saturations of P tailings layers was independent of the inclusion of a capillary layer. The silty nature of P tailings resulted in a dramatic reduction in the degree of saturation of denser tailings (≥ 90% compaction) compacted to wet of optimum water content at all depths due to evaporation. At 250 cm depth, denser P tailings (≥ 90% compaction) whether compacted to optimum or wet of optimum water content exhibited an initial minor increase in the degree of saturation due to drain down, but subsequent drying due to evaporation. Independent of placement condition, all P tailings moved to steady state saturations of less than 80%.

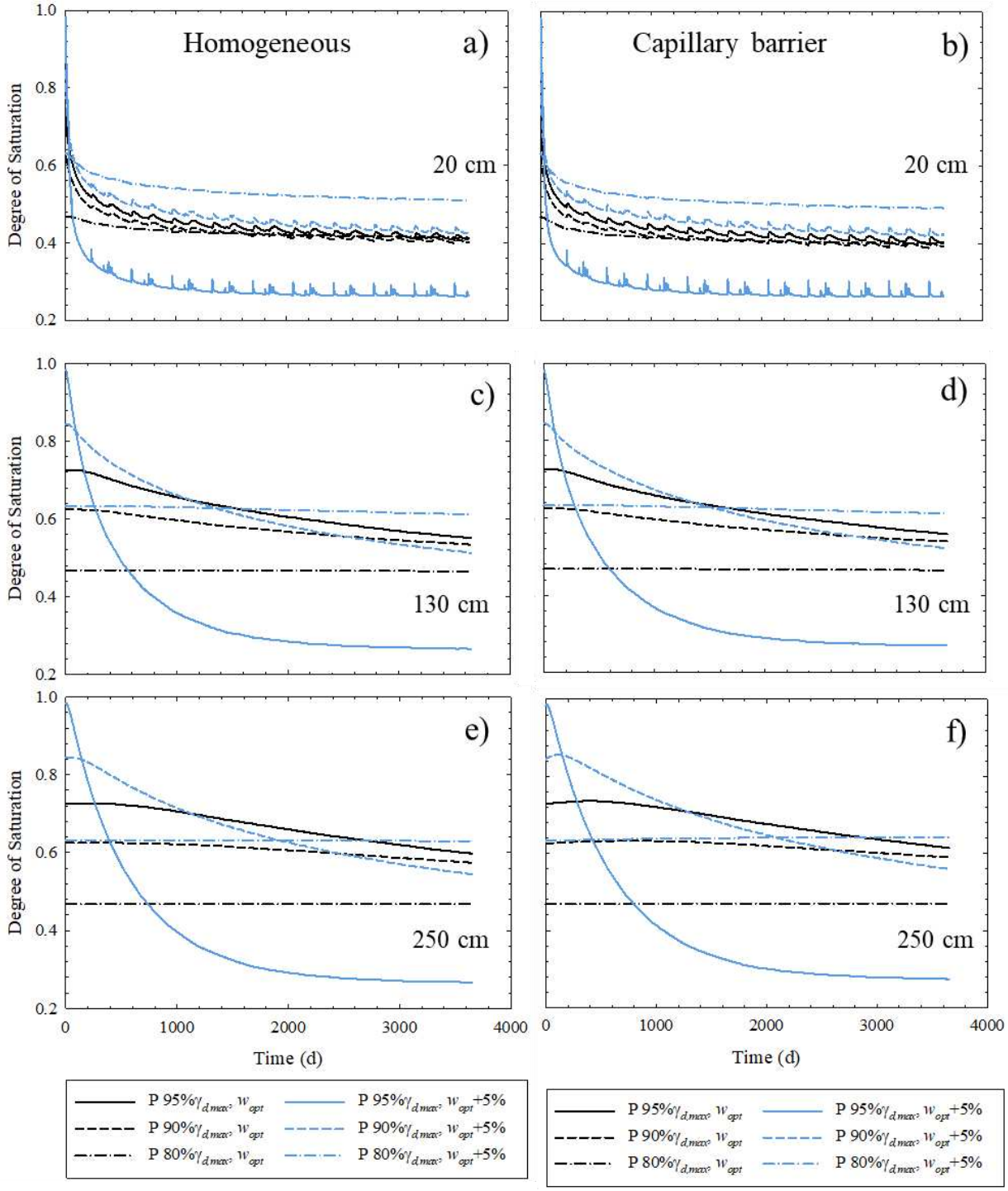

Figure 3.5 - Changes to the degree of saturation based on HYDRUS 2D outputs with arid climatic condition for a 260-cm column of P tailings at the depth of (a) 20 cm, (c) 130 cm, and (e) 250 cm from ground surface, and for a column of 260-cm P tailings atop a 100-cm sandy capillary layer at the depth of (b) 20 cm, (d) 130 cm, and (f) 250 cm from ground surface. w_{opt}: Optimum water content which is 14.2%.

3.3.1.3. Hemiboreal climate

Simulation results for M tailings considering a hemiboreal climate are presented in Figures 3.6 and 3.7. Because generated graphs from this climate had fluctuation through time, the graphs were divided into two figures so that comparing the results was visually feasible. In addition, not all graphs were generated for a full 10-year period due to model instability (described in the Methods section). The hemiboreal climate simulated has relatively high precipitation (approximately 376 mm total rainfall, 2386 mm total snowfall in 2020) and yet considerable evaporation (1086 mm total pan evaporation in 2020), resulting in significant fluctuations in the degree of saturation of tailings especially near the surface. Tailings placed at depths not affected by the high seasonal evaporation rate (in this study at depth ≥ 130 cm) experienced a considerable increase in the degree of saturation such that saturation above 80% was achieved due to downward percolation. However, the relatively high clay-size content and low hydraulic conductivity of M tailings, a degree of saturation above 80% was not initially achieved until 335 d. The lower the initial compaction of the tailings the faster the increase in the degree of saturation occurred.

Simulation results for P tailings considering a hemiboreal climate are presented in Figures 3.8 and 3.9. The oscillations in the degree of saturation were more significant for P tailings compared to M tailings. P tailings went from fully saturated to 40% saturation in about 100 d. The silty P tailings exhibited an unsteady degree of saturation, when placed 95% compacted and wet of optimum water content. Except for P tailings at 95% compacted wet of optimum, P tailings placed at depth ≥ 130 cm exhibited a considerable increase in the degree of saturation such that 80% saturation was achieved within a year.

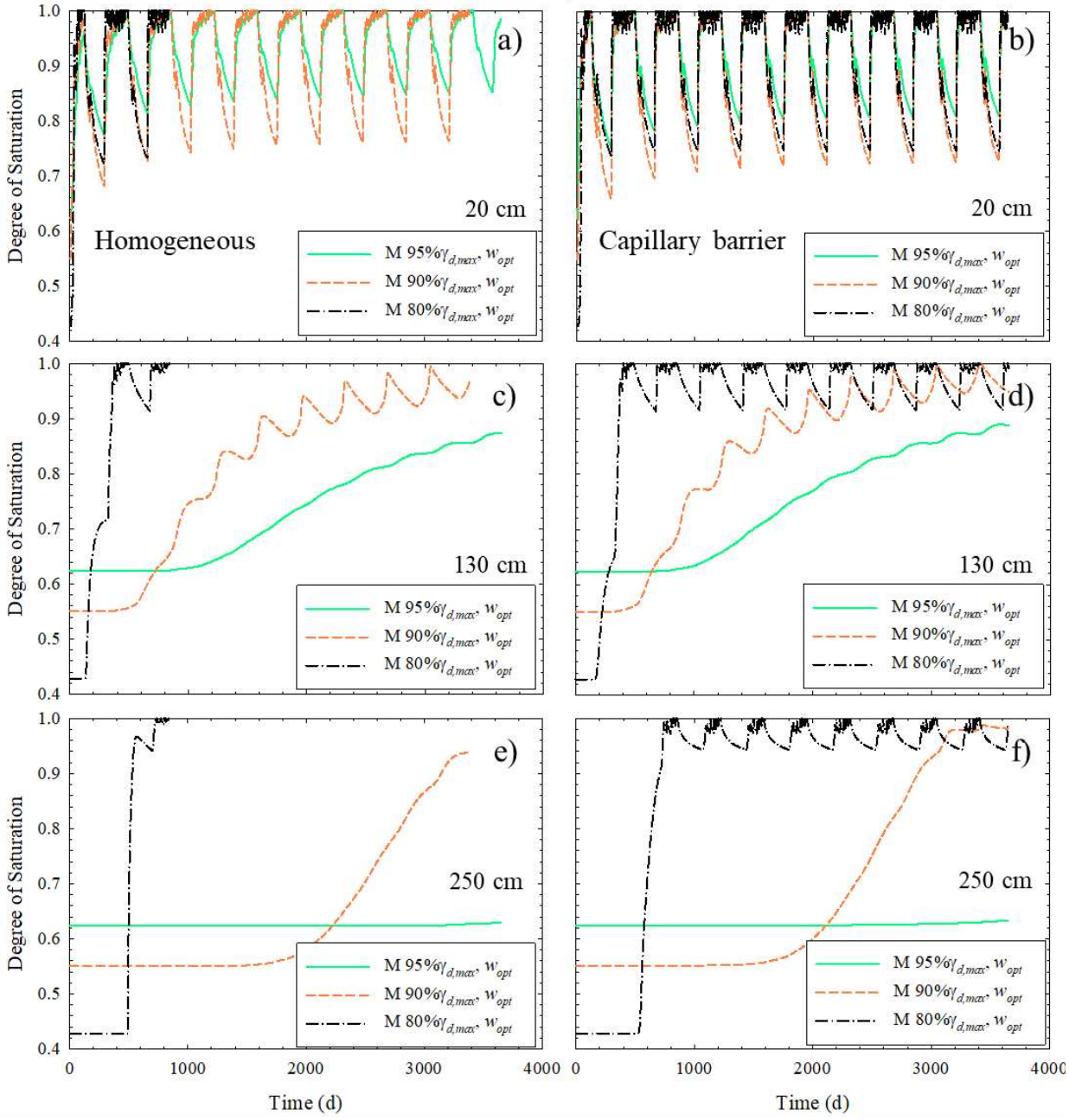

Figure 3.6 - Changes to the degree of saturation based on HYDRUS 2D outputs with hemiboreal climatic condition for a 260-cm column of M tailings initially placed at w_{opt}. Results are shown for the depth of (a) 20 cm, (c) 130 cm, and (e) 250 cm from ground surface, and for a column of 260-cm M tailings atop a 100-cm sandy capillary layer at the depth of (b) 20 cm, (d) 130 cm, and (f) 250 cm from ground surface. w_{opt}: Optimum water content which is 15.8%.

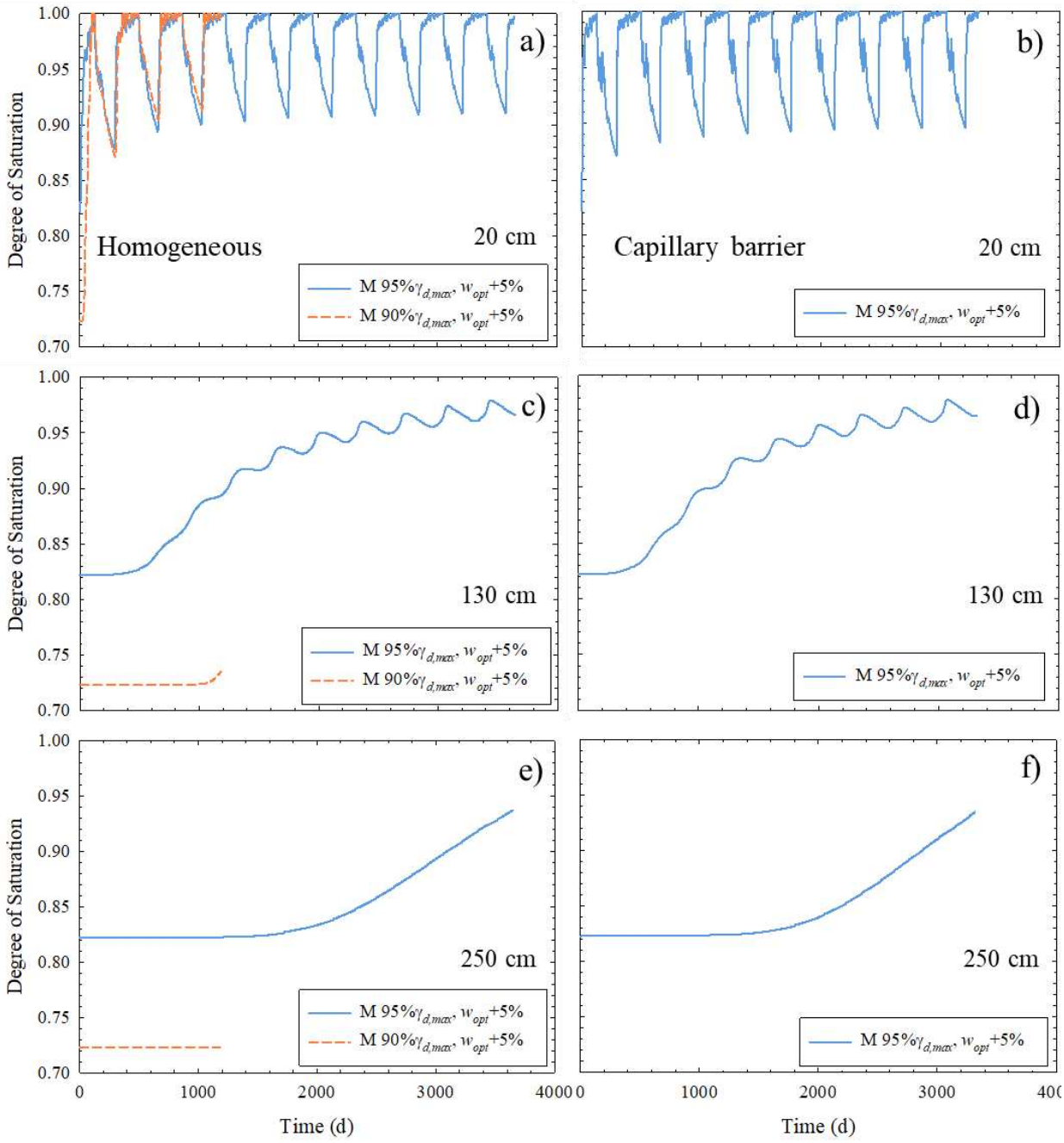

Figure 3.7 - Changes to the degree of saturation based on HYDRUS 2D outputs with hemiboreal climatic condition for a 260-cm column of M tailings initially placed at w_{opt} +5%. Results are shown for the depth of (a) 20 cm, (c) 130 cm, and (e) 250 cm from ground surface, and for a column of 260-cm M tailings atop a 100-cm sandy capillary layer at the depth of (b) 20 cm, (d) 130 cm, and (f) 250 cm from ground surface. w_{opt}: Optimum water content which is 15.8%.

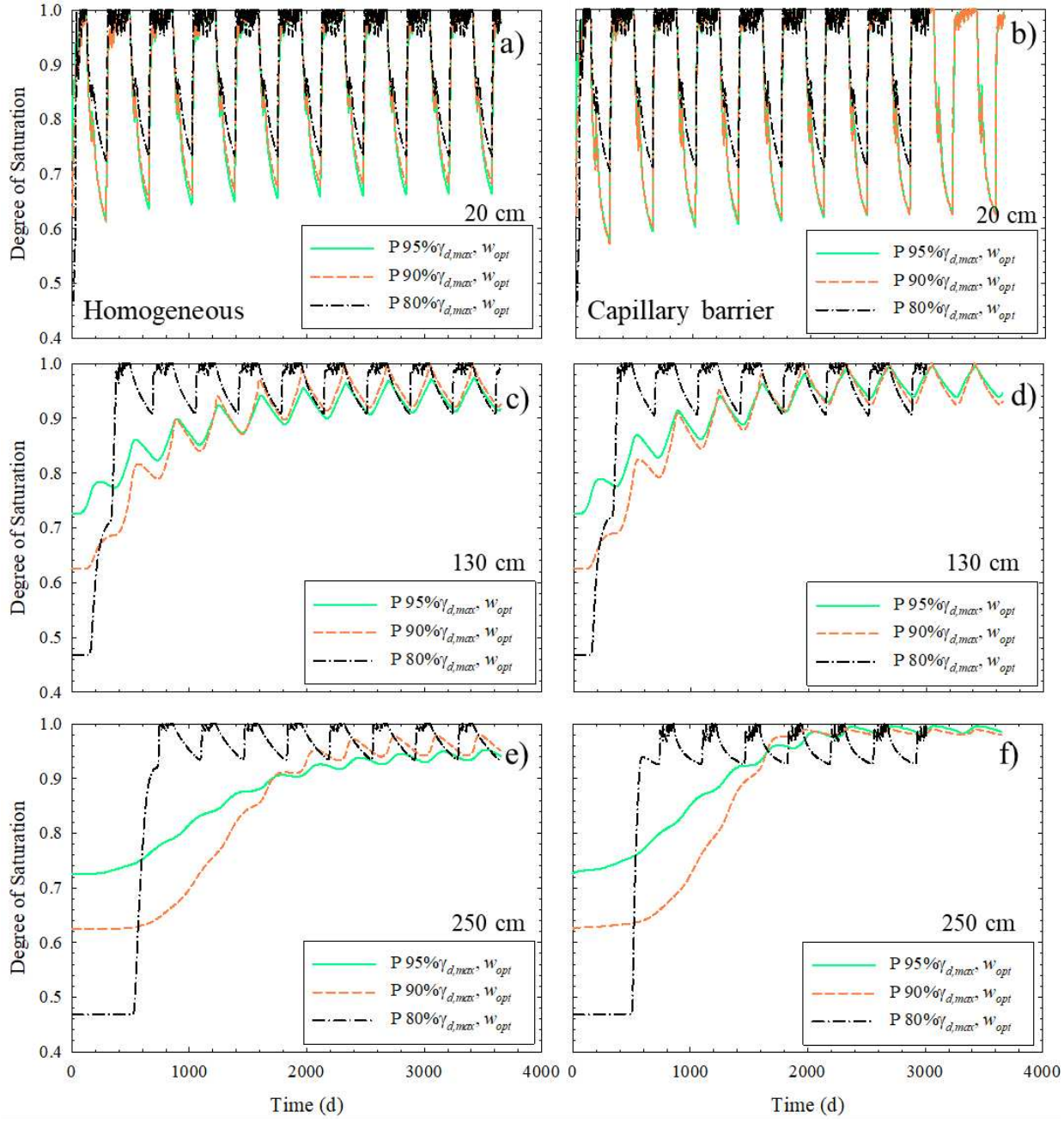

Figure 3.8 - Changes to the degree of saturation based on HYDRUS 2D outputs with hemiboreal climatic condition for a 260-cm column of P tailings initially placed at w_{opt}. Results are shown for the depth of (a) 20 cm, (c) 130 cm, and (e) 250 cm from ground surface, and for a column of 260-cm P tailings atop a 100-cm sandy capillary layer at the depth of (b) 20 cm, (d) 130 cm, and (f) 250 cm from ground surface. w_{opt}: Optimum water content which is 14.2%.

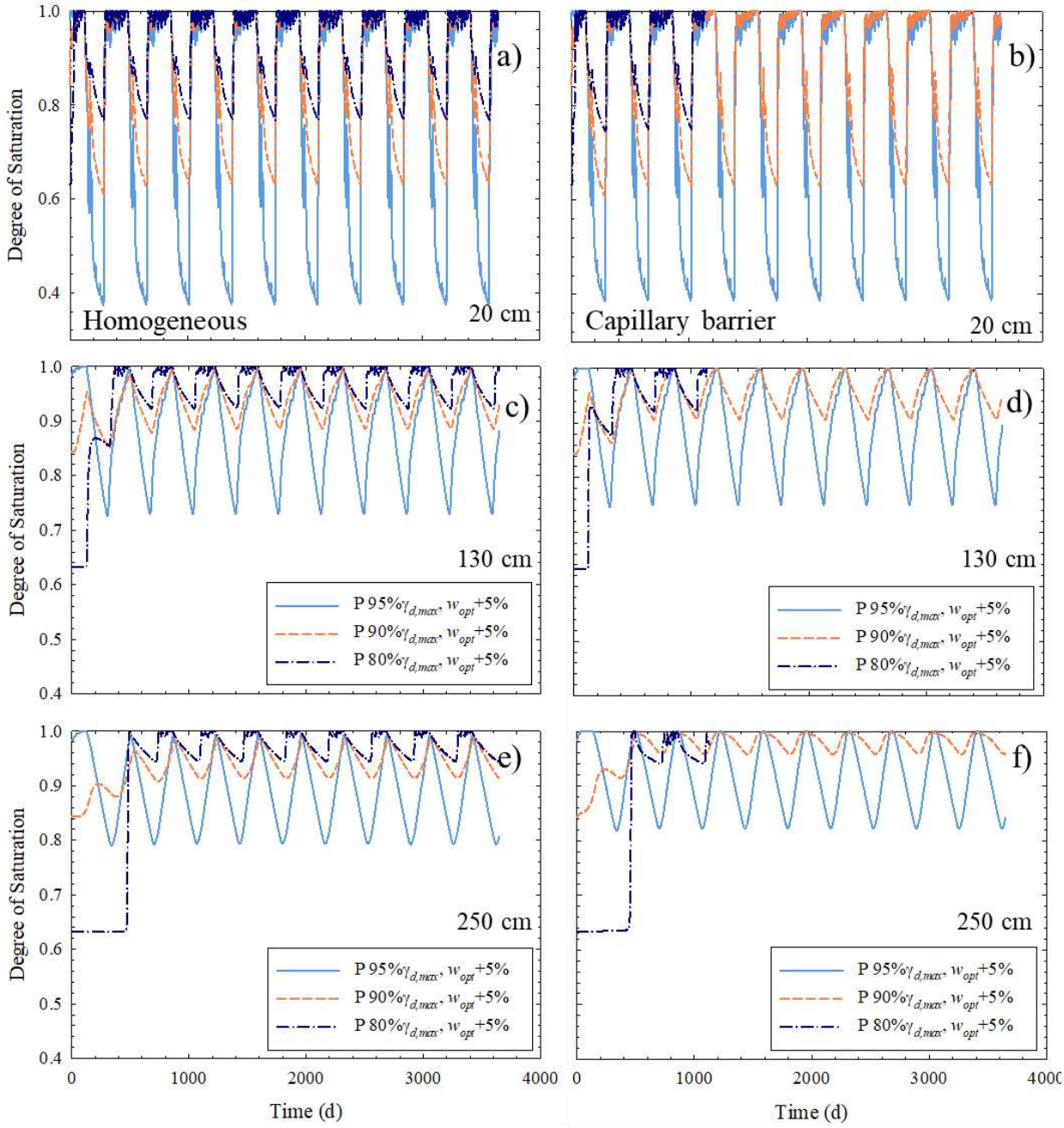

Figure 3.9 - Changes to the degree of saturation based on HYDRUS 2D outputs with hemiboreal climatic condition for a 260-cm column of P tailings initially placed at w_{opt} +5%. Results are shown for the depth of (a) 20 cm, (c) 130 cm, and (e) 250 cm from ground surface, and for a column of 260-cm P tailings atop a 100-cm sandy capillary layer at the depth of (b) 20 cm, (d) 130 cm, and (f) 250 cm from ground surface. w_{opt}: Optimum water content which is 14.2%.

3.3.1.4. Wet climate

Simulation results for M tailings considering a wet climate are presented in Figure 3.10. M tailings placed close to the ground surface were fully saturated within a few days and remained saturated thereafter. M tailings placed at any degree of compaction tended towards saturation; however, saturation at depth took more than six years depending on the initial compaction of tailings and the depth of tailings. Nonetheless, the saturated top is anticipated to be sufficient to prevent oxygen ingress.

Simulation results for P tailings considering a wet climate are presented in Figure 3.11. HYDRUS struggled to simulate the wet climate. Because full saturation was achieved rapidly in many cases and large amounts of ponded water were at the top boundary of simulated tailings, the model could not proceed with computations and crashed. Therefore, only models with sufficient visible data were presented in Figures 3.10 and 3.11. P tailings exhibited similar behavior as M tailings and thus oxygen ingress would not be the main concern in a climate as wet and cold as the climate simulated. On the other hand, the generation of excess pore water pressure and resulting geotechnical impacts are anticipated to be more important in this climate.

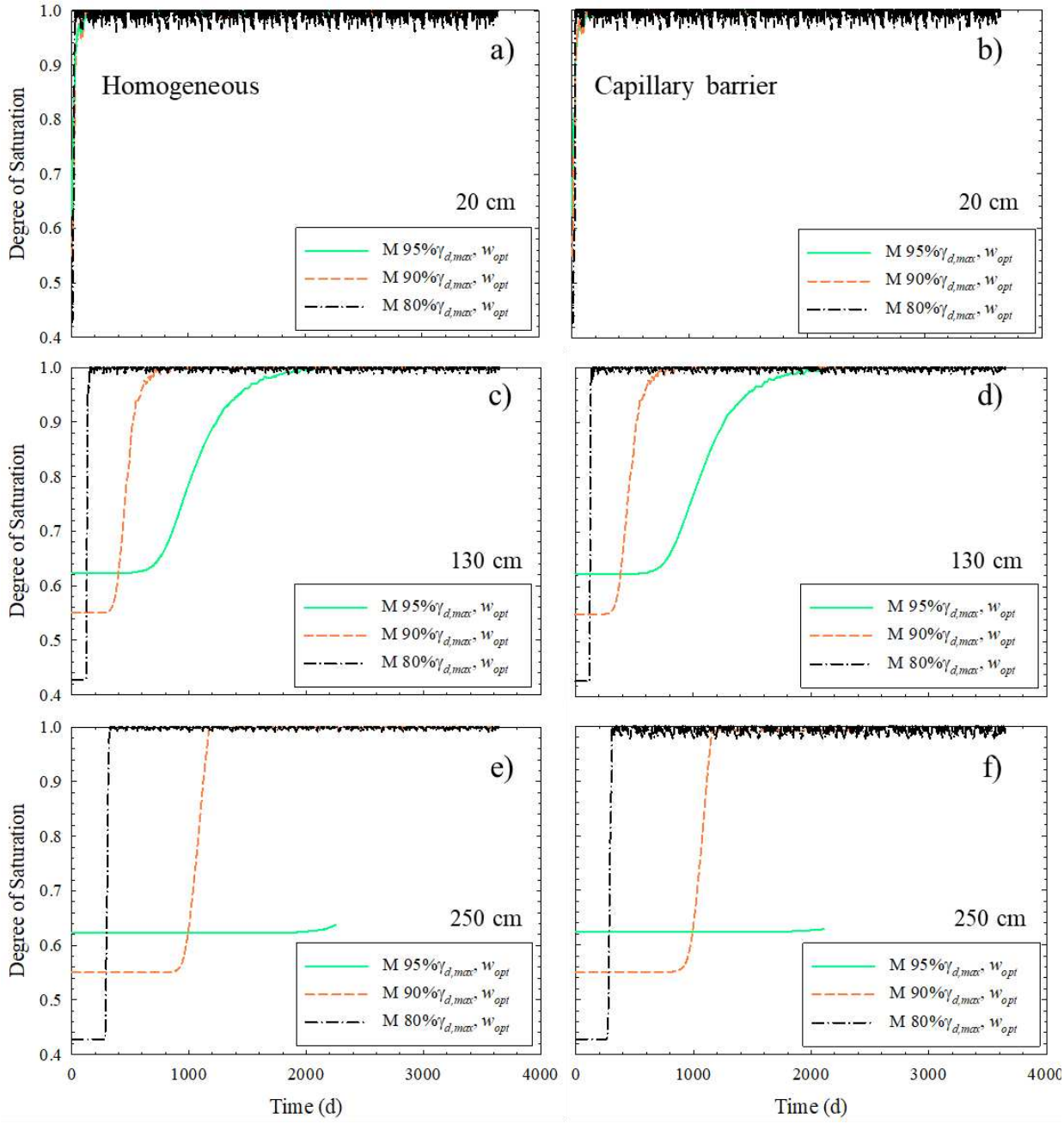

Figure 3.10 - Changes to the degree of saturation based on HYDRUS 2D outputs with the wet climatic condition for a 260-cm column of M tailings at the depth of (a) 20 cm, (c) 130 cm, and (e) 250 cm from ground surface, and for a column of 260-cm M tailings atop a 100-cm sandy capillary layer at the depth of (b) 20 cm, (d) 130 cm, and (f) 250 cm from ground surface. w_{opt}: Optimum water content which is 15.8%.

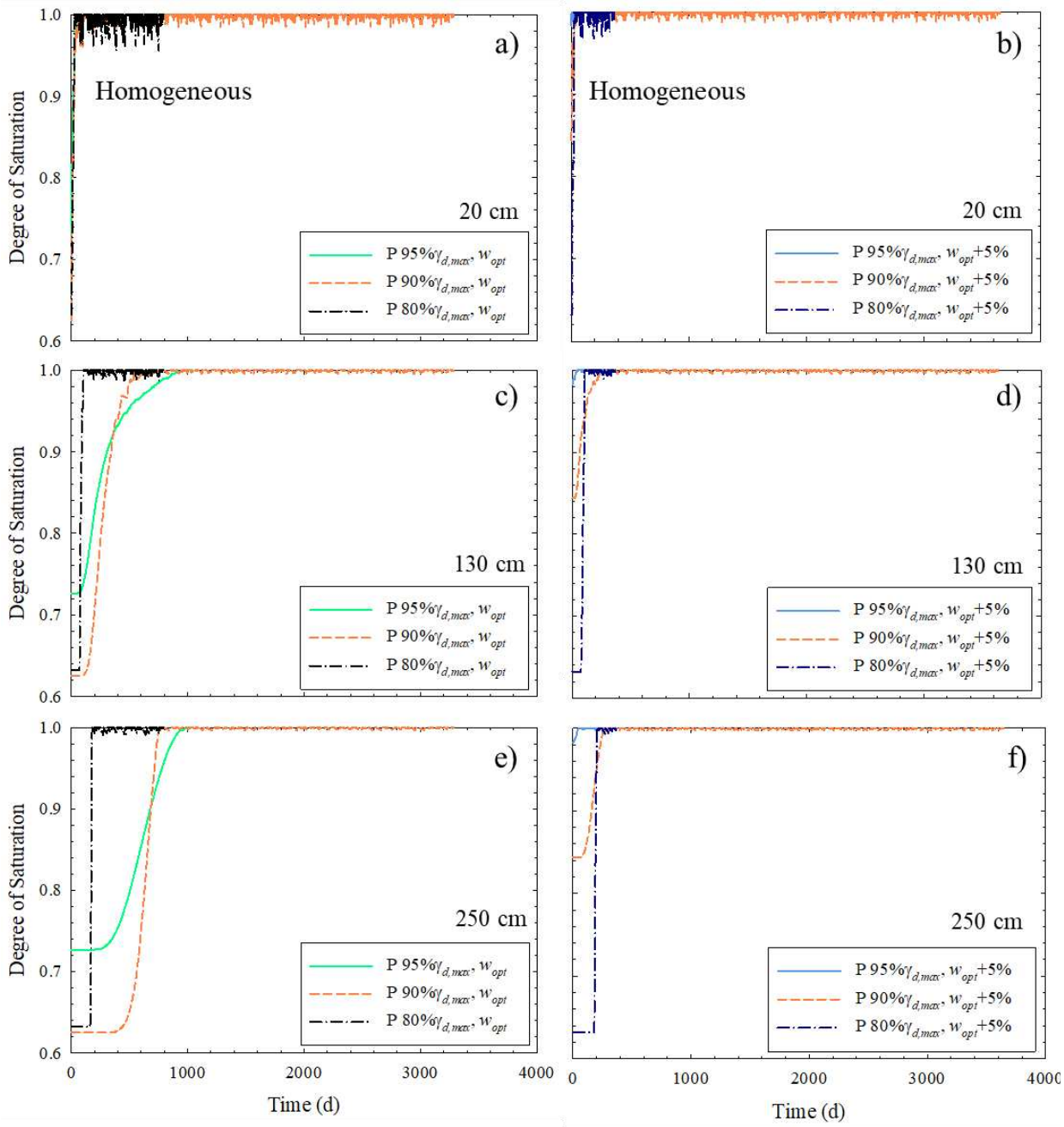

Figure 3.11 - Changes to the degree of saturation based on HYDRUS 2D outputs with the wet climatic condition for a 260-cm column of P tailings at the depth of (a, b) 20 cm, (c, d) 130 cm, and (e, f) 250 cm from ground surface. w_{opt}: Optimum water content which is 14.2%.

3.4. DISCUSSION

3.4.1. Impact of hydraulic conductivity on modeling results

Plots of unsaturated hydraulic conductivity versus matric suction of M and P tailings generated using van Genuchten (1980) method are presented in Figure 3.12. The hydraulic conductivity models in Figure 3.12 are extended to no more than 600 kPa as the van Genuchten (1980) model could not fit a curve to all the SWCC data from a tailings specimen (discussed in Chapter 2). Higher compaction of tailings resulted in lower unsaturated hydraulic conductivities for matric suctions less than 10 kPa. For matric suctions greater than 10 kPa, the unsaturated hydraulic conductivities were higher for more compacted tailings.

Figure 3.13 illustrates the relationship between unsaturated hydraulic conductivity and degree of saturation of M and P tailings. Hydraulic conductivities of more compacted tailings are generally lower than those of less compacted tailings for a given degree of saturation. M tailings, due to a higher clay-size content, showed a sharper decrease in hydraulic conductivity with decreasing saturation relative to P tailings (Figs. 3.12 and 3.13).

The degree of saturation versus time graphs in the Results section agree with the hydraulic conductivity plots in Figures 3.12 and 3.13. For instance, the extreme fluctuations of the degree of saturation of P tailings compacted wet of optimum water content in Figure 3.9 compared to less extreme fluctuations in Figure 3.8 were likely driven by the higher unsaturated hydraulic conductivity of P tailings compacted wet of optimum water content. As shown in Figure 3.13, hydraulic conductivity values of highly compacted tailings decreased markedly with small decrease in saturation. Full saturation of 95% compacted tailings does not mean all the pores filled with moisture are interconnected. Thus, a slight decrease in the degree of saturation would result in a significant reduction in the hydraulic conductivity by filling large but conductive pores with

air. The propensity of M tailings in maintaining a near constant degree of saturation at arid climates (Fig. 3.4) and hemiboreal climate (Figs. 3.6 and 3.7) appears to be driven by the low unsaturated hydraulic conductivity of these materials.

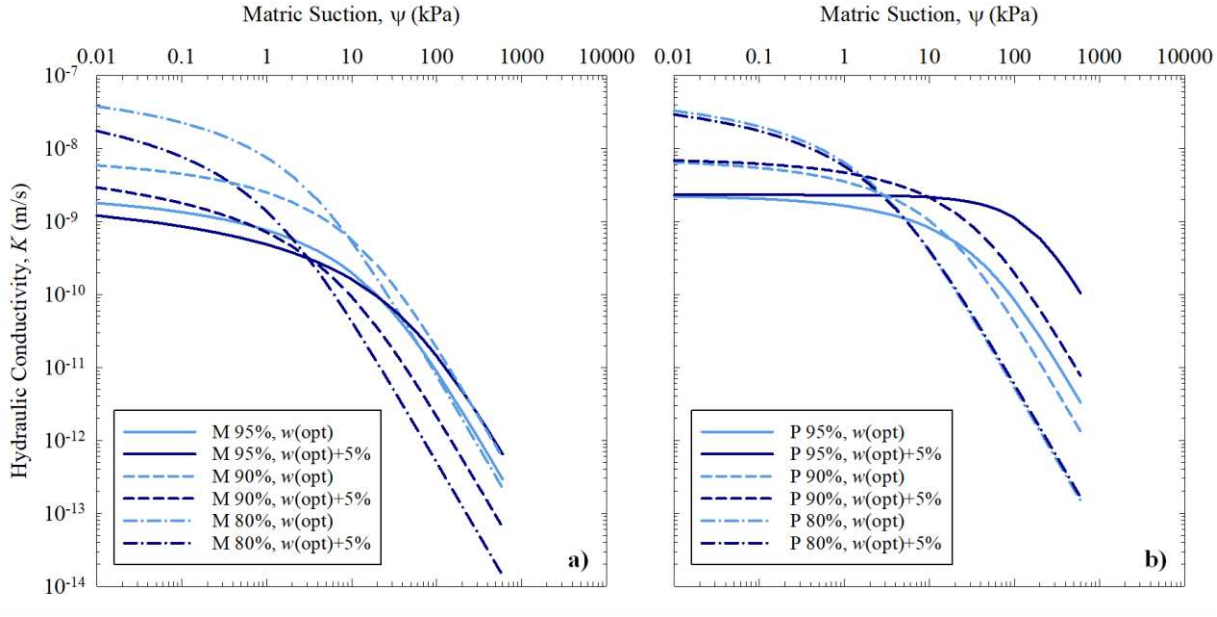

Figure 3.12 - Unsaturated hydraulic conductivity of a) M and b) P tailings versus matric suction fitted to van Genuchten (1980) model considering various initial conditions.
M = mine M tailings. P = mine P tailings, 95%: 95% compaction (95%$\gamma_{d,\,max}$), *w*(opt) = optimum water content which is 15.8% and 14.2% for M and P tailings, respectively.

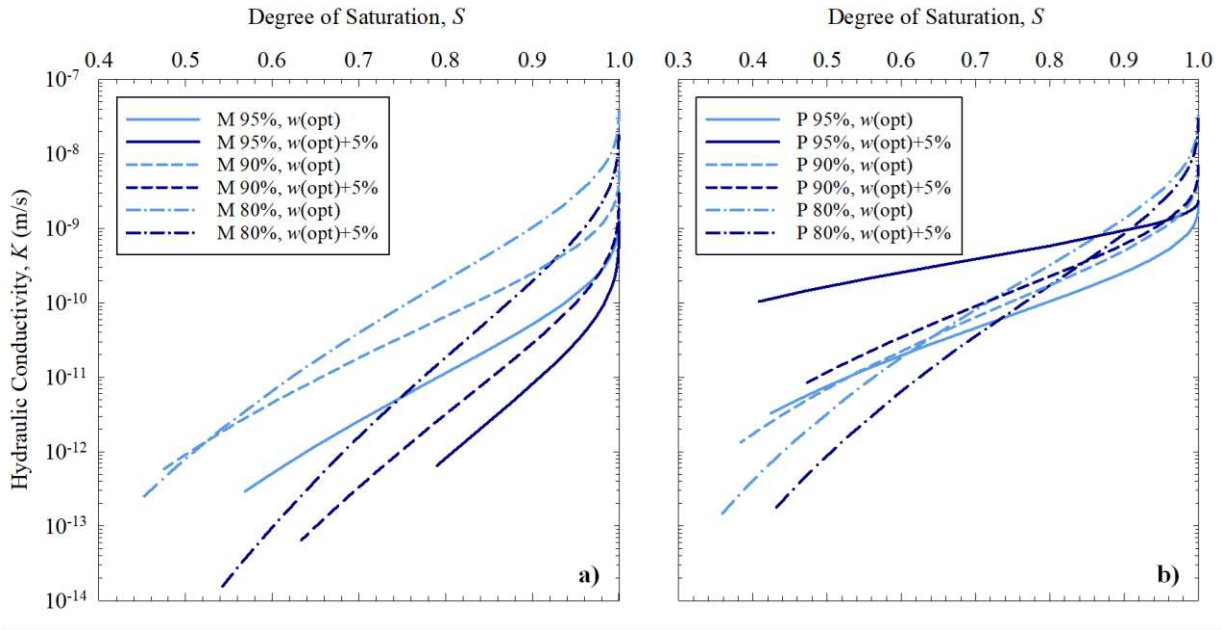

Figure 3.13 - Unsaturated hydraulic conductivity of a) M and b) P tailings versus saturation fitted to van Genuchten (1980) model considering various initial conditions.
M = mine M tailings. P = mine P tailings, 95%: 95% compaction (95%$\gamma_{d,\,max}$), w(opt) = optimum water content which is 15.8% and 14.2% for M and P tailings, respectively.

3.4.2. Impacts of considered scenarios on seepage from filtered tailings

HYDRUS provides infiltration from the top boundary and the cumulative flux from the bottom boundary which both depend on the simulated climate. In this section, seepage from filtered tailings is investigated for each climate. Cumulative downward fluxes (downward percolation) are divided by infiltration values to investigate the layer water balance. These ratios are obtained from models of one-year and two-year run time representing drain down during construction. Due to model instability, not all models were successfully run for longer durations (e.g., 10 years) but most of the models had results for two years of run time.

3.4.2.1. Arid climate

Seepage ratios from simulated M and P tailings columns in an arid climate are provided in Table 3.4. As expected, seepage ratios from tailings simulated in the arid climate were low, due to

the high evaporation rate and temperature, and low precipitation. Moreover, capillary layers reduced seepage ratios to zero, in short term or long term. Although oxygen ingress might not be prevented for tailings with the same PSD of P tailings in an arid region (Fig. 3.5), the low seepage rates from such tailings in an arid climate show a minimum risk of ARD.

Table 3.4 - The ratios of cumulative bottom seepage over the cumulative infiltration from the top of tailings columns resulting from HYDRUS 2D model in the arid climate.
ΣFlux/ΣInf: Cumulative flux from the bottom boundary over the cumulative infiltration from the top boundary. w_i: Initial gravimetric water content. w_{opt}: Optimum water content which is 15.8% and 14.2% for M and P tailings, respectively. T (tailings): A column of tailings only. T-S (Tailings-Sand): A column of tailings atop a layer of sand.

Compaction	95%		90%		80%		95%		90%		80%	
w_i	w_{opt}						w_{opt} + 5%					
M tailings	T	T-S	T	T-S	T	T-S	T	T-S	T	T-S	T	T-S
1-year ΣFlux/ΣInf (%)	0.02	0.00	0.06	0.00	0.00	0.00	0.04	0.00	0.02	0.00	0.00	0.00
2-year ΣFlux/ΣInf (%)	0.02	0.00	0.06	0.00	0.00	0.00	0.04	0.00	0.02	0.00	0.00	0.00
P tailings												
1-year ΣFlux/ΣInf (%)	1.71	0.00	0.89	0.00	0.05	0.00	21.0	0.00	9.17	0.00	0.34	0.00
2-year ΣFlux/ΣInf (%)	1.68	0.00	0.89	0.00	0.05	0.00	13.6	0.00	7.35	0.00	0.34	0.00

3.4.2.2. Hemiboreal climate

Seepage ratios from simulated M and P tailings columns in a hemiboreal climate are provided in Table 3.5. Seepage ratios were low. In this climate, substantial precipitation left the domain as runoff driven in part by the low unsaturated hydraulic conductivity of the filtered tailings. Unlike results from the arid climate, seepage rates generally increased with time in the

hemiboreal climate, however, the increase was minimal (maximum increase of 1.8% for M tailings and 7.7% for P tailings in 2 years).

Table 3.5 - The ratios of cumulative bottom seepage over the cumulative infiltration from the top of tailings columns resulting from HYDRUS 2D model in the hemiboreal climate.
ΣFlux/ΣInf: Cumulative flux from the bottom boundary over the cumulative infiltration from the top boundary. w_i: Initial gravimetric water content. w_{opt}: Optimum water content which is 15.8% and 14.2% for M and P tailings, respectively. T (tailings): A column of tailings only. T-S (Tailings-Sand): A column of tailings atop a layer of sand. NA: Not available.

Compaction	95%		90%		80%		95%		90%		80%	
w_i			w_{opt}				w_{opt} + 5%					
M tailings	T	T-S	T	T-S	T	T-S	T	T-S	T	T-S	T	T-S
1-year ΣFlux/ΣInf (%)	0.00	0.00	0.00	0.00	0.00	0.00	0.00	0.00	0.00	0.00	NA	NA
2-year ΣFlux/ΣInf (%)	0.00	0.00	0.00	0.00	1.85	0.00	0.00	0.00	0.00	0.00	NA	NA
P tailings												
1-year ΣFlux/ΣInf (%)	0.11	0.00	0.06	0.00	0.00	0.00	2.61	0.24	0.95	0.00	0.02	0.00
2-year ΣFlux/ΣInf (%)	0.16	0.00	0.07	0.00	6.02	6.16	2.09	0.16	1.68	0.50	7.16	7.75

3.4.2.3. Wet climate

Seepage ratios from simulated M tailings columns in a wet climate are provided in Table 4.6. Except for M tailings with 80% initial compaction, both filtered tailings and filtered tailings underlain by sand generated low seepage ratios. High precipitation primarily exited the model domain as runoff due to the low hydraulic conductivity of the filtered tailings. These results illustrate the potential importance of proof rolling and managing runoff to prevent ponding and erosion, but also that flux of dissolved oxygen may not be a substantial driver of ARD due to low hydraulic conductivities for M type tailings.

Table 3.6 - The ratios of cumulative bottom seepage over the cumulative infiltration from the top of M tailings and P tailings columns resulting from HYDRUS 2D model in the wet climate.
ΣFlux/ΣInf: Cumulative flux from the bottom boundary over the cumulative infiltration from the top boundary. w_i: Initial gravimetric water content. w_{opt}: Optimum water content which is 15.8% for M tailings. Optimum water content which is 14.2% for P tailings. T (tailings): A column of tailings only. T-S (Tailings-Sand): A column of tailings atop a layer of sand.

Compaction	95%		90%		80%		95%		90%		80%	
w_i			w_{opt}				w_{opt} + 5%					
M tailings	T	T-S	T	T-S	T	T-S	T	T-S	T	T-S	T	T-S
1-year ΣFlux/ΣInf (%)	0.00	0.00	0.01	0.00	7.09	5.26	NA	NA	NA	NA	NA	NA
2-year ΣFlux/ΣInf (%)	0.00	0.00	0.01	0.00	28.7	27.8	NA	NA	NA	NA	NA	NA
P tailings												
1-year ΣFlux/ΣInf (%)	0.21	NA	0.10	NA	25.8	NA	11.3	NA	7.75	NA	20.5	NA
2-year ΣFlux/ΣInf (%)	0.27	NA	0.26	NA	36.5	NA	NA	NA	13.8	NA	NA	NA

Seepage ratios from simulated P tailings columns in a wet climate are also provided in Table 3.6. The higher unsaturated hydraulic conductivity of P tailings in comparison to M tailings led to considerable seepage ratios.

3.5. SUMMARY AND CONCLUSIONS

The potential efficacy of filtered tailings, and filtered tailings with internal capillary barriers in creating conditions to minimize ARD was investigated. This study focused on the during-construction water balance, and how the geochemical of a filtered tailings stack is driven by a combination of climate, storage, and unsaturated hydraulic conductivity. The investigations were performed by numerical modeling via HYDRUS-2D for arid, hemiboreal, and wet climates,

and for no-climatic inputs (baseline) conditions. Numerical models were parameterized with lab-derived material parameters and SWCCs of two mine tailings (M and P tailings) with various initial as-placement conditions. The interpretations provided in this study can assist practitioners to understand how filtered tailings layers will hydrologically influence ARD behavior in different climates. Conclusions drawn from this study are summarized subsequently.

- The characteristics of M tailings with relatively higher clay-size content and lower unsaturated hydraulic conductivity was sufficient to maintain the as-placed degree of saturation when no climatic inputs were modeled. However, internal capillary barriers were found to be efficient for more silty P tailings to prevented sharp reductions in the degree of saturation due to drain down.

- The degree of saturation decreased substantially in models with the arid climate for both M and P tailings independent of capillary layer inclusion. The high evaporation rate and temperature, and low precipitation drove water removal. However, seepage rates from simulated filtered tailings in the arid climate were *de minimis* or zero leading decreased likelihood of ARD.

- Internal capillary barriers reduced seepage rate from filtered tailings in the hemiboreal and wet climatic conditions for M and P tailings. However, inclusion of capillary layers did not impact the degree of saturation in simulated M and P tailings mainly due to the relatively high evaporation rate compared to precipitation in the hemiboreal climate, and high precipitation in the wet climate. Filtered tailings rapidly reached saturation in both climatic conditions independent of capillary layer installation, lowering concerns for oxygen ingress.

- Dense M and P tailings (≥ 90% compaction) simulated with a hemiboreal climate reached 80% saturation but underwent seasonal fluctuations in saturation. In addition, higher compaction was effective at minimizing seepage via low hydraulic conductivities. Capillary barriers were not effective at preventing seepage in hemiboreal climatic conditions

- Generation of excess pore pressure could be the main concern independent of the degree of compaction in the wet climate because tailings reached 80% saturation rapidly and maintained that degree of saturation. Seepage was also largely minimized by the low hydraulic conductivity of the filtered tailings despite near saturated conditions.

References

Akcil, A., and Koldas, S. (2006). "Acid mine drainage (AMD): causes, treatment and case studies," *Journal of Cleaner Production*, 14(12-13), 1139-1145.

Aghazamani N., Scalia VI, J., Bareither, C.A. (2021). "Assessing the generation of positive excess pore pressure during undrained compression of unsaturated filtered tailings," Tailings and Mine Waste Conference, Banff, Alberta, Canada.

ASTM D422-63, (2007). "Standard test method for particle-size analysis of soils," West Conshohocken, PA, www.astm.org, DOI: 10.1520/D0422-63R07E02.

ASTM D2487-11, (2011). "Standard practice for classification of soils for engineering purposes (unified soil classification system)," West Conshohocken, PA, www.astm.org, DOI: 10.1520/D2487-11.

ASTM D4318-10, (2014). "Standard test methods for liquid limit, plastic limit, and plasticity index of soils," West Conshohocken, PA, PA, www.astm.org, DOI: 10.1520/D4318-10.

ASTM D698-12, (2014). "Standard test methods for laboratory compaction characteristics of soil using standard effort (12400ft-lbf/ft3 (600 kN-m/m3))," West Conshohocken, PA.

ASTM D854-14, (2014). "Standard test methods for specific gravity of soil solids by water pycnometer," West Conshohocken, PA, www.astm.org, DOI: 10.1520/D0854-14.

ASTM D6836-16, (2016). "Standard test methods for determination of the soil water characteristic curve for desorption using hanging column, pressure extractor, chilled mirror hygrometer, or centrifuge," ASTM International, West Conshohocken, PA, www.astm.org.

Barbour, S. L. (1998). "The soil-water characteristic curve: A historic perspective," *Canadian Geotechnical Journal*, Vol. 35, No. 5, 873-894.

Barden, L., Madedor, A.O., Sides, G.R. (1969). "Volume change characteristics of unsaturated clay," *Journal of the Soil Mechanics and Foundation Division*, ASCE.

Bicalho, K.V., Znidarcic, D., Ko, H.Y. (2000). "Air entrapment effects on hydraulic properties," Geo-Denver Conference, Denver, Colorado, DOI: 10.1061/40510(287)34.

Bishop, A.W. (1959). "The principles of effective stress," *Teknisk ukeblad*, Vol. 39 (106), 849-863.

Bolduc, F., Aubertin, M. (2014). "Numerical investigation of the influence of waste rock inclusions on tailings consolidation," *Canadian Geotechnical Journal*, 51, 1021-1032, DOI: 10.1139/cgj-2013-0137.

Borja, R., and Bareither, C. (2020). "Shear behavior of waste rock and filtered tailings." In proceedings of Geo-Congress 2020: Geotechnical Earthquake Engineering and Special Topics, American Society of Civil Engineers, USA.

Bossé, B., Bussière, B., Hakkou, R., Maqsoud, A, Benzaazoua, M. (2013). "Assessment of phosphate limestone wastes as a component of a store-and-release cover in a semiarid climate," *Mine Water Environment*, 32, 152-167, DOI 10.1007/s10230-013-0225-9.

Brawner, C.O. (1978). "Concepts and experience for subsurface storage of tailings," In proceeding of the 2nd International Tailings Symposium, Denver, Colorado, Edited by Argall, G.O., *Miller Freeman Publications Inc.*, San Francisco, California, 153-177.

Burland, J.B. (1965). "Some aspects of the mechanical behavior of partly saturated soils," Moisture equilibria and moisture changes beneath covered areas, symposium, Butterworths, Sydney, 270–278.

Bussière, B., Aubertin, M., Chapuis, R. (2003). "The behavior of inclined covers used as oxygen barriers," *Canadian Geotechnical Journal*, Vol. 40, 512-535, DOI: 10.1139/T03-001.

Bussière, B. (2007). "Hydrogeotechnical properties of hard rock tailings from metal mines and emerging geo-environmental disposal approaches," *Canadian Geotechnical Journal*, Vol. 44, 1019-1052.

Casey, B. (2014). "The consolidation and strength behavior of mechanically compressed fine-grained sediments," PhD dissertation, Massachusetts Institute of Technology.

Childs, E. C. (1969). "Soil Water Phenomena," Wiley Inter-science, New York.

Chiu, T.F., Shackelford, C.D. (1998). "Unsaturated hydraulic conductivity of compacted sand-kaolin mixtures," *Journal of Geotechnical Engineering, ASCE*, Vol. 124(2), 160-170.

Compton, P.V. (1970). "A study of the swelling behavior of an expansive clay as influenced by the clay microstructure, soil suction, and external loading," Technical report No. AFWL-TR-70-26, Air Force Weapons Laboratory, New Mexico.

Corey, A.T. (1994). "Mechanics of immiscible fluids in porous media," 3rd Edition Water Resources Publications, Highlands Ranch, Colorado.

Daniel, D. (1994). State-of-the-art: laboratory hydraulic conductivity tests for saturated soils. ASTM STP 1142. American Society for Testing and Materials, Philadelphia, PA, USA.

Davies, M. (2018). "Filtered Dry Stacked Tailings-The Fundamentals," Tailings & Mine Waste Conference 2018, Vancouver, BC, Canada, DOI: 10.14288/1.0107683.

Dong, Y., Lu, N. (2017) "Measurement of Suction-Stress Characteristic Curve under Drying and Wetting Conditions," *Geotechnical Testing Journal*, Vol. 40, N. 1, 107-121, DOI: 10.1520/GTJ20160058.

Drumright, E.E. (1989). “The contribution of matric suction to the shear strength of unsaturated soils,” PhD dissertation, Colorado State University, Ft Collins.

Dunn, C.S. (1965). “Developments in the design of triaxial equipment for testing compacted soils,” Proceedings of symposium on the economic use of soil testing in site investigation, Birmingham.

Escario, V., Saez, J. (1986). “The shear strength of partly saturated soils,” *Geotechnique*, 36 (3), 453-456, DOI: 10.1680/geot.1986.36.3.453.

Ferdosi, B., James, M. (2015). “Investigation of the Effect of Waste Rock Inclusions Configuration on the Seismic Performance of a Tailings Impoundment,” *Geotechnical and Geological Engineering Journal* ,33, 1519-1537, DOI: 10.1007/s10706-015-9919-z.

Fonseca do Carmo, F., Kamino, L., Tabias Jr. R., Christina de Campos, I., Fonseca do Carmo, F., Silvino, G., Xavier de Castro, K., Mauro, M., Rodrigues, N., Miranda, M., and Pinto, C. (2017). Fundão Tailings Dam Failures: The Environment Tragedy of the Largest Technological Disaster of Brazilian Mining in Global Context. *Perspectives in Ecology and Conservation*, 15, 145-151. DOI: 10.1016/j.pecon.2017.06.002.

Fredlund, D.G. (1973), “Volume change behavior of unsaturated soils,” PhD dissertation, University of Alberta, Edmonton, Canada.

Fredlund, D.G., Hasan, J. (1973). “One-dimensional consolidation theory: unsaturated soils,” *Canadian Geotechnical Journal*, 16 (3), 521-531, DOI: 10.1139/t79-058.

Fredlund, D.G., Morgenstern, N.R. 1977. “Stress state variables for unsaturated soils,” Journal of the Geotechnical Engineering Division, ASCE, 103 (GT5), 447-466.

Fredlund, D. G., Xing, A. (1994). “Equations for the soil-water characteristic curve,” *Canadian Geotechnical Journal*, 31(3): 521-532.

Fredlund, D.G., Xing, A., Huang, S. (1994). “Predicting the permeability function for unsaturated soils using the soil-water characteristic curve,” *Canadian Geotechnical Journal*, 31(3): 521-532.

Fredlund, D. G., Xing, A., Fredlund, M. D., Barbour, S. L. (1996). “The relationship of the unsaturated soil shear strength to the soil-water characteristic curve,” *Canadian Geotechnical Journal*, Vol. 33, pp. 440–448.

Fredlund, M. D. (2000). “The role of Unsaturated Soil Property Functions in the Practice of Unsaturated Soil Mechanics,” PhD Dissertation, University of Saskatchewan, Saskatoon, Saskatchewan, Canada.

Fredlund, M. D., Wilson, G.W., and Fredlund, D.G. (2002). "Representation and estimation of the shrinkage curve," UNSAT 2002, Proceedings of the Third International Conference on Unsaturated Soils, Recife, Brazil, March 10–13, pp. 145–149.

Fredlund, D.G., Rahardjo, H., Fredlund, M.D. (2012). "Compressibility and Pore Pressure Parameters," John Wiley & Sons Inc.

Fredlund, D.G., Houston, S.L. (2013). "Interpretation of soil-water characteristic curves when volume change occurs as soil suction is changed," Advances in Unsaturated Soils - Proceedings of the 1st Pan-American Conference on Unsaturated Soils, PanAmUNSAT, Cartagena de Indias, Colombia, 15-31.

Gorakhki, M.R.H., Bareither, C.A., Scalia, J, and Jacobs, M. (2019). Hydraulic conductivity and soil water retention of waste rock and tailings mixtures, GeoCongress 2019 GSP 312, ASCE, 41-50. DOI: 10.1061/9780784482148.005.

Gorakhki, M.R. (2020). "Enhancing mine waste disposal using tailings-dominated waste rock and tailings mixture," Ph.D. dissertation, Colorado State University, Fort Collins, Colorado.

Hamade, M. M. (2017). "Undrained Shear Behavior of Mixed Mine Waste Rock and Tailings," MS Thesis, Civil and Environmental Engineering, Colorado State University, Fort Collins, Colorado, 95 p.

ICOLD 2018. "Tailings Dam Design Technology Update." International Commission on Large Dams Commission Internationale des Grands Barrages, Paris, France.

James, M., Aubertin, M., Bussière, B., PEdnault, C., Pépin, N., Limoges, M. 2017. "A research project on the use of waste rock inclusions to improve the performance of tailings impoundments," GEO Ottawa-2017 conference.

Khalili, N., Khabbaz, M.H. 1996. "The concept of effective stress in unsaturated soils," UNICIV Report No. R-360, ISBN: 85841 327 2, The University of New South Wales, Sydney, Australia.

Liu, J.C., Znidarčić, D. (1991). "Modeling one-dimensional compression characteristics of soils," *Journal of Geotechnical Engineering*, 117(1), 162-169, DOI: 10.1061/(ASCE)0733-9410(1991)117:1(162).

Lu, N., Likos, W.J. (2004). "Unsaturated Soil Mechanics," John Wiley & Sons Inc.

Lu, N., Likos, W.J. (2006). "Suction Stress Characteristic Curve for Unsaturated Soil," *Journal of Geotechnical and Geoenvironmental Engineering, ASCE*, DOI: 10.1061/(ASCE)1090-0241(2006)132:2(131).

Lu, N., Godt, J.W., Wu, D.T. (2010). "A closed-form equation for effective stress in unsaturated soil," *Water Resources Research Journal*, Vol. 46, W05515, DOI: 10.1029/2009WR008646.

Lu, N. (2016) "Generalized soil water retention equation for adsorption and capillarity," *Journal of Geotechnical and Geoenvironmental Engineering*, Vol. 142, DOI: 10.1061/(ASCE)GT.1943-5606.0001524.

Lupo, J., Hall, J. (2010). "Dry Stack Tailings – Design Considerations," 14th Tailings & Mine Waste Conference 2010, Vail, Colorado, 327-335, ISBN 978-0-415-61455-9.

Matyas, E.L. (1967). "Air and water permeability of compacted soils," ASTM STP 417 American Society of Testing and Materials, Philadelphia, PA, 160-175.

Matyas, E.L., Radhakrishna, H.S. (1968). "Volume change characteristics of partially saturated soils," *Geotechnique*, 18 (4), 432-448.

Mendoza, C.A., Therrien, R., Sudicky, E.A. (1991). ORTHOFEM User's Guide, Version 1.02. Waterloo Centre for Groundwater Research, Univ. of Waterloo, Waterloo, Ontario, Canada.

Morgenstern, N., van Zyl, D., and Vick, S. (2015). Independent Expert Engineering Investigation and Review Panel Report on Mount Polley Tailings Storage Facility Breach. Government of British Columbia. January 30, 2015.

Morgenstern, N., Vick, S., Viotti, C., and Watts, B. (2016). Fundão Tailings Dam Review Panel Report on the Immediate Causes of the Failure of the Fundão Dam. August 25, 2016.

Munroe, E.A., McLemore,V.T., Kyle, P. (1999). "Waste rock pile characterization, heterogeneity, and geochemical anomalies in the Hillsboro Mining District, Sierra County, New Mexico," *Journal of Geochemical Exploration*, Vol. 67, 391–405.

National Centers for Environmental Information website (*www.ncdc.noaa.gov*).

Petticrew, E., Albers, S., Baldwin, S., Carmack, E., Derby, S., Gantner, N., Graves, K., Laval, B., Morrison, J., Owens, P., Selbie, D., and Vagle, S. (2015). The Impact of a Catastrophic Mine Tailings Impoundment Spill into One of North America's Largest Fjord Lakes: Quesnel Lak, British Columbia, Canada. *Geophysical Research Letters*, 3347-3355. DOI: 10.1002/2015GL063345.

Pham, H. Q., Fredlund, D. G., Barbour, S. L. (2002). "A simple soil-water hysteresis model for predicting the boundary wetting curve," Proceedings of the fifty fifth Canadian geotechnical conference, Ground and water-Theory to practice, Niagara Falls, ON, 1261-1267.

Pham, H. Q., Fredlund, D. G., Barbour, S. L. (2003a). "A practical hysteresis model for the soil-water characteristic curve for soils with negligible volume change," *Geotechnique*, Vol. 53, No. 2, 293-298.

Pham, H. Q., Fredlund, D. G., Barbour, S. L. (2003b). "Estimation of the hysteresis soil-water characteristic curves from the drying boundary curve," Proceedings of the fifty sixth Canadian geotechnical conference, Winnipeg, MB, Vol. 2, 115-121.

Qiu, Y., Sego, D.C (2001). "Laboratory properties of mine tailings," *Canadian Geotechnical Journal*, Vol. 38, 183-190, DOI: 10.1139/cgj-38-1-183.

Robertson, P., Melo, L., Williams, D., and Wilson, G. (2019). Report of the Expert Panel on the Technical Causes of the Failure of Feijão Dam I.

Simms, P. (2021). "The role of unsaturated soil mechanics in unconventional tailings deposition," *Soils and Rocks*, 44 (3), DOI: 10.28927/SR.2021.066721.

Somogyi, F. (1979). "Analysis and Prediction of Phosphatic Clay Consolidation," Implementation Package, Lakeland, Florida: Florida Phosphatic Clay Res.

Song, Y. (2014) "Suction stress in unsaturated sand at different relative densities," *Journal of Engineering Geology*, 1-10

Terzaghi, K. (1936). "The shearing resistance of saturated soils and the angle between the planes of shear," on Proceedings of the international conference on Soil Mechanics and Foundation Engineering by Casagrande, A., Rutledge, P.C., Watson, J.D. (eds.), Vol. I, 54–56. Harvard University.

Terzaghi, K. (1943). "Theoretical soil mechanics," Wiley, New York.

van Genuchten, M. T. (1980). "A closed-form equation for predicting the hydraulic conductivity of unsaturated soils." *Soil Science Society of America Journal*, Vol. 44 (5): 892.

Wang, X., Benson, C., H. (2004). "Leak-free pressure plate extractor for measuring the soil water characteristic curve," *Geotechnical Testing Journal, ASTM*, Vol. 27, No. 2.

Wang, C., Harbottle, D., Liu, Q., Xu, Z. (2014). "Current state of fine mineral tailings treatment: A critical review on theory and practice," *Minerals Engineering Journal*, Vol. 58, 113-131.

Western Region Climatic Center, *wrcc.dri.edu*.

Wickland, B.E., Wilson, G.W. (2005). "Self-weight consolidation of mixtures of mine waste and tailings," *Canadian Geotechnical Journal*, Vol. 42, 327-339.

Wickland, B.E., Wilson, G.W., Wijewickreme, D., Klein, B. (2006). "Design and evaluation of mixtures of mine waste rock and tailings," *Canadian Geotechnical Journal*, Vol. 43, 928-945.

Wickland, B.E., Wilson, G.W., Wijewickreme, D. (2010). "Hydraulic conductivity and consolidation response of mixtures of mine waste rock and tailings," *Canadian Geotechnical Journal*, Vol. 47, 472-485.

Zhang, C., and Lu, N. (2018). "What is the range of soil water density? Critical reviews with a unified model," *Reviews of Geophysics*, Vol. 56 (3), 532– 562.

Zhang, C., Lu, N. (2020). "Unified Effective Stress Equation for Soil," *Journal of Engineering Mechanics, ASCE*, 146(2): 04019135, DOI: 10.1061/ (ASCE) EM.1943-7889.0001718.

Appendix

A1. ROWE CELL TEST SETUP

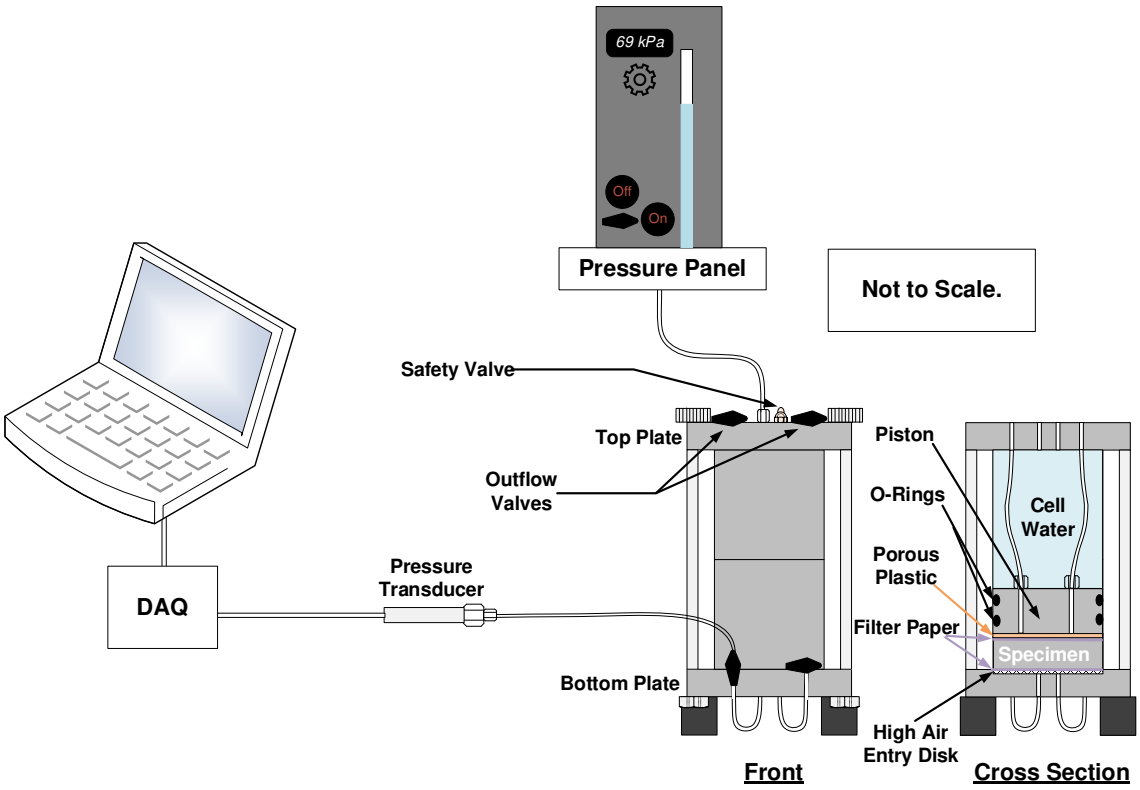

Figure A1 - Schematic of Rowe cell test setup components, running an undrained compression test

A2. INITIAL COMPRESSION TEST METHOD, MATERIAL, AND RESULTS

The undrained compression test method explained in section 2.3.3 was the result of early trials. In this section, initial compression test method, which has led to the final method, is explained. The results from these early-stage tests are discussed later in this section. Large strain compression tests at CSU were first performed on nine filtered tailings samples provided by the industry as part of a preliminary assessment of the use of filtered tailings for a planned mine; these tests are summarized in Table A1. All the compression tests mentioned in Table A1 were semi-drained compression tests as requested by the industry sponsor. In a semi-drained compression test, air is allowed to exit the system because one of the top outflow valves of the apparatus is open to the atmosphere.

Table A1 - Filter cake samples properties (initial tests).

Tailings #	w (%)	w_{opt} (%)	Wet/Dry of Optimum	Max Dry Unit Weight (pcf)	G_s	Significant u_e Measured?
T1	44.0	19.5	24.5	102	2.71	Yes
T2	29.1	33.0	-3.90	86.8	2.80	No
T3	30.0	29.2	0.800	91.5	2.67	Yes
T4	33.0	37.0	-4.00	80.4	2.76	No
T5	33.0	48.0	-15.0	75.5	3.21	Yes
T6	42.0	41.6	0.400	76.0	2.72	Yes
T7	36.0	33.0	3.00	86.0	2.74	Yes
T8	41.1	41.1	0.000	78.5	2.77	Yes
T9	23.4	24.2	-0.800	97.1	2.75	No

One partially full 1-gallon Ziploc bag of each filter cake was received for testing. Received filter cakes had been dewatered to the gravimetric water contents anticipated to be relevant for a

tailings stack. No additional information regarding the composition of these materials (soil characteristics, mineralogy, etc.) was received. Prior to testing, filter cakes were passed through a #4 sieve (Figure A2).

Figure A2 - Filter cake samples getting passed through a #4 sieve

Because the test was new, different methods were being evaluated. Tailings T2, T3, T4, T5, T6, and T7 were deposited into the cell to a height of approximately 4 cm, without compaction. Tailings T1, however, as the first experiment was filled to approximately 9 cm of the cell in Figure A3.

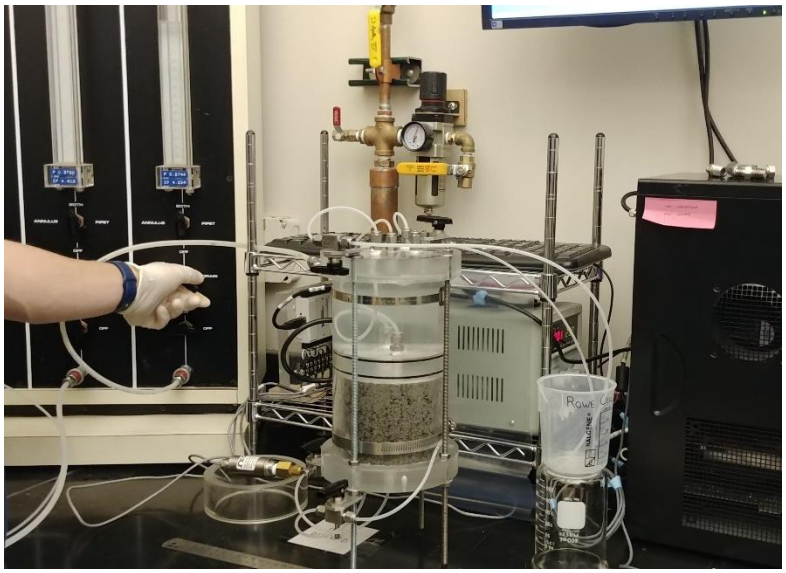

Figure A3 - Undrained compression apparatus used for testing sample T1.

The setup shown in Figure A3 was used for T1 test, and the rest of the samples were tested using the setup shown in Figure 2.2. For tests on T8 and T9, the specimens were compacted to 95% standard Proctor maximum dry unit weight, $\gamma_{d,max}$, into the cell to a height of 2.5 cm. Higher thicknesses for the specimens elongated test duration incredibly based on the experience with T1 test. Compaction of filtered tailings inside the cell of the initial setup in Figure A3 could not be sufficiently accurate, while compaction inside the cell of the setup in Figure 2.2 was easier and more precise.

The cell water is pressurized incrementally at each load step to apply total vertical stress on the specimen. The σ_v applied in compression tests were (numbers in parentheses are in psi) 14 (2,) 34 (5), 69 (10), 103 (15), 138 (20), 172 (25), 207 (30), 241 (35), 276 (40), 310 (45), 345 (50), 379 (55), 414 (60), 448 (65), 483 (70), 517 (75), and 552 (80) kPa respectively. Based on testing requirements provided by the industry sponsor, the magnitude of generated u_e did not matter, and only the load magnitude which generated a positive u_e was targeted. Tests on samples listed in

Table A1 were continued until a measurable amount of u_e (more than 0.1 V ≅ 2.1 kPa) was captured by the pressure transducer, and then tests were terminated. However, the test on T1 was continued for more load steps to see the trend of potential increase/decrease in u_e.

In the initial seven tests, specimens were loaded rapidly, such that as soon as the rate of specimen compression began to slow noticeably, the next load was added (typically < 1 min). These specimens were all loosely placed.

For the test on T8, a 24 h time interval was chosen between each load step; however, at load step of 103 kPa, more time was allowed to evaluate how long the dissipation of the generated u_e would require. The generated u_e did not dissipate for seven days under constant load, instead continued to increase until termination of the test. Even though this test was semi drained, the rate of water leaving the specimen was negligible.

For the test on T9, a 24 h time interval was also used between each load step; however, due to the COVID-19 CSU closure, the test had to be expedited and starting at the 69 kPa load step, load increments lasted for only an hour. No u_e generation was observed for T9.

Table A2 provides a summary of initial conditions for all nine tests along with the critical degree of saturation, S_{crit} at which a measurable u_e was generated.

Table A2 - Filtered tailings specifications for the initial nine compression tests.

Tailings #	w (%)	Wet/Dry of Optimum	Initial Degree of Compaction	Initial S (%)	S_{crit} (%)	Test Speed	Significant u_e Measured?
T1	44.0	24.5	Not compacted	52.0	75.0	Fast	Yes
T2	29.1	-3.90	Not compacted	26.0	-	Fast	No
T3	30.0	0.800	Not compacted	25.0	83.0	Fast	Yes
T4	33.0	-4.00	Not compacted	38.0	-	Fast	No
T5	33.0	-15.0	Not compacted	29.0	66.0	Fast	Yes
T6	42.0	0.400	Not compacted	36.0	63.0	Fast	Yes
T7	36.0	3.00	Not compacted	42.0	75.0	Fast	Yes
T8	41.1	0.000	95% $\gamma_{d,max}$	86.3	87.4	Slow	Yes
T9	23.4	-0.800	95% $\gamma_{d,max}$	67.0	-	Slow then Fast	No

Compression test results are presented in Figure A4. Time intervals between each load increments substantially affected test results, such that if a load step was maintained for 24 h, u_e generation might have been observed for some of the rapid-loading experiments. Figure A5 provides trends of u_e generation for the six tests for which u_e was observed. Specimens T1, T6, and T8 show a jump in u_e and a reduction afterward. This trend was due to the test being semi drained and the specimens not compacted.

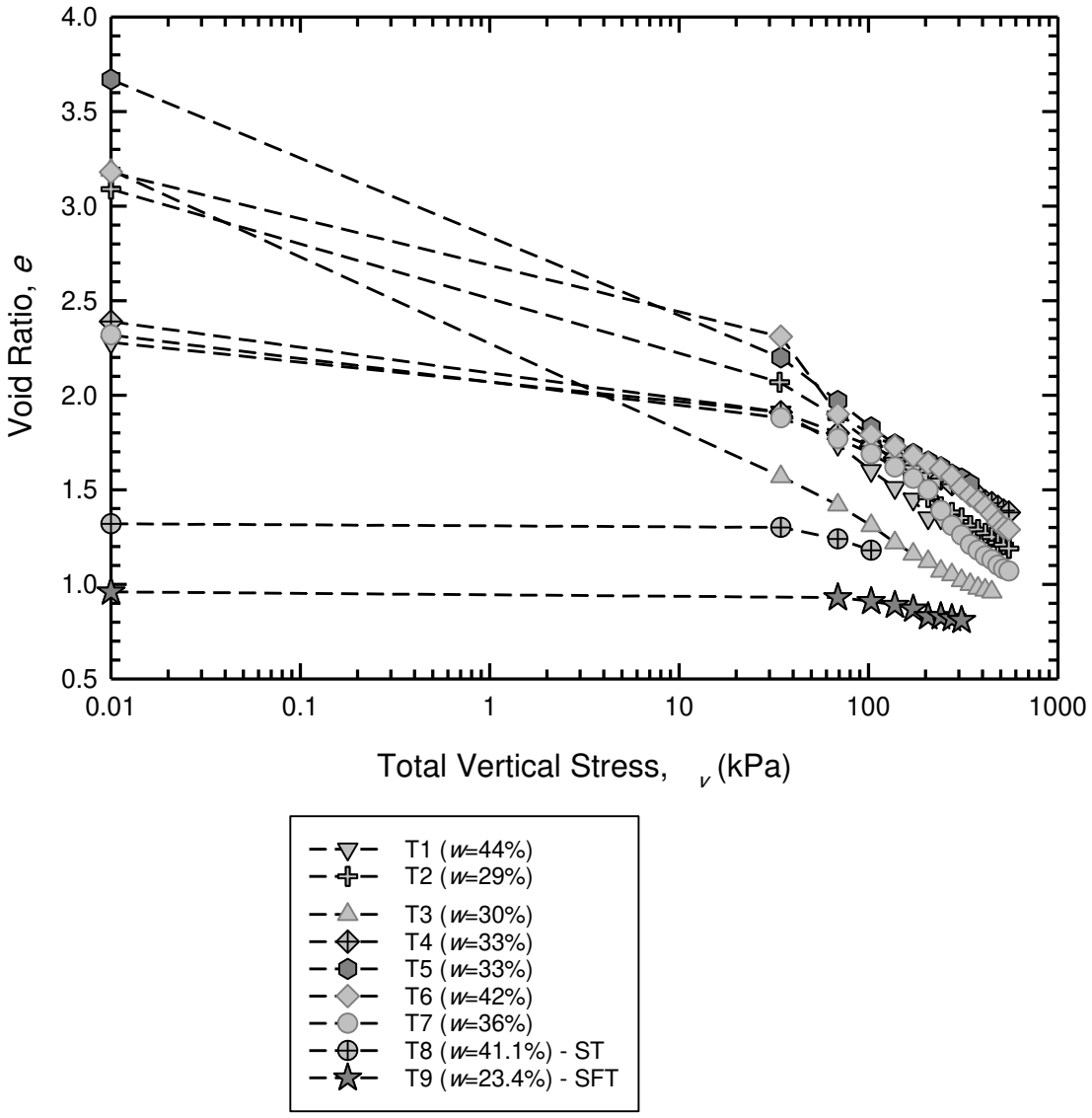

Figure A4 - Initial compression test results. ST: Slow Test. SFT: Slow then Fast Test.

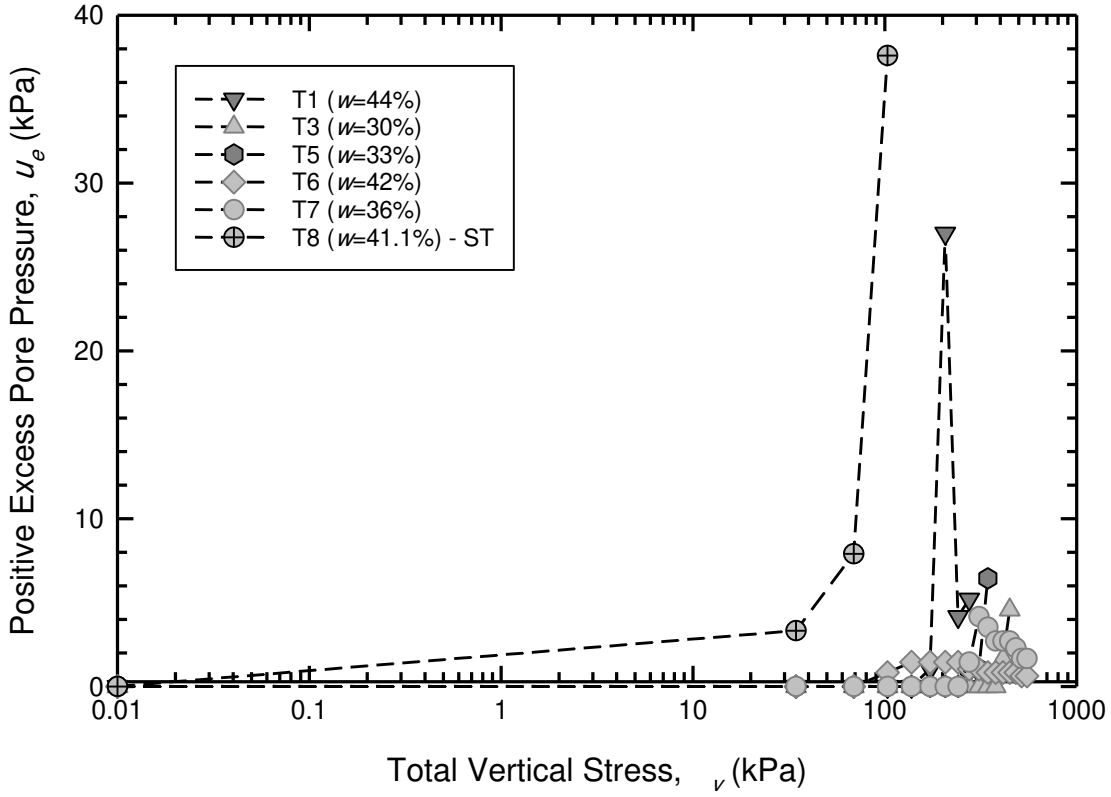

Figure A5 - Specimens that exhibited positive u_e generation during testing. ST: Slow Test.

Figure A6a shows the relationship between the degree of saturation and the generation of positive u_e. Figure A6b shows the relationship between ρ_d of the specimen and generation of positive u_e. Figures A6 illustrates that if sufficient time is not provided between load steps, the increase in u_e compounds. These compression tests generally show that specimens with high initial void ratios (2.3 to 3.67) exhibited u_e generation at higher stresses (103 to 413 kPa), independent of how frequently successive load increments were added. When specimens were not fully compacted, u_e was able to be dissipated rapidly. Results from these tests indicate that although u_e can be generated at medium S in filtered tailings, the rapid dissipation of the generated u_e can be expedited when the filter cake is not compacted initially.

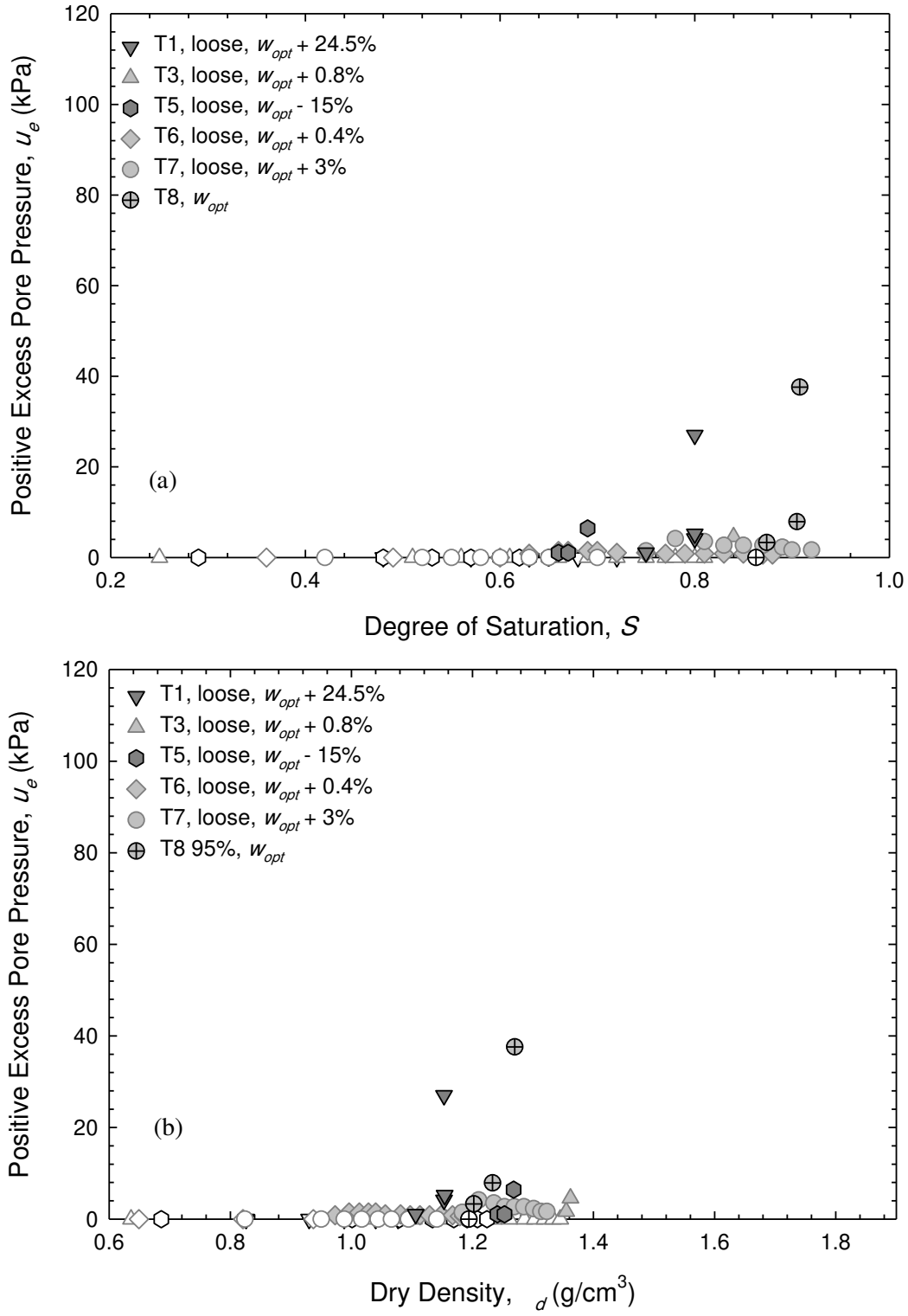

Figure A6 - a) Trend of positive u_e generation as S increases. b) Trend of positive u_e generation as ρ_d increases. Empty symbols: significant u_e not generated.

A3. RESULTS FROM COMPRESSION TESTS AND CONFIRMATORY TESTS

Results from the undrained large-strain compression tests and unsaturated and saturated confirmatory tests on M tailings and P tailings are provided in Figures A7 and A8, respectively.

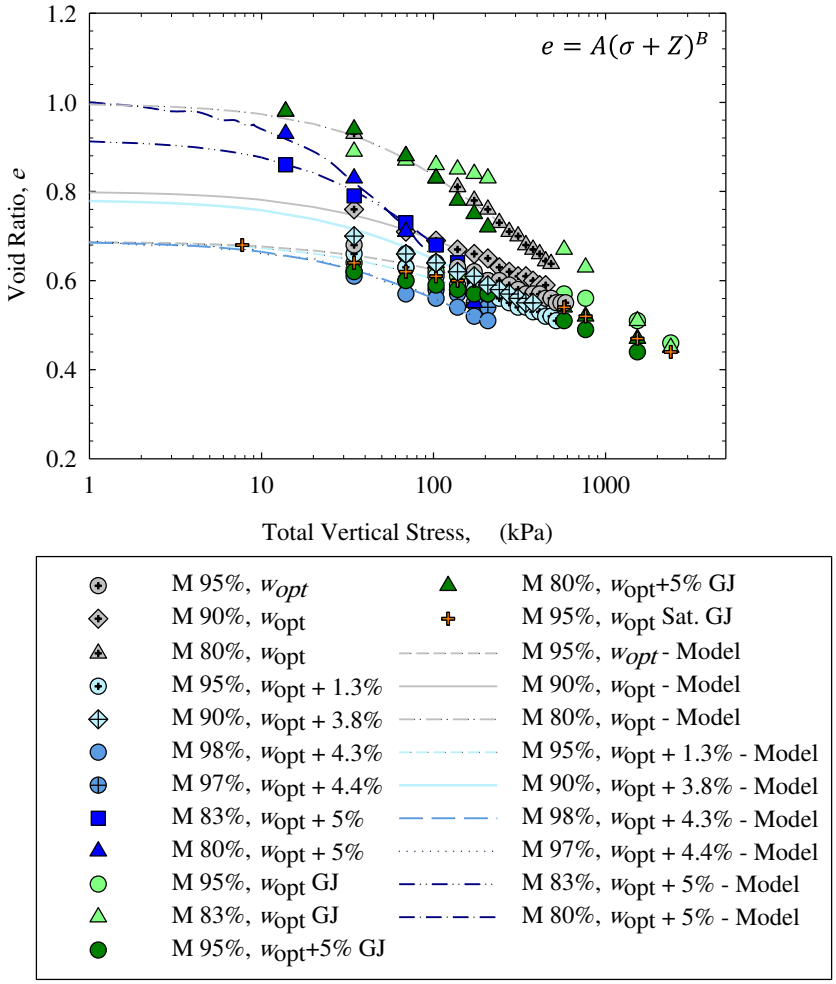

Figure A7 - Results from undrained large-strain compression tests and saturated and unsaturated confirmatory tests on M tailings.
Tests identified in the legend include the percent of maximum dry unit weight and water content relative to optimum water content (w_{opt}), which is 15.8%. $e = A(\sigma + Z)^B$, a constitutive relationship by Liu and Znidarčić (1991). GJ: GeoJac apparatus, Sat: saturated.

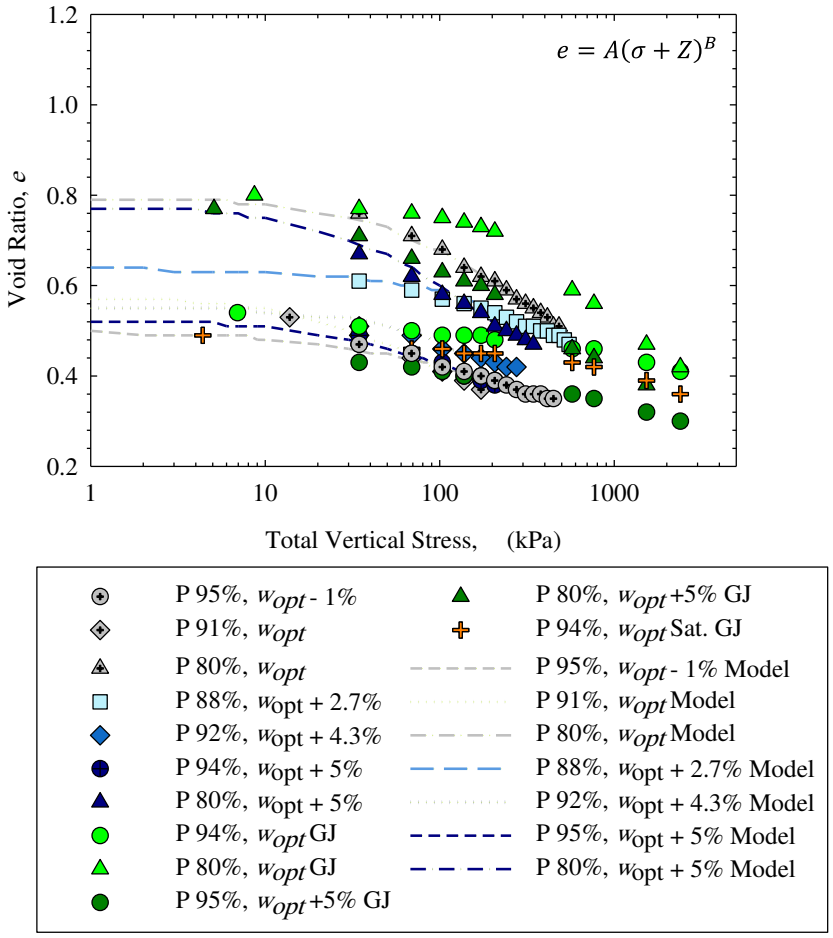

Figure A8 - Results from undrained large-strain compression tests and saturated and unsaturated confirmatory tests on P tailings.
Tests identified in the legend include the percent of maximum dry unit weight and water content relative to optimum water content (w_{opt}), which is 14.2%. $e = A(\sigma + Z)^B$, a constitutive relationship by Liu and Znidarčić (1991). GJ: GeoJac apparatus, Sat: saturated.

A4. SUPPLEMENTARY DATA FOR CHAPTER 4

Locations descriptions

Climatic data of year 2020 from Tucson-AZ, Juneau-AK, and Bozeman-MT were used in the simulations performed via HYDRUS-2D. Climatic data were obtained from the National Centers for Environmental Information website (*www.ncdc.noaa.gov*) and from Western Region Climatic Center (*wrcc.dri.edu*). In 2020, Tucson had approximately 106 mm total rainfall, zero snowfall, and 2820 mm total pan evaporation, Juneau had approximately 1974 mm total rainfall, 2329 mm total snowfall, and 12 mm total pan evaporation, and Bozeman had approximately 376 mm total rainfall, 2386 mm total snowfall, and 1086 mm total pan evaporation. The average temperature in 2020 was 22.5°C in Tucson, 5.9°C in Juneau, and 7.4°C in Bozeman.

Saturated hydraulic conductivies of investigated tailings

Table A3 provides fitting parameters optimized for the constitutive hydraulic conductivity model by Somogyi (1979) for M and P tailings. The model is described in the main manuscript.

Table A3- Fitting parameters used for the saturated hydraulic conductivity constitutive model.

Fitting Parameter	Mine M Tailings	Mine P Tailings
C (m/s)	7.6×10^{-8}	2.9×10^{-7}
D	9.08	7.17

Heat transport package inputs

Table A4 provides the temperature amplitudes and the initial temperatures of the three climatic conditions of arid (Tucson-AZ), wet (Juneau-AK), and hemiboreal (Bozeman-MT), which were needed to activate the heat transport package within the HYDRUS-2D program.

Table A4 - Heat transport package parameters for the three considered climates

Climate	Temperature Altitude (°C)	Initial Temperature (°C)*
Bozeman, MT	13.5	0.25
Juneau, AK	6.31	4.60
Tucson, AZ	15.9	8.10

*Corresponds to the average temperature of Jan. 1, 2020.

Soil water characteristic curve of sand

The drying SWCC parameters and saturated hydraulic conductivity (K_s) of sand were already available within the Rosetta Package of the HYDRUS program and are provided in Table A5. The SWCC of sand is shown in Figure A9.

Table A5 - Soil water characteristic curve parameters of sand obtained from the Rosetta Package of HYDUS.
θ_r = residual volumetric water content. θ_s = saturated volumetric water content. α, and n, are fitting parameters ($m = 1 - n^{-1}$), K_{sat}: saturated hydraulic conductivity.

	θ_r	θ_s	α*	n	K_{sat} (m/s)
Sand	0.045	0.430	1.45	2.68	8.2×10^{-5}

* in 1/kPa.

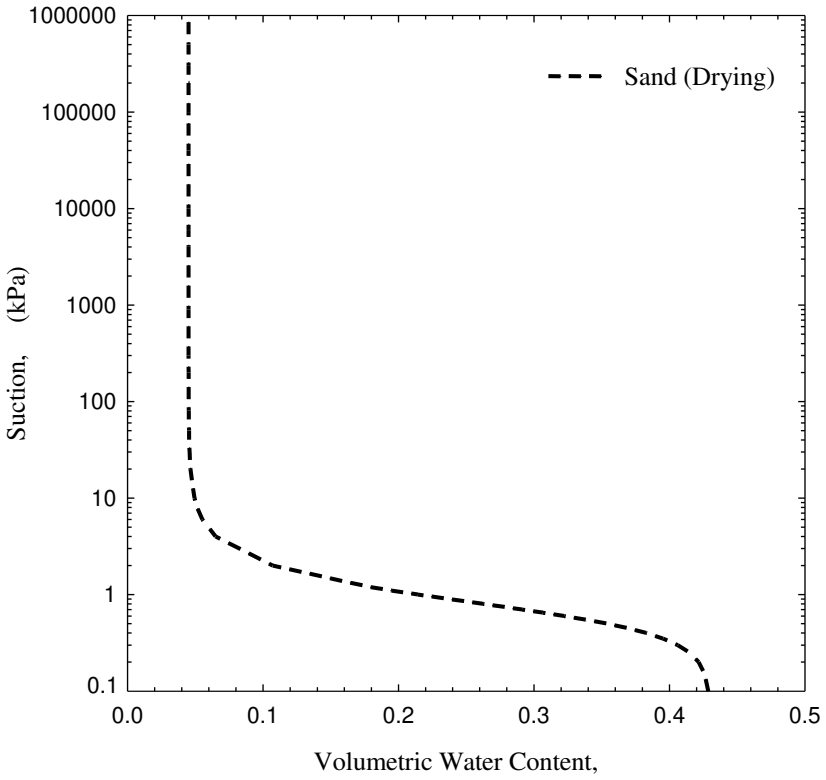

Figure A9 - Drying soil water characteristic curve of sand generated using the parameters from the Rosetta Package within HYDRUS.